BIOGEOCHEMISTRY OF ENVIRONMENTAL GRADIENTS IN SERPENTINIZATION-INFLUENCED GROUNDWATER AT THE COAST RANGE OPHIOLITE MICROBIAL OBSERVATORY, CALIFORNIA

By

Mary C. Sabuda

A THESIS

Submitted to
Michigan State University
in partial fulfillment of the requirements
for the degree of

Geological Sciences--Master of Science

2017

ABSTRACT

BIOGEOCHEMISTRY OF ENVIRONMENTAL GRADIENTS IN SERPENTINIZATION-INFLUENCED GROUNDWATER AT THE COAST RANGE OPHIOLITE MICROBIAL OBSERVATORY, CALIFORNIA

By

Mary C. Sabuda

Serpentinization of ultramafic rock in ophiolite complexes along continental margins leads to the mobilization of volatiles and reduced carbon compounds that can be used as sources of energy by subsurface microbial communities. The extent to which sulfur compounds can serve as electron acceptors in anoxic serpentinizing systems and their role in biogenic carbon cycling remains to be elucidated. Large scale processes at CROMO were studied using geochemical analyses, bioenergetics calculations, microscopic cell counts, and 16S rRNA sequencing to identify the population of sulfate reducers and methane cyclers. Shotgun metagenomic and metatranscriptomic sequencing identified the production of key genes for sulfate reduction, sulfide oxidation, and thiosulfate disproportionation. Small scale processes at CROMO were identified through a depth profile of CSW1.1. With water pumped directly from the well, microcosms were created to measure the growth of microbial communities in the presence of $^{13}CH_4$. Thiosulfate or $Fe(OH)_3$ were injected as electron acceptors, with the addition of O_2 gas in designated “oxic” bottles. The highest cell growth and biogenic ^{13}DIC production occurred in “anoxic” $^{13}CH_4$ + thiosulfate amended bottles, with Trueperaceae dominating both the profile of CSW1.1 and the microcosms. The biogeochemistry of CROMO yields insight into the potential for sulfur and methane cycling within this cryptic serpentinite environment found throughout the world.

ACKNOWLEDGEMENTS

This work was made possible with the advice and support of many people. First, a huge, endless thank you to Dr. Matt Schrenk for his support, guidance, and unwavering confidence in me throughout the past two years. You have been an incredible mentor and I deeply value all the opportunities I have had while a member of your laboratory. Thank you for encouraging me to earn a Ph.D. I would also like to thank Dani Morgan-Smith, Lindsay Putman, Heather Miller, and Lauren Seyler for being great lab mates and for making room 144 feel like home. You all have made my experience at MSU one that I will strive to find again through my Ph.D. work and beyond.

I would like to thank the entire CROMO team, including Dr. Tom McCollom, Dr. Dawn Cardace, Dr. Tori Hoehler, Mike Kubo, and Dr. Masako Tominaga, I want to extend an extra thank you to Dr. Tori Hoehler and Mike Kubo for hosting and mentoring me throughout my time at NASA Ames Research Center throughout the summer of 2016. Working on a part of my thesis project at NASA was incredible, and I thank Tori and Mike for this once in a lifetime opportunity. It was an honor working with you both. Additionally, thanks to the NASA Astrobiology Institute for funding this research at CROMO through the NAI CAN-7 Rock Powered Life grant. Thank you to my committee members, Dr. Matt Schrenk, Dr. Kazem Kashefi, Dr. David Long, and Dr. Jay Zarnetske for their essential advice and input on this work. Thanks to the Michigan State Department of Earth and Environmental Sciences for the guidance, fellowships, and scholarships that made my research possible.

Thanks to Lindsay Putman, Megan Hudak, Jordan Salley, and Laney Hart for being the best friends and lab mates throughout our time at MSU. You kept me sane throughout these past few years and I am extremely thankful.

A big thank you is for my incredible family, including my mother Mrs. Karen Sabuda for inspiring me to earn a Master's degree and reach higher. Thanks to my father, Mr. David Sabuda, for his constant encouragement, daily notes to "have a day", and conversations about environmental politics. Thank you to my brother, Mr. Steven Sabuda, for always knowing how to make me laugh, and for always being there for me. We have been through everything together, and I am so lucky to have you. Thanks to my family for always relaying me to and from the airport at any hour whenever I had to travel for this research. I am thankful for those unfortunately short car rides, infrequent nights at home, and care packages of groceries before leaving for the next destination or heading back to MSU. Thank you to my amazing grandparents for their support and encouragement, and for always reminding me that there's more to life than work. Thank you to Mr. Sean Hughes, my rock, for his unwavering support and advice throughout the countless struggles of my Master's degree. I love you all, and I thank you very much.

PREFACE

This work was written for publication in *Nature Geoscience* and *Geochemistry, Geophysics, Geosystems (G^3)*, for chapters two and three, respectively.

TABLE OF CONTENTS

LIST OF TABLES

LIST OF FIGURES

KEY TO ABBREVIATIONS

AOM: Anaerobic Methane Oxidation

ANME: Anaerobic Methanotrophic Archaea

ARC: Ames Research Center (NASA)

DAPI: 4',6-diamidino-2-phenylindole

DNA: Deoxyribonucleic Acid

CH_2O: Formaldehyde

CH_4: Methane

CO: Carbon Monoxide

CO_2: Carbon Dioxide

CO_3^{2-}: Carbonate Ion

CROMO: Coast Range Ophiolite Microbial Observatory

CSW: Core Shed Well

DIC: Dissolved Inorganic Carbon

DO: Dissolved Oxygen

DOC: Dissolved Organic Carbon

Dsr: Dissimilatory Sulfite Reductase

F-AOM: Iron reduction coupled to AOM

HCO_3^-: Bicarbonate

ICP-MS: Inductively Coupled Plasma Mass Spectrometry

IRMS: Isotope Ratio Mass Spectrometry

LCHF: Lost City Hydrothermal Vent

LCY: Lost City

LIG: Liguria, Italy

MSU: Michigan State University

NAI: NASA Astrobiology Institute

NASA: National Aeronautics and Space Administration

OA: Organic Acids

ORP: Oxidation Reduction Potential

QV: Quarry Valley

rRNA: Ribosomal Ribonucleic Acid

RPL: Rock Powered Life

S-AOM: Sulfate Reduction coupled to AOM

UV: Ultraviolet

XRD: X-Ray Diffraction

XRF: X-Ray Fluorescence

CHAPTER 1

Introduction

Serpentinization

Along the ocean floor at various tectonic settings, ultramafic rocks can be uplifted which allows seawater to infiltrate to extensive depths and interact with primitive basement rock such as basalt, gabbro, and peridotite. During this process, water can hydrate the olivine and pyroxene minerals that comprise peridotite, dunite, etc. and alter it to become the serpentine minerals, lizardite, antigorite, and chrysotile (Proskurowski et al., 2008; Frost et al., 2013; McCollom et al., 2013). This process can happen in low-temperature environments (50-300°C) where the serpentine mineral, lizardite, dominates, or in high temperature settings where antigorite is the predominant form (Evans et al., 2010). The general serpentinization reaction is presented below (Equation 1.1).

$$3Fe_2SiO_4 + 5Mg_2SiO_4 + 9H_2O \rightarrow 3Mg_3Si_2O_5(OH)_4 + Mg(OH)_2 + 2Fe(OH)_2 \qquad \text{(Eq. 1.1)}$$

Throughout the process of serpentinization, inorganic carbon is precipitated out as carbonate (Equation 1.2), and as a result reduced, volatile carbon compounds such as methane are one of the most available and mobile carbon compounds in this setting (Barnes et al., 1978; Schrenk et al., 2013). Because of this, it is important to understand the processes that control its concentrations, including microbial metabolic activities. In

circumneutral waters, magnesium can react with bicarbonate in solution to form magnesite, carbon dioxide, and water (Equation 1.3).

$$Ca^{2+} + CO_3^{2-} \rightarrow CaCO_{3(s)} \quad \text{(Eq. 1.2)}$$

$$Mg^{2+} + 2HCO_3^{-} \rightarrow MgCO_{3(s)} + CO_2 + H_2O \quad \text{(Eq. 1.3)}$$

$$3Fe(OH)_2 \rightarrow Fe_3O_4 + 2H_2O + H_2 \quad \text{(Eq. 1.4)}$$

During this process, water reacts with carbon dioxide in solution to produce methane and hydrogen (McCollom and Seewald, 2013). Reduced iron in olivine can also react with water and contribute high concentrations of hydrogen (Suda et al., 2014; Equation 1.4). Hydrogen gas produced from this secondary reaction can further react with carbon dioxide or carbon monoxide to form hydrocarbons in Fisher-Tropsch Type reactions (Szponar et al., 2013).

Natural gradients in water chemistry develop as serpentinization reactions occur, and as end-member fluids mix. Measured serpentine waters range from circumneutral pH 7.5 to hyperalkaline pH 12.5 and above due to an influence of hydroxides. In marine settings, the ions associated with seawater can interact with the ultrabasic waters associated with serpentinization, creating complex concentrations of compounds and therefore unique environments to sustain life. Similarly, in ophiolite complexes where oceanic crust has been emplaced on continental crust, meteoric water can percolate into the groundwater and mix with ultrabasic serpentinite-and-seawater fluids.

CROMO Field Site

The Coast Range Ophiolite Microbial Observatory (CROMO) is located at the Donald and Sylvia McLaughlin Natural Reserve, near Lower Lake, California. The Homestake Mining Company, Inc. first drilled exploratory cores for gold prospecting and provided the preliminary water and core data from environmental monitoring, which sparked scientific interest in the area. Later, the University of California Davis established the McLaughlin Natural Reserve on site and the CROMO scientific party drilled a total of eight wells in August 2011 to explore the geology, geochemistry, microbiology, hydrology, and geophysical characteristics of the area (Cardace et al., 2013) in addition sampling to four pre-existing HMC wells (N08-A, N08-B, N08-C, CSWold).

The Reserve and respective wells are located on and drilled into the mélange of the northern Coast Range Ophiolite (CRO) of mid to late Jurassic age (Shervais et al., 1985; Huot and Maury, 2002). The Coast Range Ophiolite extends north from San Francisco to the Klamath Mountains and beyond Oregon's Coast Range, and west from the east end of the Franciscan Complex to the Great Valley of California (Cardace et al., 2013) as fragments of ophiolite scattered throughout the area (Shervais et al., 2004). The CRO is tectonically altered and overlain by the Jurassic-Cretaceous Great Valley Sequence and is in contact with the geologically younger Jurassic-Paleogene Franciscan Complex (Shervais et al., 1985; Shervais et al., 2004). Work by Peters, (1993) reveals a single source of water for the Coast Range Mountains as trapped Cretaceous seawater. The McLaughlin Natural Reserve's geology is diverse, with

serpentinite, gabbro, metasediment, pyroxenite, and peridotite influence (Carnevale et al., 2013).

In monitoring wells at CROMO influenced by water from a deeper aquifer source, groundwater exhibits high pH levels, increased salinities, and extremely reducing conditions (-300 mV). Across the site, dissolved oxygen and nitrate concentrations are minimal, whereas sulfate and methane concentrations are high (~300 μM, ~500 μM respectively), which reveals the need to assess the potential energy organisms surviving these extreme conditions could gain from metabolizing sulfur through a variety of reactions. The range of groundwater chemistries and microbial communities between wells only meters apart indicate complex hydrology due to the fractured serpentine matrix. When the two main wells at CROMO were experimentally purged, *in situ* dataloggers reveal none of the surrounding wells responded, and that it took weeks to fully recharge the two boreholes. This reveals the isolated hydrology comprising the area near CSW1.1 and QV1.1.

Microbial Metabolic Potential

Previous work at CROMO has clearly shown that Betaproteobacteria and Clostridiales are dominant members of this system (Twing et al., 2017). Microcosm experiments inoculated with CROMO fluids, hydrogen atmosphere, and a suite of carbon sources (CO_2, CH_4, acetate, formate) showed growth when provided methane or acetate. The addition of nutrients or electron acceptors had no significant effect on the growth (Crespo-Medina et al., 2014), except in bottles amended with sulfur compounds, where community compositions changed to favor *Dethiobacter* and Comamonadaceae.

An analysis of methane isotopologues within natural CROMO groundwater revealed both thermogenic and microbial sources for methane (Wang et al., 2015). Similarly, recent work by Twing et al., 2017 showed pH, CO, and CH_4 best explained the variability in bacterial community composition across the site, with significant positive correlations between both *Dethiobacter* and Comamonadaceae to methane. This foundational work helps to elucidate which factors control community composition and the importance of sulfur and carbon in this system.

The work described throughout this thesis assesses the distribution and activities of microorganisms in the context of environmental gradients (oxygen, pH, conductivity, DIC, sulfate, methane, etc.) with depth at CROMO to gain insight into how fluctuations in chemistry impact the extremophiles able to thrive within this challenging environment. This thesis addresses the biogeochemistry of sulfur and methane in serpentinite systems, and reveals the importance of intermediate sulfur compounds (e.g. thiosulfate) in microbial metabolisms within these systems. In addition to assessing the large-scale processes occurring at CROMO, this is the first study to date that has combined aqueous geochemical measurements, microbiological characterization (metagenomics and metatranscriptomics), thermodynamic calculations, and microcosm experiments to develop a comprehensive depth profile of a terrestrial serpentinite-hosted groundwater well.

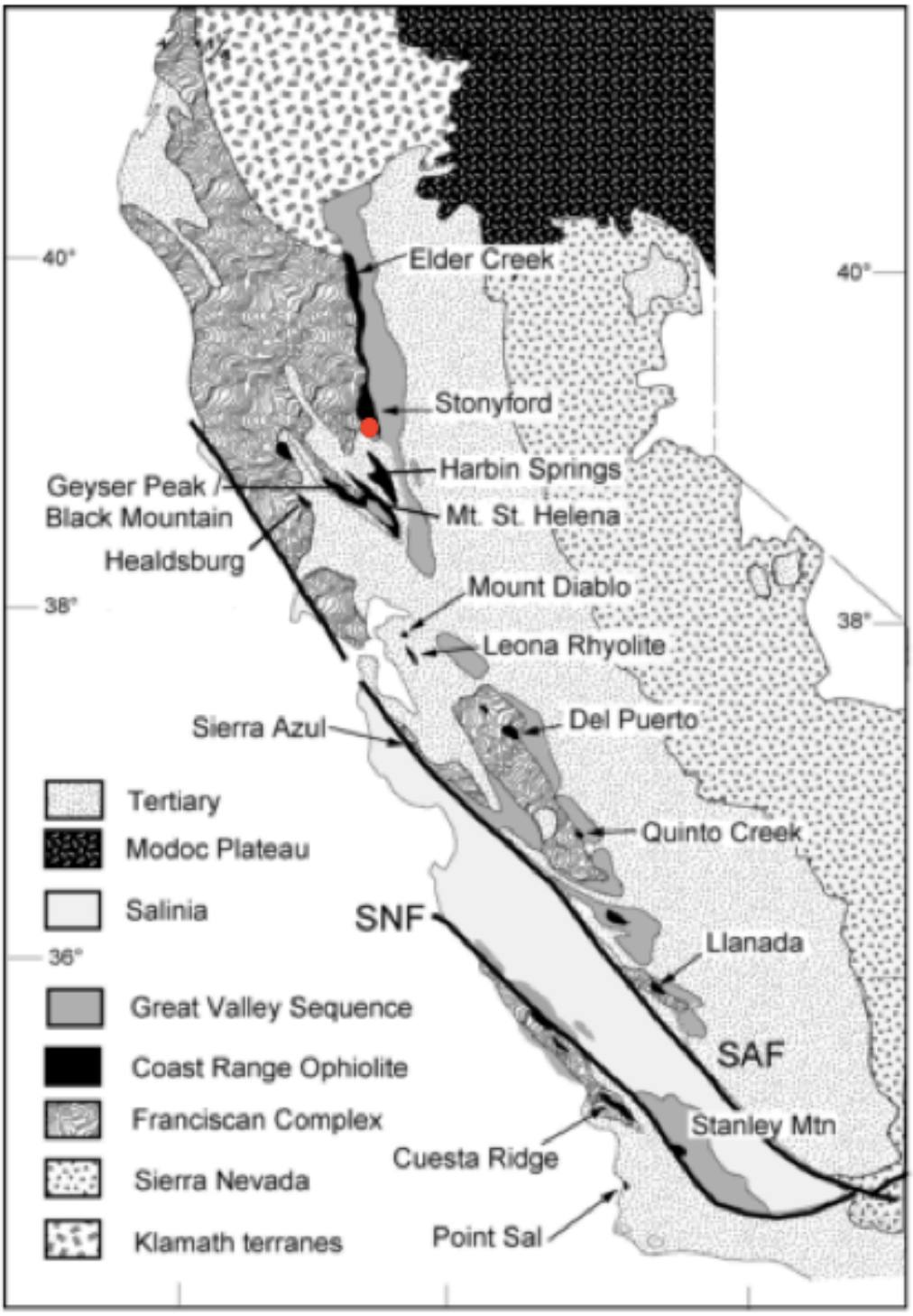

Figure 1 - Geologic Map Indicating the CROMO Field Site Location. Also shown are California's Great Valley Sequence, Coast Range Ophiolite, Franciscan Complex, Del Puerto Ophiolite, and others modified from Shervais et al., (2004). A red circle indicates the location of the CROMO field site, northeast of San Francisco, CA

REFERENCES

REFERENCES

Barnes, I., Oneil, J. R. & Trescases, J. J. Present Day Serpentinization in New-Caledonia, Oman and Yugoslavia. *Geochim. Cosmochim. Acta* **42,** 144–145 (1978).

Cardace, D. *et al.* Establishment of the Coast Range ophiolite microbial observatory (CROMO): Drilling objectives and preliminary outcomes. *Sci. Drill.* 45–55 (2013). doi:10.5194/sd-16-45-2013

Carnevale, D.C. Carbon sequestration potential of the Coast Range Ophiolite in California. (Master's thesis). Retrieved from: Open Access Master's Theses. Paper 46. (2013).

Crespo-Medina, M. *et al.* Insights into environmental controls on microbial communities in a continental serpentinite aquifer using a microcosm-based approach. *Front. Microbiol.* **5,** 604 (2014).

Evans, B. W. Lizardite versus antigorite serpentinite: Magnetite, hydrogen, and life(?). *Geology* **38,** 879–882 (2010).

Frost, B. R., Evans, K. A., Swapp, S. M., Beard, J. S. & Mothersole, F. E. The process of serpentinization in dunite from new caledonia. *Lithos* **178,** 24–39 (2013).

McCollom, T. M. Laboratory Simulations of Abiotic Hydrocarbon Formation in Earth's Deep Subsurface. *Rev. Mineral. Geochemistry* **75,** 467–494 (2013).

McCollom, T. M. & Seewald, J. S. Serpentinites, hydrogen, and life. *Elements* **9,** 129–134 (2013).

Peters, E. K. D-18O enriched waters of the Coast Range Mountains, northern California: Connate and ore-forming fluids. *Geochim. Cosmochim. Acta* **57,** 1093–1104 (1993).

Proskurowski, G. *et al.* Abiogenic hydrocarbon production at lost city hydrothermal field. *Science* **319,** 604–7 (2008).

Schrenk, M. O., Brazelton, W. J., Carolina, N. & Lang, S. Q. Serpentinization, Carbon, and Deep Life. *Rev. Mineral.* **75,** 575–606 (2013).

Shervais, J. W. & Kimbrough, D. L. Geochemical evidence for the tectonic setting of the Coast Range ophiolite: a composite island arc-oceanic crust terrane in western California. *Geology* **13,** 35–38 (1985).

Shervais, J. W. *et al.* Multi-Stage Origin of the Coast Range Ophiolite, California: Implications for the Life Cycle of Supra-Subduction Zone Ophiolites. *Int. Geol. Rev.* **46,** 289–315 (2004).

Suda, K. *et al.* Origin of methane in serpentinite-hosted hydrothermal systems: The CH4-H2-H2O hydrogen isotope systematics of the Hakuba Happo hot spring. *Earth Planet. Sci. Lett.* **386,** 112–125 (2014).

Szponar, N. *et al.* Geochemistry of a continental site of serpentinization, the Tablelands Ophiolite, Gros Morne National Park: A Mars analogue. *Icarus* **224,** 286–296 (2013).

Twing, K. I. *et al.* Serpentinization-influenced groundwater harbors extremely low diversity microbial communities adapted to high pH. *Front. Microbiol.* **8,** 308 (2017).

Twing, K. I. Microbial Diversity and Metabolic Potential of the Serpentinite Subsurface Environment. *ProQuest* (2015).

Wang, David T. *et al.* Nonequilibrium clumped isotope signals in microbial methane. *Science (80-.).* **348,** (2015).

CHAPTER 2

Sulfur Biogeochemistry is an Important Link Between Marine and Terrestrial Serpentinizing Systems[1]

Abstract

The hydration and oxidation of mantle rock that can occur in ancient ocean crust emplaced along continental margins can result in a process known as serpentinization. Reduced gases such as hydrogen and methane are mobilized and reduced carbon compounds are produced that lead to distinct serpentinite-hosted groundwater chemistries. Seawater, in particular, can be stored within these aquifers and interact with hyperalkaline fluids and neutral meteoric waters. The aqueous sulfur chemistry can vary dramatically between serpentinites in ophiolite complexes due to this mixing effect and harbor microbial communities able to metabolize sulfur and thrive within the extreme conditions. At the Coast Range Ophiolite Microbial Observatory (CROMO), sampled water chemistries indicate a substantial influence of seawater with increasing depth. This seawater can contribute to the high concentrations of sulfate measured, which may serve as a key oxidant for native microbial populations, as oxygen, nitrate, and iron concentrations in the system are extremely limited. This idea was tested by supplementing measured geochemical data with 16S rRNA sequencing and shotgun metagenomic and metatranscriptomic approaches to identify organisms capable of metabolizing sulfur compounds. These results demonstrate an abundance of sulfur cycling activities within microbial communities at CROMO, such as sulfate reduction,

[1] The work described in this chapter is currently in submission to the journal Nature Geoscience for publication: M.C. Sabuda, T.M. McCollom, M.D. Kubo, L.I. Putman, W. Brazelton, K.I. Twing, D. Cardace, and M.O. Schrenk. Sulfur biogeochemistry is an important link between marine and terrestrial serpentinizing systems

sulfide oxidation, and thiosulfate disproportionation. Thermodynamic calculations indicate intermediate sulfur species (i.e. thiosulfate) are key compounds in these systems that have been previously overlooked, and the anaerobic oxidation of methane (AOM) coupled to sulfate reduction is energetically favorable. The metagenomic and metatranscriptomic findings outlined in this study reveal striking similarities between metabolic processes within ancient CROMO groundwaters and the marine Lost City Hydrothermal Field. Together, these results demonstrate the important role sulfur holds in understanding the biogeochemistry of serpentinizing systems.

Introduction

Serpentinization is a geochemical reaction that occurs following the exposure of mafic and ultramafic lithologies to hydrothermal fluid. This process can occur as deeply seated rocks are obducted onto the continents in the form of ophiolite sequences (Dilek et al., 2011; Morrill et al., 2013), or as detachment faulting on the ocean floor uplifts ultramafic rock allowing the interaction of mineral assemblages, water, and heat (Sleep et al., 2004; Schwarzenbach et al., 2016). Typical groundwater chemistries hosted by serpentinites can range from sulfate-chloride dominated waters rich in magnesium, to intermediate magnesium-bicarbonate dominated fluids, or waters with abundant calcium hydroxides (Schwarzenbach et al., 2016). As a result, the pH of these systems can range from 7.5 to greater than 12.5. As the ferrous iron in these ultramafic minerals are oxidized by water, hydrogen gas (H_2) is released (Okland et al., 2012), creating a predominantly anoxic environment within the subsurface. Microorganisms within this unique habitat are able to metabolize the products of serpentinization (Sleep et al.,

2004; Brazelton et al., 2011; Lang et al., 2012; Ménez et al., 2012; Quéméneur et al., 2014; Mei et al., 2016) and facilitate biogeochemical cycling of the limited nutrients (i.e. hydrogen, methane, acetate, formate) and electron acceptors (oxygen, nitrate, sulfate, iron, etc.) when present.

Because the three most favorable terminal electron acceptors, dissolved oxygen, nitrate, and iron can be extremely limiting in serpentinizing systems, the occurrence of alternative oxidants, such as sulfate, must be considered. At the Coast Range Ophiolite Microbial Observatory (CROMO), CA, outstanding questions remain about the role of sulfur in microbial metabolic activity within serpentinite-hosted groundwaters, and were addressed using genomic and geochemical approaches. In addition to shotgun metagenomics, geochemical analyses, and thermodynamic bioenergetics calculations, for the first time in a serpentinizing system, a shotgun metatranscriptomics approach was applied to address these unknowns.

CROMO Chemistry Is Unique Among Ophiolites

CROMO is located on the University of California- Davis McLaughlin Natural Reserve and consists of twelve wells drilled into the mélange of the northern Coast Range Ophiolite (CRO) of Middle to Late Jurassic age (Shervais et al., 1985; Huot and Maury, 2002). The CRO was emplaced in a supra-subduction zone setting, and structurally overlies the Franciscan Complex (Shervais et al., 2004; Choi et al., 2008; Wakabayashi, 2012). Among ophiolitic serpentinite-influenced waters (e.g. Oman, Liguria, Cyprus, Leka, Santa Elena, etc.) the aqueous geochemistry at CROMO hosts distinct concentrations of major cations and anions (Table 1) relative to other recorded

terrestrial serpentinizing systems. Interestingly, sodium and chloride concentrations at CROMO indicate that the water is characteristic of both dilute seawater and evaporite deposits (Fig. 2). Though the wells are split into two clusters, Core Shed Wells (CSW) located 1.4 km down-valley from the Quarry Valley wells (QV, N08), when compared to published data for other ophiolite complexes, collectively CROMO wells are among the most saline while other sites plot further down the seawater dilution line (Fig. 2, Table 2). To emphasize this, the Cyprus ophiolite, Prony Bay in New Caledonia, and the Genova Province in Italy, are three systems that reflect sodium chloride values most similar to CROMO. Work from Cyprus suggests the most saline waters are those that interact with a saline end member and evaporite minerals (Neal and Shand, 2002). Work by Peters (1991, 1993) reveals Coast Range waters are derived from Cretaceous seawater that underwent diagenetic processes to varying degrees by water-rock interactions.

Seawater geochemical indicators such as sodium, bromide, and chloride values, strontium concentrations, and specific conductivity measurements, reported here for CROMO (Table 1) suggest that wells drilled to greater than 27m sample groundwater influenced by a deeper formation with a dilute seawater composition (Hem et al., 1992; Alcalá et al., 2008; Katz et al., 2011). If CROMO showed evidence for halite dissolution at depth, the trajectory of the sodium chloride plot for the deeper wells would steepen and reflect that of 1:1 Na Cl rather than seawater dilution (Fig. 2). Other wells at the site drilled to less than 27m (shallow and medium wells; Table 1), exhibit sodium and chloride concentrations reflective of both dilute seawater and evaporite dissolution. Increases in salinity can occur from mixing with deeper brine formation water,

dissolution of evaporite minerals (e.g. marine salts), or by the evaporation of water (Neal and Shand, 2002). Subsurface evaporites can be deposited in serpentinite lithologies over time as relatively buoyant brines migrate vertically, mix, and drain, as discussed in Scribano et al., 2017. While ophiolitic serpentines can lose evaporite deposits during water circulation and obduction, fluid inclusions can be composed of saline brines and contain salt as they cool (Scribano et al., 2017). These fluid inclusions can reveal ancient recycling of original seawater-derived fluids (Scambelluri et al., 1997). It is worth noting that the Feather River Ophiolite located ~300 km East of CROMO, hosts chemistries reflective of peridotite serpentinized by seawater prior to obduction onto the continent, and a secondary stage of serpentinization hypothesized to be due to the exhumation of the hydrothermally altered peridotite (Li and Lee, 2006).

As suggested by Boscetti and Toscani, 2008 and Chavagnac et al., 2013, among others, deviations of sodium from the seawater dilution line can indicate the influence of sodium-containing minerals such as plagioclase. Furthermore, because small single charged ions are the most mobile (White, 1965), sodium has a higher potential to migrate into solution. Bromide is typically considered conservative during evaporation and diagenesis of seawater (Carpenter, 1978), until evaporation conditions reach almost 90 times that of seawater (McCaffrey et al., 1987). At CROMO, bromide is enriched in these fluids relative to the dilute seawater concentrations observed (Fig. 2), which is consistent with results of Peters (1993) for this area of the Coast Range region.

In order for water chemistries to reflect that of a dilute seawater composition, hyperalkaline fluids at CROMO must be additionally influenced to varying degrees by meteoric water. Sodium and conductivity are positively correlated to well depth, and

conductivity is additionally correlated to chloride, sodium, and methane (Table 6). Sulfate, and strontium concentrations generally increase with depth, though CSW 1.1 and QV 1.1 deviate from this trend as the wells are uncased below 5m and 17m depths, respectively, and thus can sample water influenced more heavily by surficial sources. Shallower wells (e.g. Group 1: CSW1.4, N08-C, QV1.2, CSW1.2) exhibit meteoric-alkaline water conditions, with pH values in the 7.8-9.5 range, whereas wells drilled to medium depths (e.g. Group 2: CSW1.1, CSW1.3, QV 1.1, and N08-B) sample a mixture of water sources, and wells drilled to deeper depths (e.g. Group 3: CSW1.5, CSWold, QV1.3, N08-A) are more exclusively influenced by this deep seawater source (Fig. 2). The mixing of these waters leaning in the direction of seawater composition may represent the transition between a marine and terrestrial serpentinizing system. Additionally, mixing can have numerous implications for biogeochemical cycling of key microbial nutrients (C, N, and P compounds) reductants such as methane, and hydrogen, and oxidants such as nitrate, sulfate, and thiosulfate.

To understand how CROMO and its saline waters relate to marine systems, this ancient seafloor system was compared to the Lost City Hydrothermal Field, an actively serpentinizing system located on the Atlantis Massif along an off-axis traverse of the Mid-Atlantic Ridge (Ludwig et al., 2005; Delacour et al., 2008). The Lost City hosts a gradient of water chemistries influenced by seawater as one end member and the high pH, Ca-OH dominated vent fluids as the other. Sulfate concentrations for the hydrothermal fluids range from 1000 to 4000 μM (Kelley et al., 2005; Table 2), sulfide ranges from 245 to 2880 μmol/kg, and magnesium is depleted (Lang et al., 2012). Microbial communities in both locations can take advantage of energy available from

these variations in chemistry and thrive in conditions where seawater mixes with hydrothermal fluids. In addition to similar chemistries between systems, metagenomic data show striking similarities, as described below.

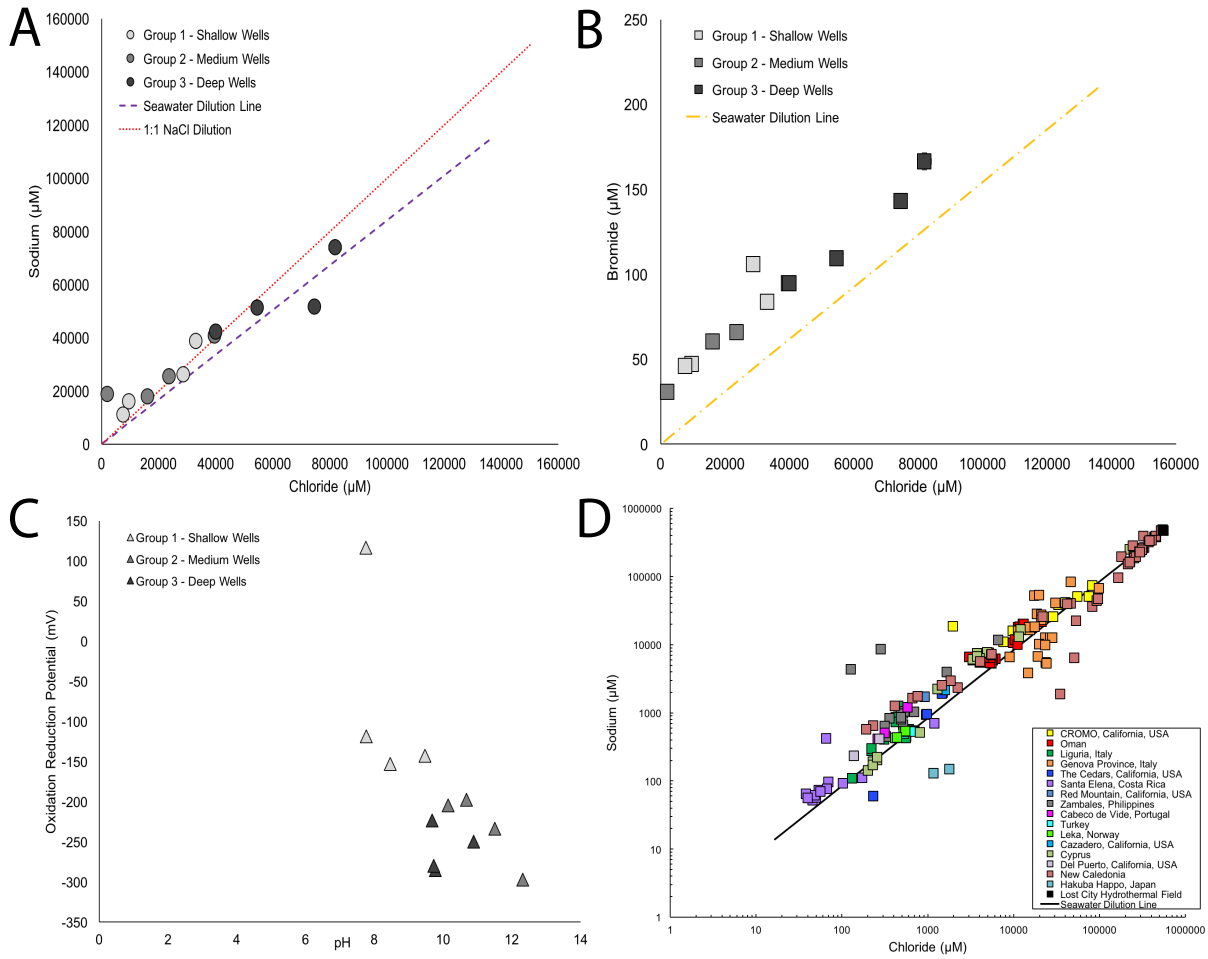

Figure 2 - CROMO Water Chemistry. a,b, The amount of sodium and bromide are respectively compared to chloride in micromolar concentrations, and c, ORP is plotted against pH. Each point represents a CROMO monitoring well. Wells were grouped evenly into three clusters based upon their drilled depth. Shallow represents wells drilled to less than 15 m, medium represents wells drilled between 15 and 20 m depth, and deep represents wells drilled to depths greater than 20 m depth. Error bars represent analytical uncertainty of the ion measurements. d, Sodium chloride values in micromolar concentrations are plotted for published terrestrial serpentinizing systems worldwide, with the seawater dilution line plotted for reference. CROMO wells plot as yellow squares.

Sulfur Metabolisms Are Energetically Favorable

CROMO is designed to sample the subsurface at discrete depths, and thus it is possible to obtain insight into the existing suite of chemistry and life that persists within serpentinizing systems without substantial interference of atmospheric processes. Previously published work in Liguria (Chavagnac et al., 2013), the Philippines (Cardace et al., 2015), the Cedars (Morrill et al., 2013) and the Genova Province (Cipolli et al., 2004) among others, sample sulfur chemistry at springs, and therefore are influenced to a relatively stronger degree by the atmospheric conditions. CROMO is characterized by higher concentrations of sulfate compared to sulfide in low dissolved oxygen, high conductivity, and high pH waters, which presents favorable conditions for sulfate reduction (Schrenk et al., 2013). CROMO wells were drilled using 143.09m^3 of purified water in the summer of 2011 (Cardace et al., 2013; Ortiz et al., submitted). This created an artificial wet season in California and considerably diluted the *in situ* water chemistry, but since this time drilling perturbation has dissipated. Where data is available, seasonal sampling campaigns since 2011 indicate sulfate and sulfide concentrations have stabilized over time to their present concentrations of hundreds and tens of micromolar, respectively, and fluctuate small amounts between sampling. Dissolved oxygen, electrical conductivities, oxidation-reduction potential, and pH similarly fluctuate, but remain relatively stable (Table 3).

Serpentinizing systems have stimulated a great deal of interest in recent years in terms of their habitability, as have the adaptations of resident microbial communities in these ecosystems (e.g. Brazelton et al., 2012; Okland et al., 2012; Schrenk et al, 2013; Tiago et al., 2013; Suzuki et al., 2014; Rempfert et al., 2016;). In addition to constraining

the concentrations of the dominant chemical components and investigating potential physiological adaptations, it is important to identify how these serpentinization-driven compounds provide a source of energy for microbes in this oxygen-and-carbon-limited environment (Cardace and Hoehler, 2009; Amend et al., 2011). Sixteen reactions that involve sulfur species coupled to various electron donors such as hydrogen, methane, formate and acetate, were considered for Gibbs free energy calculations based upon geochemical data from CROMO, and provide a foundation for understanding how these organisms can facilitate biogeochemical cycling of sulfur and survive within these extreme anaerobic conditions.

Results of these bioenergetic calculations indicate that sulfide oxidation coupled to nitrate reduction hosts the greatest energy gain across all wells, implicating the key role of this process in sulfur transformations. It is interesting to note that thiosulfate disproportionation to sulfate and elemental sulfur, and thiosulfate oxidation coupled to nitrate reduction yielded more free energy than reactions such as sulfate reduction coupled to hydrogen oxidation (Table 4). This has profound implications for the importance of intermediate sulfur species in the energy exchange within serpentinizing systems, as it provides a key piece of information as to how microbes facilitate the cycling of sulfur to create energy for use in ATP synthesis.

It is also notable that sulfate reduction coupled to methane oxidation (i.e. the anaerobic oxidation of methane, AOM), has the greatest free energy yield of the four sulfate reduction reactions considered in this study. Terrestrial serpentinizing systems around the world have indicated this process can occur (i.e. Brazelton et al., 2006; Tiago et al., 2013; Miller et al., 2016), and at the Santa Elena Ophiolite in Costa Rica,

the free energy yield for AOM coupled to sulfate reduction can range from $-4.84x10^{-3}$ to -4.82 J/L of fluid (Crespo-Medina et al., 2017). CROMO fluids host substantially higher free energy yields for AOM coupled to sulfate reduction (S-AOM) in all wells (-0.03 to -14.29 J/L), yet remarkably through numerous years of field studies, neither ANME nor any Archaea have been detected in CROMO fluids in greater than 1% abundance (Twing et al., 2017), but have been identified in core analyses (Twing, 2015). It is evident from these calculations that S-AOM can provide sufficient energy for metabolic activity and is one of the most energetically favorable reactions in this serpentinizing environment. As a large percentage of the community composition is unknown, organisms in the system capable of facilitating these reactions either have yet to be isolated or characterized (Crespo-Medina et al., 2014), or have escaped detection due to primer selection.

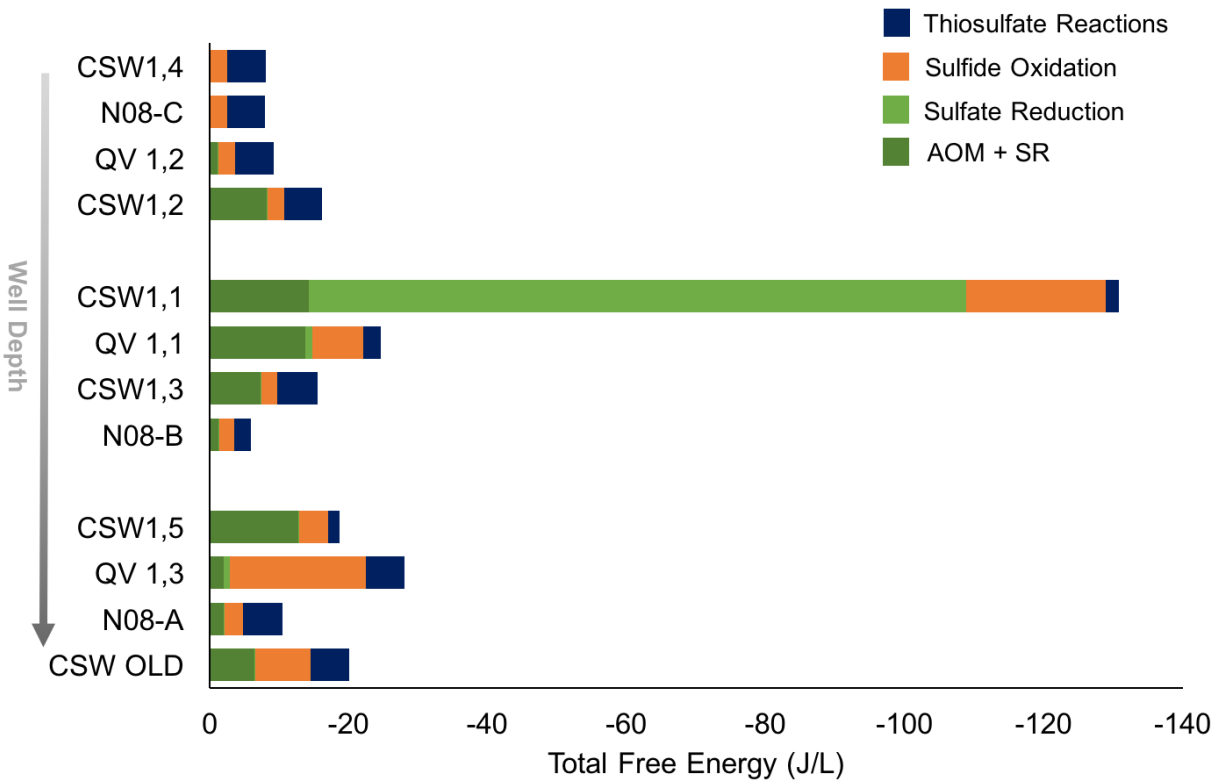

Figure 3 - Bioenergetics of Select Sulfur Reactions. Total Gibbs free energy (kJ/L) available was calculated using aqueous geochemistry data in Table 1 for reactions listed in Table 4.

Shotgun -Omics Analyses Confirm Microbes Cycle Sulfur Compounds

In this complex mixture of aqueous chemistry where hyperalkaline fluids present a challenging environment for organisms to survive, microorganisms can take advantage of the thermodynamic disequilibrium sustained from mixing fluid sources and various abiotic sulfur redox processes. For the first time in a serpentinizing system, 16S rRNA gene sequencing, metagenomics, and metatranscriptomics analyses were performed to assess community diversity, gene function, and gene production surrounding sulfur metabolisms. These data were compared to previously analyzed metagenomes from the Lost City and Voltri Massif sites. Predicted protein annotations were obtained by aligning to KEGG orthologies. Normalized abundances of key genes involved in sulfur cycling obtained from CROMO wells QV1.1, QV1.2, N08-B, CSWold, and Lost City locations H08 and 3862, confirm that organisms have the biochemical capacity to cycle sulfur and actively generate transcripts for four key metabolic processes: sulfate reduction, sulfide oxidation, thiosulfate disproportionation, and thiosulfate oxidation.

In addition to high concentrations of sulfate coupled to a thermodynamic incentive to metabolize sulfate as an electron acceptor, 16S rRNA sequences of known sulfate cycling Clostridia members *Dethiobacter*, *Desulfitispora, Family XIV, and Candidatus 'Desulforudis'* positively correlate with depth and specific conductance in the CROMO fluids (Table 6). *Dethiobacter* also significantly correlated with increasing pH. The clear relationships defined above indicate the deeply-sourced dilute seawater has in important role in controlling community composition. The sulfate- reducing '*Candidatus Desulforudis'*, isolated from the Mponeng gold mine in South Africa

(Chivian et al., 2008), is similarly abundant in the deepest well, CSWold, where elevated concentrations of hydrogen and sulfate are measured in addition to dilute seawater chemistries. Functional genes related to facilitating the complete dissimilatory sulfate reduction pathway to sulfide, *sat, aprAB, and dsrAB* were identified in all four CROMO wells analyzed, and in both Lost City locations, H08 and 3862 (Fig. 4). The phylogeny of *dsrA*,*B* (Fig. 5) illustrates the abundance of organisms capable of sulfate reduction in both marine and terrestrial serpentinites, while also highlighting the complexity associated with interpreting the phylogeny of this gene. Organisms in the serpentinite subsurface are actively contributing to producing concentrations of aqueous sulfide in the groundwater, as transcripts for the synthesis of sulfate reducing genes at CROMO were identified in comparable normalized-abundances to their respective genes. Pairwise Pearson's correlation analyses between amplicon sequence variants (ASVs) and aqueous chemical compounds reveal positive correlations between hydrogen sulfide and the Betaproteobacteria and Erysipelotrichaceae groups at CROMO, and *Dethiobacter alkaliphilus* is positively correlated with pH. Methylocystaceae, a family capable of consuming methane to obtain energy, and Fusibacter, are positively correlated with hydrogen gas, and the Type I methanotrophs, Methylococcaceae are positively correlated with SRB-2 (Clostridia). This indicates important relationships exist not only between microbes and environmental parameters, but also between groups of microbes capable of metabolizing different compounds.

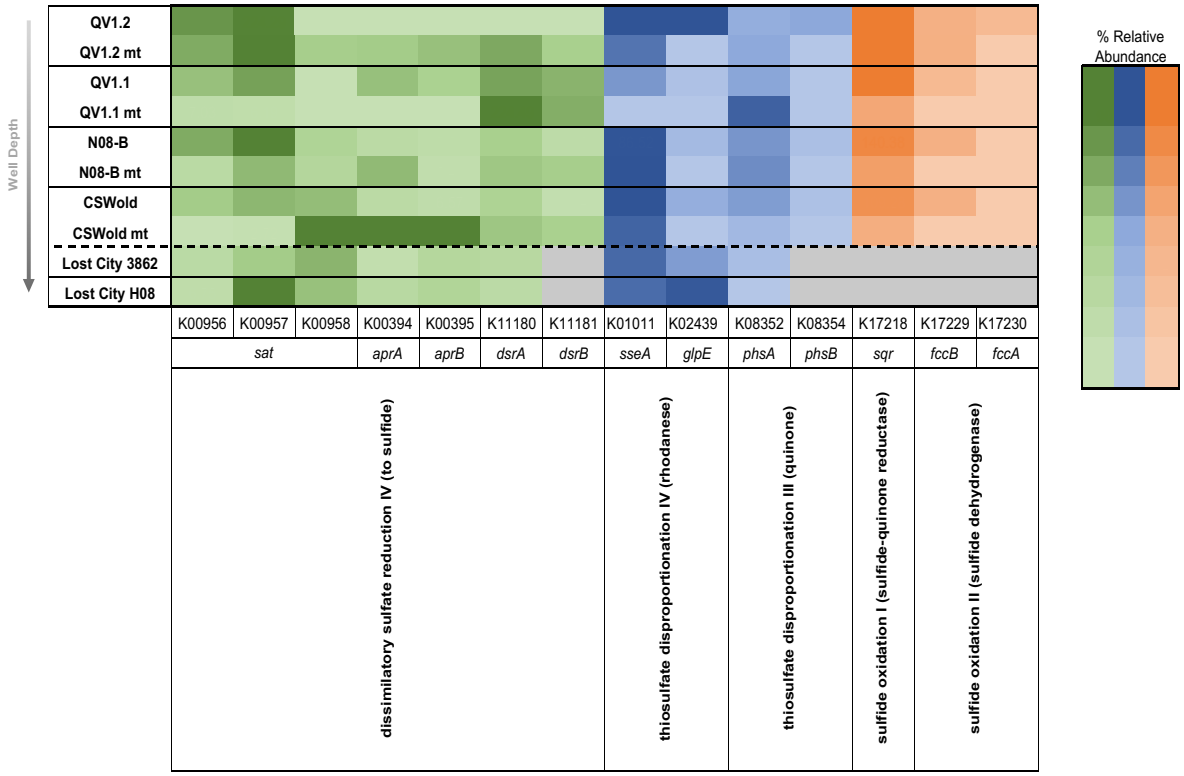

Figure 4 - Sulfur Cycling Genes and Transcripts. KEGG accessions and genes associated with various sulfur metabolic pathways (dissimilatory sulfate reduction IV, thiosulfate disproportionation IV, III, sulfide oxidation I,II) are listed on the x-axis. Lost City Hydrothermal Field and CROMO metagenome fragments per kilobase of predicted protein sequence per million mapped reads are listed on the y axis. Metatranscriptomes are listed beneath the metagenome abundance for each well using the abbreviation, mt. The color intensity relates to the percent relative abundance of that particular gene or transcript (100%: darkest color; 0% lightest color), and grey fill indicates no sequences were observed meeting the given criteria. The heat map depicts the average percentage of annotated proteins of each cluster belonging to each functional category. Table 5 in Appendix A lists additional metagenomic data for wells without matching transcript data.

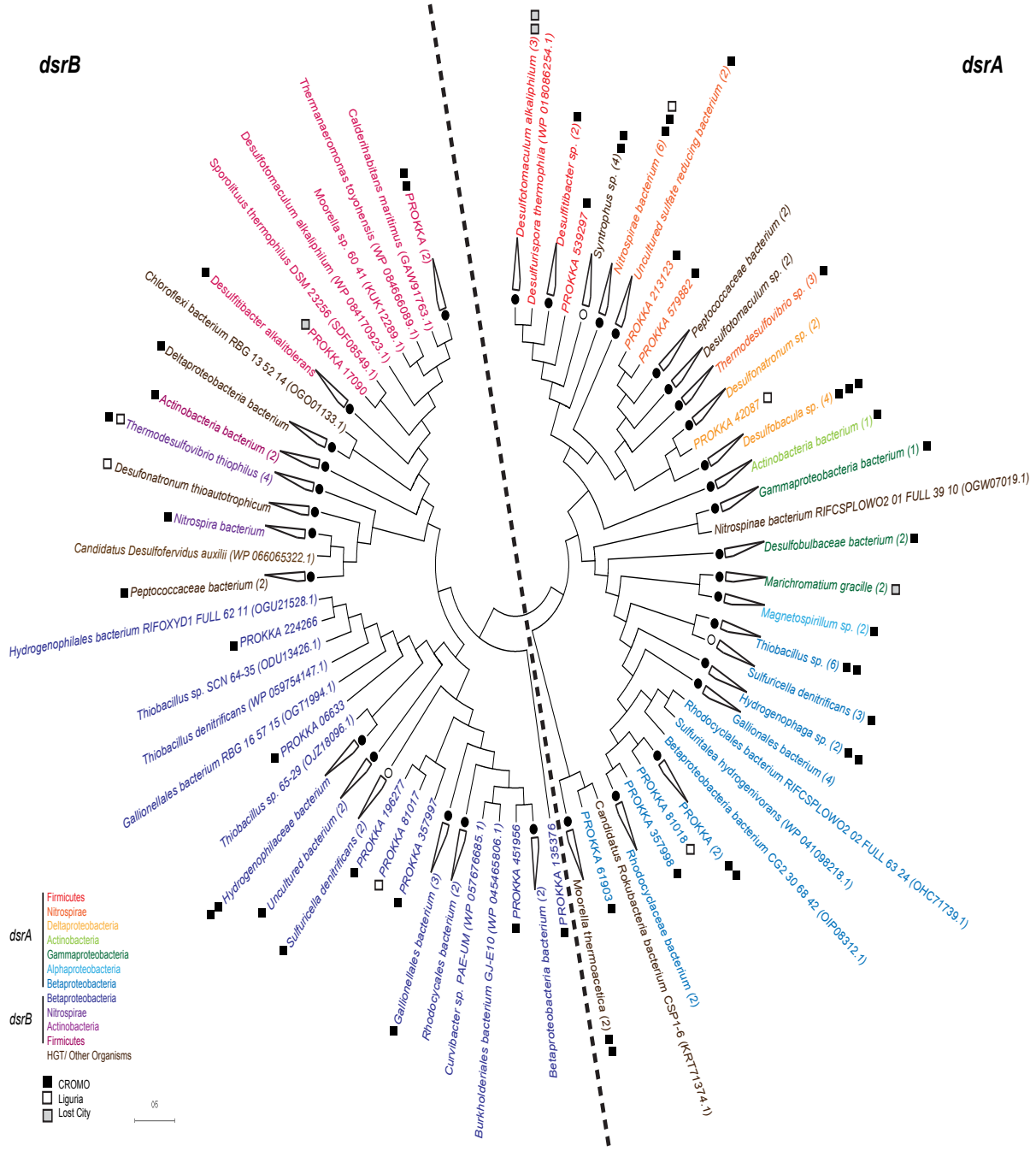

Figure 5 - DsrA,B Phylogenetic Tree. A maximum likelihood phylogenetic tree (bootstrap=1000) was constructed in MEGA6 with a cutoff value of 50% after aligning sequences in ClustalOmega (158 sequences). The relationships between CROMO (black squares), Lost City (grey squares), and Liguria (white squares) organisms and NCBI BLASTp reference organisms are represented here. Clusters were collapsed where a relationship greater than 80% (open circles), or greater than 90% (closed circles) was identified. Parentheses next to reference organism names indicate the number of that genus in the collapsed cluster. Number of squares after genus names represent amount of site-specific protein sequences identified in the respective collapsed cluster.

The Lost City Hydrothermal Field hosts biogeochemical patterns where microbial sulfate reduction impacts concentrations of sulfate, sulfide, and hydrogen across the area (Proskurowski et al., 2008; Lang et al., 2012). Organisms such as *Desulfotomaculum alkaliphilum* and *Desulfotomaculum halophilum* have been identified (Brazelton et al., 2006; Gerasimchuk et al., 2010) and, as evidenced by metagenomic data for H08 and 3862 locations, can reduce sulfate and disproportionate thiosulfate (Fig. 4). Functional gene abundance for the sulfate reduction pathway in Lost City organisms is most comparable to the deepest well, CSWold, at CROMO.

Sulfide oxidation is similarly an exergonic process at CROMO, though much less so compared to reactions involving sulfate reduction. The sulfide oxidation I pathway containing the sulfide-quinone reductase enzyme, as identified in the MetaCyc database (Caspi et al., 2014), is the dominant pathway by which organisms metabolize sulfide at CROMO (Fig. 4). The sulfide oxidation II and sulfide dehydrogenase enzyme is strikingly less abundant (<10% relative abundance in all wells; Fig. 4). *Chlorobia*, a salt tolerant sulfur oxidizing bacteria, is found in almost every well and *Thiomicrospira*, a strictly aerobic sulfur oxidizing bacteria (Sorokin et al., 2006) is present predominantly in the shallowest wells. A striking complication to biogenic sulfur cycling recently discovered in *Desulfurivibrio alkaliphilus* reveals the activation of the genes related to sulfate reduction while facilitating the oxidation of sulfide (Thorup et al., 2017). Further, while it might be expected that the shallowest well considered in metagenome and metatranscriptome data analysis, QV1.2, would demonstrate the highest total free energy yield and also the highest gene and transcript abundance as it hosts the most circumneutral chemistries, it strikingly indicates very little free energy yield for this

reaction involving either oxygen or nitrate reduction, and similarly, CSWold shows the fewest genes and transcripts related to sulfide oxidation, yet the free energy available for this reaction is much higher than the remaining wells. This result indicates kinetics of these reactions have an important role in this system, organisms at CROMO may not be actively oxidizing sulfide to sulfate at rates representative of transcript abundance or free energy yield, microbes may be facilitating a reverse reaction through their sulfur-related genes, or that microbes may be utilizing intermediate sulfur species more than previously considered.

Though it is evident serpentinite-hosted organisms are capable of performing redox reactions involving sulfate and sulfide, strikingly, thiosulfate is a prominent contributor to the biogeochemical transformation and metabolic availability of sulfur in both CROMO and Lost City waters. The *sseA* and *glpE* genes encoding for thiosulfate disproportionation to thiocyanate and sulfite via rhodanese are detected in all wells (Fig. 4). The *sseA* gene is actively transcribed on multiple contigs most frequently in the two deepest wells, CSWold and N08-B, though it is ubiquitous throughout CROMO (Fig. 4). Metagenomic (PhyloPythiaS+) data indicate production of *sseA* in the methanotroph, *Methylomonas* (Gammaproteobacteria). Interestingly, Truepera, from the extremely radioresistant Deinococcales Phyla, dominates the CSW1.1 community, as evidenced by 16S rRNA results, and has the genetic framework necessary to synthesize both the *sseA* and *phsA,B* genes, which may indicate this group plays a key role in the transformation of thiosulfate to sulfide. Truepera were positively correlated to acetate, formate, and lithium concentrations in the Pearson correlation coefficient analysis.

Thiobacillus denitrificans is an organism found collectively throughout the CROMO groundwaters and can facilitate sulfate reduction, sulfide oxidation, and thiosulfate disproportionation, and is also known to be capable of thiosulfate oxidation (Beller et al., 2006). Similarly, the *Dechloromonas aromatica* genome encodes for the disproportionation of thiosulfate and the reduction of sulfate to sulfide through the entire suite of sulfate reduction genes (*dsrAB*, *aprAB*, and *sat*).

The abundance and diversity of sulfur cycling organisms implicates the key function of sulfur metabolisms in energy-limited serpentinite groundwaters. Thiosulfate metabolisms, in particular, may be increasingly utilized in fluids influenced by mixing of water sources, such as those where high sulfate concentrations in the deep seawater source and dissolution of evaporite minerals can interact with meteoric waters and the highly reducing fluids from serpentinization. This work brings to light the previously overlooked role thiosulfate metabolisms can have in both an active marine serpentinizing system and an ancient seawater-influenced ophiolitic serpentine environment.

Methods

Aqueous Geochemistry

All CROMO wells (CSW, QV, N08) were sampled for their biogeochemistry in July 2014. Fluids were pumped from discrete depths via positive displacement Teflon bladder pumps (Geotech Environmental Equipment, Denver, CO, USA) to the surface, where they were flushed through a YSI 3059 flow cell attached to a digital YSI multiprobe (Yellowsprings, OH, USA) for pH, ORP, dissolved oxygen (DO), specific

conductance, and temperature measurements once DO stabilized. Fluids were collected via tubing attached directly to the flow cell, which allowed syringes to directly sample water pumped anoxically from the well bottom. Aqueous samples were preserved for anion (Br^-, Cl^-, NO_2^-, NO_3^-, and SO_4^{2-}) and cation (Ca, Na, Mg, K, Fe, Li, Si) analysis as described below, and dissolved gas (CH_4, CO, H_2), organic acid (acetate, lactate, propionate, formate), and dissolved inorganic carbon (DIC) quantification according to previously published protocols in Crespo-Medina et al., (2014) and Twing et al., (2017).

Well water was pumped and immediately filtered through a 0.22 μm Sterivex syringe filter (Millipore, Billerica, MA, USA) into sterile 15 mL Falcon tubes (Fisher Scientific) and stored at 4ºC. Anions were measured using a Dionex ICS-2100 Ion Chromatography System (ThermoScientific), generating data for the concentrations of chloride (limit of detection (LOD) 0.02 mg/L, uncertainty 2.7%), nitrite (LOD 0.1 mg/L, uncertainty 3.15%), nitrate (LOD 0.1 mg/L, uncertainty 2.2%), bromide (LOD 0.1 mg/L, uncertainty 4.0%), fluoride (LOD 0.02 mg/L, uncertainty 6.5%), and sulfate (LOD 0.15 mg/L, uncertainty 0.41%).

Hydrogen sulfide concentrations were determined via colorimetry according to previously published protocols for the methylene blue method (Cline, 1969; Joye et al., 2004; Weber et al., 2016). Fluid samples (45mL) from each well were preserved immediately in the field using 600 μL of a 20% zinc acetate solution to preserve volatile sulfide in the form of solid zinc sulfide. In the laboratory, solutions were vortexed and 1.2 mL aliquots of this solution were placed into individual 2 mL centrifuge tubes in triplicate (Sigma-Aldrich). Prior to analysis, 0.096 μL of the appropriate diamine reagent

for sulfide concentration in the sample (0-3 μM, 3-40 μM, 40-250 μM, or 250-1000 μM) was added to each tube to develop the characteristic blue color. Standard curves were created for the range of each diamine reagent using the same method of preservation and stock solutions of hydrogen sulfide. Stock solutions were generated by dissolving 1.2 mg and 12 mg of sodium sulfide anhydrous (FisherScientific; for 50 uM and 500 uM stocks respectively) into sterile serum bottles (Wheaton Industries, Inc., Millville, NJ, USA) filled with 100 mL of 18 mΩ water and fitted with a 20mm thick blue butyl stopper (Chemglass Life Sciences, Vineland, NJ) in a COY anaerobic chamber (COY Lab Products, Grass Lake, MI, USA) with 80:20 H_2:N_2 gas headspace. These stock solutions were then transferred to new clean, sterile serum vials capped in the COY chamber and filter sterilized using a 0.22 μm syringe filter. Once the appropriate reagent was added to these samples and standards, the tubes were quickly vortexed to mix and let stand for 20 minutes in order to develop the methylene blue color and surpass the inhibition stage created by thiosulfate, as described by Cline (1969). After this allotted time, samples and standards were immediately run in parallel to an 18 mΩ water, 0.22 μm syringe filtered, zinc acetate-preserved, 0-3 μM diamine-reacted blank on an Ultraviolet-1800 Shimadzu UV spectrophotometer at 670 nm wavelength at Michigan State University.

Cations were preserved by addition of 600 μL of a 20% zinc acetate solution to 45 mL of sample water and stored at 4ºC in order to preserve volatile H_2S and obtain an accurate value for aqueous sulfur. These values obtained are comparable to CROMO samples preserved in nitric acid (Sabuda, Cardace, unpublished data). Cation samples were sent to the Analytical Geochemistry Laboratory at the University of New Mexico for

analysis and immediately run using an Inductively Coupled Plasma Optical Emission Spectrometer (ICP-OES).

Gibbs Free Energy Calculations

Free energy values for 16 energy-yielding reactions involving the various states of sulfur speciation (Table 4) were calculated using the measured cation, anion, organic acid, and dissolved gas concentrations (Table 1). Conservative approximations of formate, acetate, and thiosulfate were used in the calculations as data were available for only some components of the fluid. Speciation calculations were performed to determine activities of dissolved species for each sample location fluid in the modeling software Geochemist's Workbench© (Aqueous Solutions LLC, Champaign, IL) with the SUPCRT92 (Johnson et al., 1992) package. Using the equation:

$$\Delta G^0 = \Delta G_r^0 + RT\ln Q \qquad (1)$$

ΔG^0 is the Gibbs energy of reaction (J/mol), ΔG_r^0 is the standard Gibbs energy (J/mol), R is the universal gas constant (J/mole*K), T is the temperature in Kelvin, and Q is the reaction quotient of the compounds involved in the respective reaction. The reaction quotient was calculated using the activities established by the fluid speciation models. ΔG_r^0 values for the selected reactions were cited from the work of Amend & Shock, 2001. These were then used in the given equation to calculate a total ΔG (J/L) for the respective reaction and factored in the concentration of the limiting reactant (McCollom and Shock, 1997).

Microbial Cell Enumeration

Unfiltered well fluids containing microbial cells were collected in 50 mL Falcon tubes, preserved in 3.7% formaldehyde, and kept at 4°C. In lab, this water was filtered onto 0.22 μm black polycarbonate filters (Millipore, Billerica, MA, USA), stained with 1 μg/mL of 4',6-diamidino-2-phenylindole (DAPI), and analyzed using epifluorescence microscopy using previously published protocols (Hobbie et al., 1977; Schrenk et al., 2003).

Extraction of DNA and RNA

In concert with aqueous geochemistry and cell enumeration preservations, four liters of well fluids were pumped from each well bottom and immediately filtered through respective Sterivex 0.2 μm filter cartridges (Millipore, Billerca, MA) using a portable peristaltic pump. Cartridges were kept on ice during filtration, immediately stored in liquid nitrogen upon completion, shipped to the home laboratory, and stored at -80˚C until processing. Total genomic DNA extractions were completed as previously described by Brazelton et al., (2017), Crespo-Medina et al., (2017) and Twing et al., (2017) and briefly described here. Freeze/thaw cycles and lysozyme/Proteinase K treatment were performed to lyse cells, followed by purification with phenol-chloroform, precipitation using ethanol, and purification using QiaAmp (Qiagen, Hilden, Germany) columns according to manufacturer instructions. A Qubit 2.0 fluorometer (ThermoFisher) was used to quantify extracted DNA using a Qubit® dsDNA High Sensitivity Assay kit.

Extractions for RNA were performed as described in MacGregor et al., 1997 and Lin et al., 1995 with slight modifications. Briefly, frozen 0.2 μm Sterivex filter cartridges were broken open, cut into four equal pieces, and divided into two screw-cap Eppendorf tubes containing phenol, 20% sodium dodecyl sulfate, 5× low-pH buffer, and 0.2 to 0.5g baked zirconium beads. Samples were bead beaten for 3 minutes, heated in a 60°C water bath for 10 minutes, bead beaten again for 3 minutes, and centrifuged at 4°C and 14,000 rpm to separate phases. Supernatant was transferred to a fresh Eppendorf tube and chilled. 1× low-pH buffer was added to remaining sample in tube, and bead beating was repeated. Supernatants were combined and phenol, 1:1 phenol: chloroform, and chloroform were added in series with vortex and centrifugation in between. Between steps, aqueous phases were transferred to clean Eppendorf tubes. The final aqueous phase was transferred to a clean Eppendorf tube with additions of ammonium acetate, isopropanol, and magnesium chloride before vortex and incubation at -20°C overnight. Samples were centrifuged for 30 minutes at 4°C, washed with ethanol, and dried under vacuum before suspension in RNase-free water and storage at -80°C until analyzed.

Bacterial 16S rRNA Amplicon Sequencing, and Data Analysis

Purified samples were submitted to the Genomics Core Facility at Michigan State University for processing using an Illumina MiSeq instrument. The V4 region of the 16S rRNA gene (515F/806R primers) was amplified using dual indexed Illumina fusion primers (Kozich et al., 2013). An Invitrogen SequalPrep DNA Normalization Plate was then used to normalize and pool the products. The pool was then loaded on an Illumina MiSeq v2 flow cell and sequenced using a standard 500 cycle reagent kit after library

quality control and quantitation was performed. Illumina Real Time Analysis (RTA) software v1.18.54 performed base calling. The RTA output was demultiplexed and converted to FastQ files using Illumina Bcl2fastq v1.8.4.

USEARCH 8 (Edgar et al., 2010) was then used to filter and merge paired-end sequence reads. Additional quality filtering was performed to remove sequences with ambiguous bases and more than 8 homopolymers using mothur (Schloss et al., 2009), and chimaeras were removed with mothur's implementation of UCHIME (Edgar et al., 2011). The sequences were pre-clustered with the mothur command pre.cluster (diffs=1), which reduced from 362,039 to 211,847, which removes rare sequences most likely created by sequencing errors (Schloss et al., 2011).

Sequences were aligned to the SILVA SSURef alignment (v119), and taxonomic classifications were assigned using mothur (Pruesse et al., 2007; Schloss et al., 2009), as described in Twing et al., 2017. Rather than binning sequences into Operational Taxonomic Units (OTUs) at the 3% distance threshold as was performed for the results of Twing et al., 2017, amplicon sequence variants (ASVs) for July 2014 CROMO sequences were utilized. ASVs can provide taxonomic resolution to single-nucleotide differences over the sequenced gene area while maintain sequence identities that stand independently from a specific reference database (Callahan et al., 2017). The SV's were normalized to the total number of reads for each sample. Following this, normalized SV values were averaged for wells that had more than one representative sample to negate statistical issues related to psuedoreplication (Kuhar, 2006). The data were then filtered to retain SVs that made up greater than one percent of any given sample which resulted in eighty-two unique SVs to be used for statistical analyses. The

resulting eighty-two SVs were combined into a data table along with geochemical data collected during sampling to analyze relationships between abundant species and environmental parameters.

A two-tailed Pearson correlation coefficient matrix was computed with the rcor.test function in the R package ltm (Rizopoulos, 2006) using 16S rRNA relative ASV data and aqueous chemical data for all CROMO wells. The list of *p*-values from this test was converted into a matrix and the false discovery rate (*q*-value) was calculated for each *p*-value within the matrix. Correlation coefficients were filtered to remove values that did not have *p*- and *q*-values of 0.05 or less in order to remove insignificant correlations. Pairwise correlations that fit these criteria were included in further analyses and used to guide investigations between environmental parameters and specific ASVs.

Metagenomic Sample Preparation, Sequencing, and Data Analysis

Samples were submitted to the Joint Genome Institute (JGI) for bacterial metagenomic and metatranscriptomic sequencing on an Illumina HiSeq2000 instrument and assembled as described by Hawley et al., 2014, and briefly described here. Archaea were not assessed here due to prior determination that this domain is notably absent from CROMO well fluids (Twing et al., 2017). A Corvaris LE220 focused-ultrasonicator was used to shear DNA samples into 270 bp fragments and size selection was performed using SPRI. Base pair fragments were end-repaired, A-tailed, and ligated with Illumina- compatible adapters with barcodes unique for each library. KAPA Biosystem's next-generation sequencing library qPCR kit and Roche LightCycler 280 RT PCR instrument were used to quantify libraries. 10-library pools were assembled

and prepared for Illumina sequencing in one lane each. Clustered flowcells were produced using a TruSeq paired-end cluster kit (v3) and Illumina's cBot instrument. The Illumina HiSeq2000 instrument was utilized with a TruSeq SBS sequencing kit (v3) and a 2 × 150 indexed run recipe to sequence the samples. A minimum quality score cutoff of 10 was used to trim raw reads, and SOAPdenovo v1.05 was utilized to assemble the trimmed paired-end reads. Processing and analysis of metagenomic data is described in detail by Brazelton et al., 2017, and briefly described here. Preprocessing of the sequencing data was performed by trimming reads with 5' contaminants, and replicate sequences were discarded. 3' adapters were then trimmed from reads, and reads were again trimmed based on quality and filter by length. Contaminants were then discarded, artificial replicates removed, adapters trimmed, and reads were quality trimmed.

PhyloSift v.1.0.1 (Darling et al., 2014) was used to assign phylogenetic affiliations to the quality checked, unassembled pairs. Assembly of metagenomes was executed with Ray Meta v.2.3.1 (Boisvert et al., 2012), and short-reads were mapped to the assembly using Bowtie2 v.2.2.6 (Langmead & Salzberg, 2012). Prokka v.1.12 (Seeman, 2014) to determine that Prodigal v2.6.2 (Hyatt et al., 2010) should be used to predict genes.

BLASTP v.2.3 was utilized to annotate the Kyoto Encyclopedia of Genes and Genomes (KEGG; Ogata et al., 1999) to predicted protein-coding sequences, and the default databases in Prokka were aligned to remaining un-annotated protein-coding sequences. HTSeq v.0.6.1 was used to calculate predicted protein abundances (Anders, Pyl & Huber, 2015), and the abundance of predicted protein functions in all CROMO metagenomes and metatranscriptomes were normalized to metagenome size.

Data reported here are in units of metagenome fragments per kilobase of predicted protein sequence per million mapped reads. The current version of the KEGG online database lacks orthologies for the thiosulfate disproportionation I and II pathways annotated in MetaCyc, and for that reason are not included in this discussion.

All Prokka-predicted coding sequences (CDSs) on the contigs of interest were aligned against the NCBI NR database (v. 2017-06-07) using the top two BLAST Protein hits for each predicted gene to assign taxonomy. Predicted protein sequences and their respective top two BLAST hits were aligned using Clustal Omega (Sievers et al., 2011) to produce a FASTA file for use in creation of phylogenetic trees. Maximum Likelihood Trees were assembled using a reference tree created by NJ/BioNJ in MEGA6 with the Jones-Taylor-Thornton Model and a Bootstrap Phylogeny Test with 1000 replications (Tamura et al., 2013). A bootstrap cutoff value of 50% was utilized, and clusters were assembled when a relationship greater than 80% (open circles on Fig. 5), or greater than 90% (closed circles) was identified.

APPENDIX

Table 1 - CROMO July 2014 Aqueous Geochemistry

Well	Well depth (m)	pH	T (℃)	Cond. (µS)	DO (mg/L)	ORP (mV)	Br^-	Cl^-	F^-	NO_2^-	NO_3^-	SO_4^{2-}	HS^-	Ca^{2+}	Na^+	Mg^{2+}	K^+	Mn^{2+}	Fe	Sr	H_2	CO	CH_4	DIC
CSW1.4	8.80	7.75	15.05	1950	2.36	116	46.93	9622.33	13.69	< 1.45	2.58	391.94	0.10	782.73	16082.76	826.37	118.21	<3.14	81.09	3.60	0.29	0.16	3.66	3870.12
N08-C	13.70	8.46	15.53	1372	0.42	-153	46.06	7556.82	14.21	< 1.45	13.87	51.22	0.10	487.88	11027.28	176.01	179.17	<3.14	23.98	6.07	0.26	0.04	1.13	674.65
QV 1.2	14.90	9.47	17.09	3042	0.40	-143	106.00	28676.00	11.58	< 1.45	< 1.61	32.00	0.10	559.39	26113.34	23.03	156.86	<3.14	52.95	5.13	0.49	0.17	263.77	682.16
CSW1.2	19.20	7.76	15.97	4495	0.25	-119	83.60	32994.62	18.95	78.99	< 1.61	191.65	0.10	772.23	38690.27	26.80	287.44	<3.14	14.92	10.34	0.18	0.11	783.87	1238.59
CSW1.1	19.50	12.32	16.31	4453	0.43	-297	30.79	1956.11	26.84	< 1.45	< 1.61	266.19	12.88	706.47	18847.22	3.13	1111.17	<3.14	46.01	22.70	0.79	0.18	593.90	192.00
QV 1.1	23.00	11.51	17.52	2854	0.28	-234	60.20	16172.67	16.32	< 1.45	< 1.61	257.13	4.76	1978.56	17840.16	3.13	967.73	<3.14	34.78	13.53	0.25	0.12	286.46	45.43
CSW1.3	23.20	10.15	15.64	4842	0.16	-205	94.61	39610.63	11.58	< 1.45	< 1.61	151.16	0.10	808.86	40831.81	3.13	307.55	<3.14	17.18	10.55	2.89	0.11	1138.16	254.95
N08-B	26.20	10.68	16.12	3132	0.76	-198	65.70	23610.94	15.26	< 1.45	< 1.61	27.69	0.10	1139.10	25520.89	3.13	237.87	<3.14	74.44	17.96	0.09	0.06	303.20	28.04
CSW1.5	27.40	9.77	15.80	4792	0.16	-285	94.49	40001.66	14.74	< 1.45	< 1.61	317.41	23.75	926.67	42202.20	3.13	332.29	<3.14	54.90	15.05	0.38	0.16	1075.03	438.78
QV 1.3	34.60	9.68	16.60	6507	0.26	-224	142.92	74557.95	17.90	< 1.45	< 1.61	55.69	10.13	1694.40	51677.62	9.15	333.49	<3.14	32.66	45.96	0.17	0.11	1281.63	593.43
N08-A	39.60	10.89	16.85	6335	0.09	-250	109.38	54610.27	12.63	< 1.45	< 1.61	40.18	1.14	3194.94	51245.33	3.13	450.21	<3.14	38.88	86.04	0.08	0.07	1268.96	55.77
CSW OLD	76.20	9.73	17.43	11529	0.26	-280	166.45	81853.64	15.79	< 1.45	< 1.61	139.29	8.39	1660.11	73939.94	3.13	540.29	<3.14	47.86	38.89	0.15	0.25	1316.97	44.24

Anions, cations, and dissolved gases are reported in micromolar concentrations

Gases are reported as concentration dissolved in fluid

T = temperature; Cond = conductivity; DO = dissolved oxygen ; ORP = oxidation reduction potential; DIC = dissolved inorganic carbon

Table 2 - Terrestrial Serpentinizing Systems Selected Water Chemistry Parameters

Site Name	Well/ Specific Name	Conductivity (µS/cm)	pH	SO_4^{2-} (µM)	Cl^-(µM)	Na^+(µM)	References
CROMO, California, USA	CSW 1,1	4453.00	12.32	266.19	1956.11	18847.22	This Work
CROMO, California, USA	CSW 1,2	4495.00	7.76	191.65	32994.62	38690.27	This Work
CROMO, California, USA	CSW 1,3	4842.00	10.15	151.16	39610.63	40831.81	This Work
CROMO, California, USA	CSW 1,4	1950.00	7.75	391.94	9622.33	16082.76	This Work
CROMO, California, USA	CSW 1,5	4792.00	9.77	317.41	40001.66	42202.20	This Work
CROMO, California, USA	CSW OLD	11529.00	9.86	139.29	81853.64	73939.94	This Work
CROMO, California, USA	N-08 A	6335.00	10.89	40.18	54610.27	51245.33	This Work
CROMO, California, USA	N-08 B	3132.00	10.68	27.69	23610.94	25520.89	This Work
CROMO, California, USA	N-08 C	1372.00	8.46	51.22	7556.82	11027.28	This Work
CROMO, California, USA	QV 1,1	2854.00	11.51	257.13	16172.67	17840.16	This Work
CROMO, California, USA	QV 1,2	3042.00	9.47	32.00	28676.00	26113.34	This Work
CROMO, California, USA	QV 1,3	6507.00	9.68	55.69	74557.95	51677.62	This Work
Oman	Yellowstone du pauvre	2700.00	10.10	349.00	21052.00	22086.00	Chavagnac et al., 2013
Oman	Yellowstone du pauvre	2210.00	11.90	15.00	9844.00	10740.00	Chavagnac et al., 2013
Oman	Little Grand Canon	1730.00	11.80	5.00	6091.00	6261.00	Chavagnac et al., 2013
Oman	Little Grand Canon	1690.00	11.70	1.00	5701.00	5939.00	Chavagnac et al., 2013
Oman	Izki les 2 puits	810.00	7.80	71.00	5136.00	7647.00	Chavagnac et al., 2013
Oman	Izki les 2 puits	920.00	11.20	28.00	5464.00	5373.00	Chavagnac et al., 2013
Oman	Le partage du midi	2250.00	11.70	3.00	10301.00	11965.00	Chavagnac et al., 2013
Oman	Lac bleu de Bahla	780.00	10.80	179.00	5215.00	5412.00	Chavagnac et al., 2013
Oman	Rustaq	980.00	8.20	812.00	4007.00	5489.00	Chavagnac et al., 2013
Oman	La poule au pot	1870.00	11.30	45.00	11027.00	10094.00	Chavagnac et al., 2013
Oman	L'ane blanc	1360.00	7.90	2433.00	5327.00	6446.00	Chavagnac et al., 2013
Oman	Two shoes	1480.00	11.60	40.00	4511.00	6581.00	Chavagnac et al., 2013
Oman	Two shoes	1480.00	11.60	41.00	3009.00	6691.00	Chavagnac et al., 2013
Oman	Irma (Yellowstone du pauvre)	2540.00	10.50	44.00	11154.00	18311.00	Chavagnac et al., 2013
Oman	Irma (Yellowstone du pauvre)	2540.00	10.50	46.00	11632.00	18579.00	Chavagnac et al., 2013
Oman	Irma (Yellowstone du pauvre)	2650.00	9.90	48.00	12752.00	20366.00	Chavagnac et al., 2013
Oman	Irma (Yellowstone du pauvre)	2650.00	9.90	48.00	12926.00	20304.00	Chavagnac et al., 2013
New Caledonia	La Coulee 1	n.r.	10.80	7.81	628.57	634.78	Barnes et al., 1978
New Caledonia	La Coulee 2	n.r.	10.70	60.38	465.71	1134.78	Barnes et al., 1978
Liguria, Italy	Fiorino village	n.r.	9.50	12.60	600.00	570.00	Chavagnac et al., 2013
Liguria, Italy	Fiorino village	n.r.	9.50	11.20	600.00	580.00	Chavagnac et al., 2013
Liguria, Italy	Rio Dellecave	n.r.	6.70	31.80	130.00	110.00	Chavagnac et al., 2013
Liguria, Italy	Acquasanta	n.r.	11.70	3.30	450.00	1260.00	Chavagnac et al., 2013
Liguria, Italy	Acquasanta	n.r.	11.70	3.00	450.00	1270.00	Chavagnac et al., 2013
Liguria, Italy	Acquasanta	n.r.	11.70	3.40	450.00	1270.00	Chavagnac et al., 2013
Liguria, Italy	Ponte Arma	n.r.	9.50	32.80	560.00	450.00	Chavagnac et al., 2013
Liguria, Italy	Rio Leone	n.r.	11.30	19.20	650.00	550.00	Chavagnac et al., 2013
Liguria, Italy	Rio Leone	n.r.	11.30	16.70	640.00	550.00	Chavagnac et al., 2013
Liguria, Italy	Rio Leone	n.r.	11.30	7.50	550.00	430.00	Chavagnac et al., 2013
Liguria, Italy	Rio Leone	n.r.	11.30	5.00	550.00	430.00	Chavagnac et al., 2013
Liguria, Italy	Rio Branega	n.r.	11.50	0.60	500.00	1050.00	Chavagnac et al., 2013
Liguria, Italy	Rio Branega	n.r.	11.50	0.50	500.00	1040.00	Chavagnac et al., 2013
Liguria, Italy	Gorzente (lago Lavagnina)	n.r.	11.20	10.50	220.00	280.00	Chavagnac et al., 2013
Liguria, Italy	Gorzente (lago Lavagnina)	n.r.	11.20	10.40	220.00	280.00	Chavagnac et al., 2013
Liguria, Italy	Gorzente (lago Lavagnina)	n.r.	11.50	0.80	220.00	300.00	Chavagnac et al., 2013
Liguria, Italy	Gorzente (lago Lavagnina)	n.r.	11.20	1.20	310.00	410.00	Chavagnac et al., 2013
Liguria, Italy	Gorzente	n.r.	11.60	1.40	420.00	850.00	Chavagnac et al., 2013
Liguria, Italy	Gorzente	n.r.	11.60	1.30	420.00	860.00	Chavagnac et al., 2013
Liguria, Italy	Maddalena (Don Orione)	n.r.	11.10	23.60	420.00	740.00	Chavagnac et al., 2013
Liguria, Italy	Maddalena (Don Orione)	n.r.	11.10	23.80	420.00	740.00	Chavagnac et al., 2013
Genova Province, Italy	V18	n.r.	11.37	42.68	n.r.	n.r.	Cipolli et al., 2004
Genova Province, Italy	BR1	n.r.	11.86	1.46	n.r.	n.r.	Cipolli et al., 2004
Genova Province, Italy	L43	n.r.	11.52	4.58	n.r.	n.r.	Cipolli et al., 2004
Genova Province, Italy	S70	n.r.	11.42	190.51	n.r.	n.r.	Cipolli et al., 2004
Genova Province, Italy	C11	n.r.	10.50	263.38	n.r.	n.r.	Cipolli et al., 2004
Genova Province, Italy	A1	n.r.	11.57	133.25	n.r.	n.r.	Cipolli et al., 2004
Genova Province, Italy	V18	n.r.	11.37	42.68	11700.00	16600.00	Cipolli et al., 2004
Genova Province, Italy	BR1	n.r.	11.86	1.46	21700.00	23700.00	Cipolli et al., 2004
Genova Province, Italy	L43	n.r.	11.52	4.58	18600.00	28300.00	Cipolli et al., 2004

Table 2 (cont'd)

Cyprus Ophiolite	10.00	n.r.	8.50	22.59	200.00	143.04	Neal & Shand 2002
Cyprus Ophiolite	11.00	n.r.	7.90	25.61	228.57	176.52	Neal & Shand 2002
Cyprus Ophiolite	12.00	n.r.	8.60	31.86	257.14	205.65	Neal & Shand 2002
Cyprus Ophiolite	6.00	n.r.	9.10	37.89	257.14	203.48	Neal & Shand 2002
Cyprus Ophiolite	7.00	n.r.	9.80	28.21	228.57	191.30	Neal & Shand 2002
Cyprus Ophiolite	8.00	n.r.	8.40	21.65	228.57	172.17	Neal & Shand 2002
Cyprus Ophiolite	9.00	n.r.	8.40	30.09	257.14	224.35	Neal & Shand 2002
Cyprus Ophiolite	5.00	n.r.	8.70	477.83	1285.71	2260.87	Neal & Shand 2002
Cyprus Ophiolite	13.00	n.r.	9.50	154.07	800.00	521.74	Neal & Shand 2002
Cyprus Ophiolite	1.00	n.r.	9.70	244.64	4857.14	7521.74	Neal & Shand 2002
Cyprus Ophiolite	2.00	n.r.	9.70	229.02	4857.14	7739.13	Neal & Shand 2002
Cyprus Ophiolite	21.00	n.r.	9.50	310.22	4000.00	6347.83	Neal & Shand 2002
Cyprus Ophiolite	15.00	n.r.	9.90	2592.13	3314.29	5956.52	Neal & Shand 2002
Cyprus Ophiolite	14.00	n.r.	9.60	2592.13	3314.29	6173.91	Neal & Shand 2002
Cyprus Ophiolite	17.00	n.r.	9.60	2841.97	3714.29	7521.74	Neal & Shand 2002
Cyprus Ophiolite	3.00	n.r.	11.60	4091.19	12000.00	16739.13	Neal & Shand 2002
Cyprus Ophiolite	4.00	n.r.	11.40	1134.71	12000.00	16739.13	Neal & Shand 2002
Cyprus Ophiolite	19.00	n.r.	11.20	2154.90	5428.57	7086.96	Neal & Shand 2002
Cyprus Ophiolite	18.00	n.r.	9.00	36331.46	222857.14	252173.91	Neal & Shand 2002
Cyprus Ophiolite	16.00	n.r.	9.00	26035.81	3714.29	6782.61	Neal & Shand 2002
Cyprus Ophiolite	20.00	n.r.	9.60	11451.18	11428.57	13130.43	Neal & Shand 2002
seawater	-	56000.00	8.00	28107.43	542857.14	456521.74	Culkin and Cox, 1966
Del Puerto	Adobe Springs Well	n.r.	8.73	166.56	137.14	234.78	Blank et al., 2009
Del Puerto	Del Puerto Creek	n.r.	8.52	104.10	271.43	417.39	Blank et al., 2009
New Caledonia	HP11-BdJ-Ilot1-W1C	n.r.	11.08	100.00	2220.00	2380.00	Monnin et al., 2014
New Caledonia	HP11-BdJ-Ilot1-W2	n.r.	10.48	280.00	5470.00	7290.00	Monnin et al., 2014
New Caledonia	HP11-BdJ-Ilot1-W3	n.r.	10.01	1240.00	21610.00	26140.00	Monnin et al., 2014
New Caledonia	HP11-BdJ-Ilot1-W5	n.r.	11.07	10.00	410.00	1280.00	Monnin et al., 2014
New Caledonia	HP11-BdJ-Ilot1-W6	n.r.	10.68	190.00	4020.00	5680.00	Monnin et al., 2014
New Caledonia	HP11-BdJ-Ilot1-W1	n.r.	10.87	70.00	1840.00	2980.00	Monnin et al., 2014
New Caledonia	HP11-BdJ-Dil1	n.r.	10.05	3360.00	52670.00	22630.00	Monnin et al., 2014
New Caledonia	HP11-BdJ-Dil2	n.r.	9.13	11850.00	179270.00	197980.00	Monnin et al., 2014
New Caledonia	HP11-BdJ-Dil3	n.r.	8.66	16090.00	241800.00	284150.00	Monnin et al., 2014
New Caledonia	HP11-BdJ-Dil4	n.r.	10.20	2160.00	34520.00	1910.00	Monnin et al., 2014
New Caledonia	HP11-BdJ-Dil5	n.r.	8.30	21450.00	322050.00	392810.00	Monnin et al., 2014
New Caledonia	HP11-BdJ-Dil6	n.r.	11.00	60.00	1440.00	2550.00	Monnin et al., 2014
New Caledonia	HP11-BdJ-Dil7	n.r.	10.92	20.00	660.00	1650.00	Monnin et al., 2014
New Caledonia	HP11-BdJ-Dil8	n.r.	10.88	20.00	760.00	1750.00	Monnin et al., 2014
New Caledonia	HP11-CarKao-W1	n.r.	10.80	#VALUE!	230.00	650.00	Monnin et al., 2014
New Caledonia	HP11-CarKao-W2	n.r.	10.80	#VALUE!	190.00	580.00	Monnin et al., 2014
New Caledonia	HP11-Site11-W1	n.r.	10.64	1540.00	45780.00	40520.00	Monnin et al., 2014
New Caledonia	HP11-Site11-W4	n.r.	9.58	16160.00	327740.00	270850.00	Monnin et al., 2014
New Caledonia	HP11-Site11-W5	n.r.	8.76	22560.00	451960.00	386580.00	Monnin et al., 2014
New Caledonia	HP11-Site11-W10	n.r.	9.06	15790.00	319180.00	263710.00	Monnin et al., 2014
New Caledonia	HP11-Site11-W11	n.r.	9.38	12130.00	248690.00	199400.00	Monnin et al., 2014
New Caledonia	HP11-Site12-W1	n.r.	11.00	380.00	41740.00	40050.00	Monnin et al., 2014
New Caledonia	HP11-Site12-W3	n.r.	8.92	21500.00	432700.00	384520.00	Monnin et al., 2014
New Caledonia	HP11-Site12-W4	n.r.	9.50	11530.00	247310.00	191240.00	Monnin et al., 2014
New Caledonia	HP11-Site12-W5	n.r.	8.85	21790.00	440030.00	385320.00	Monnin et al., 2014
New Caledonia	HP11-Site12-W6	n.r.	9.34	18200.00	371920.00	323690.00	Monnin et al., 2014
New Caledonia	HP11-Site12-W7	n.r.	8.60	22170.00	447210.00	393220.00	Monnin et al., 2014
New Caledonia	HP11-Site12-W8	n.r.	8.15	25890.00	515390.00	475500.00	Monnin et al., 2014
New Caledonia	HP11-Site7-W1	n.r.	9.73	12240.00	252370.00	190960.00	Monnin et al., 2014
New Caledonia	HP11-Site7-W2	n.r.	9.66	12140.00	250440.00	187730.00	Monnin et al., 2014
New Caledonia	HP11-Site7-W3	n.r.	9.67	10170.00	212430.00	154310.00	Monnin et al., 2014
New Caledonia	HP11-Site7-W4	n.r.	9.61	10820.00	225870.00	167610.00	Monnin et al., 2014
New Caledonia	HP11-Site7-W5	n.r.	9.72	12780.00	262810.00	198080.00	Monnin et al., 2014
New Caledonia	HP11-Site7-W6	n.r.	9.61	14590.00	297380.00	235440.00	Monnin et al., 2014
New Caledonia	HP11-Site7-W3Ti	n.r.	9.44	19950.00	400870.00	346460.00	Monnin et al., 2014
New Caledonia	HP11-Site7-W7	n.r.	10.00	14200.00	290680.00	232610.00	Monnin et al., 2014
New Caledonia	HP11-Site7-W8	n.r.	10.13	10640.00	223030.00	163750.00	Monnin et al., 2014
New Caledonia	HP11-Site7-W9	n.r.	9.91	15190.00	309310.00	249170.00	Monnin et al., 2014
New Caledonia	HP11-Site7-W10	n.r.	10.14	7530.00	163850.00	97320.00	Monnin et al., 2014
New Caledonia	HP11-Site7-W11	n.r.	9.96	14250.00	292430.00	228890.00	Monnin et al., 2014
New Caledonia	HP11-Site9-W1	n.r.	10.45	3310.00	81520.00	36670.00	Monnin et al., 2014

Table 2 (cont'd)

Genova Province, Italy	S70	n.r.	11.42	190.51	23300.00	5500.00	Cipolli et al., 2004
Genova Province, Italy	C11	n.r.	10.50	263.38	23200.00	12800.00	Cipolli et al., 2004
Genova Province, Italy	LER20	n.r.	11.57	133.25	26500.00	12700.00	Cipolli et al., 2004
Genova Province, Italy	BR2	n.r.	11.73	1.04	30500.00	41100.00	Cipolli et al., 2004
Genova Province, Italy	ERR20	n.r.	11.36	32.06	15400.00	16500.00	Cipolli et al., 2004
Genova Province, Italy	GOR34	n.r.	11.68	1.04	17300.00	18500.00	Cipolli et al., 2004
Genova Province, Italy	GOR34A	n.r.	11.55	5.73	15000.00	18300.00	Cipolli et al., 2004
Genova Province, Italy	LER18A	n.r.	11.38	12.28	18900.00	6800.00	Cipolli et al., 2004
Genova Province, Italy	LER2	n.r.	11.11	39.35	19700.00	10300.00	Cipolli et al., 2004
Genova Province, Italy	LER20	n.r.	11.53	15.93	27900.00	12700.00	Cipolli et al., 2004
Genova Province, Italy	LER2I	n.r.	11.49	11.56	23100.00	9900.00	Cipolli et al., 2004
Genova Province, Italy	ORB101	n.r.	10.59	34.77	14700.00	3900.00	Cipolli et al., 2004
Genova Province, Italy	PIO14	n.r.	10.69	17.49	17200.00	53000.00	Cipolli et al., 2004
Genova Province, Italy	S70	n.r.	11.48	22.28	23900.00	5400.00	Cipolli et al., 2004
Genova Province, Italy	V18	n.r.	11.31	47.89	11200.00	16100.00	Cipolli et al., 2004
Genova Province, Italy	GOR35	n.r.	11.44	1.04	8960.00	6700.00	Cipolli et al., 2004
Genova Province, Italy	L43	n.r.	11.55	4.68	20800.00	27700.00	Cipolli et al., 2004
Genova Province, Italy	BR1	n.r.	11.79	2.08	20800.00	23500.00	Cipolli et al., 2004
Genova Province, Italy	BR3	n.r.	11.72	15.62	17400.00	18400.00	Cipolli et al., 2004
Genova Province, Italy	PIO14	n.r.	10.49	26.23	19600.00	53600.00	Cipolli et al., 2004
Genova Province, Italy	GOR36	n.r.	9.95	30.71	46100.00	84000.00	Cipolli et al., 2004
Genova Province, Italy	V99	n.r.	11.28	212.37	97400.00	68100.00	Cipolli et al., 2004
The Cedars, California, USA	NS1	740.00	11.50	1.00	945.00	945.00	Morrill et al., 2013
The Cedars, California, USA	BS5	870.00	11.60	1.00	1490.00	1980.00	Morrill et al., 2013
The Cedars, California, USA	CREEK	3010.00	8.70	8.00	230.00	60.00	Morrill et al., 2013
The Cedars, California, USA	NS1	740.00	11.50	1.00	970.00	960.00	Suzuki et al., 2013
The Cedars, California, USA	BS5	800.00	11.50	1.00	1450.00	1940.00	Suzuki et al., 2013
Santa Elena, Costa Rica	Camino al inglés	425.00	7.85	26.34	45.14	52.57	Sanchez-Murillo et al., 2014
Santa Elena, Costa Rica	Poza del General	404.00	8.45	23.63	69.14	96.83	Sanchez-Murillo et al., 2014
Santa Elena, Costa Rica	Río Murciélago springs	428.00	7.45	18.22	53.43	74.35	Sanchez-Murillo et al., 2014
Santa Elena, Costa Rica	Casa de Zinc	369.00	8.43	20.92	66.86	76.96	Sanchez-Murillo et al., 2014
Santa Elena, Costa Rica	Río Calera 4	397.00	8.53	18.01	49.43	57.57	Sanchez-Murillo et al., 2014
Santa Elena, Costa Rica	Río Calera 3	401.00	8.24	16.55	48.00	62.17	Sanchez-Murillo et al., 2014
Santa Elena, Costa Rica	Nancite spring	681.00	8.77	30.50	171.71	112.52	Sanchez-Murillo et al., 2014
Santa Elena, Costa Rica	Los Pargos Spring	560.00	7.42	21.03	101.71	92.57	Sanchez-Murillo et al., 2014
Santa Elena, Costa Rica	Casa de Zinc	545.00	8.46	24.05	56.00	70.43	Sanchez-Murillo et al., 2014
Santa Elena, Costa Rica	Río Murciélago	643.00	7.26	14.68	38.00	65.65	Sanchez-Murillo et al., 2014
Santa Elena, Costa Rica	Quebrada Danta	412.00	8.30	21.03	65.14	426.09	Sanchez-Murillo et al., 2014
Santa Elena, Costa Rica	Río Calera	558.00	8.40	15.30	39.71	56.96	Sanchez-Murillo et al., 2014
Santa Elena, Costa Rica	Pozo Aguas Calientes	535.00	7.20	59.75	1181.43	704.78	Sanchez-Murillo et al., 2014
Red Mountain, California, USA	Red Mountain	n.r.	11.78	14.57	914.29	1739.13	Barnes et al., 2015
Zambales, Philippines	Manleluag 1, ML1	315.00	10.90	7.29	514.29	1000.00	Cardace et al., 2015
Zambales, Philippines	Manleluag 2, ML2	337.00	10.80	7.29	534.29	1060.87	Cardace et al., 2015
Zambales, Philippines	Manleluag 3, ML3	307.00	10.80	8.33	485.71	982.61	Cardace et al., 2015
Zambales, Philippines	Bigbiga well, BB1	349.00	9.30	492.40	125.71	4369.57	Cardace et al., 2015
Zambales, Philippines	Poon Bato 1, PB1	505.00	11.30	1.04	685.71	1039.13	Cardace et al., 2015
Zambales, Philippines	Poon Bato 2, PB2 [star pool]	229.00	9.20	1.04	322.86	447.83	Cardace et al., 2015
Zambales, Philippines	Poon Bato 3, PB3	606.00	11.30	0.00	511.43	678.26	Cardace et al., 2015
Zambales, Philippines	San Isidro Spr, SI1	516.00	10.50	40.60	1640.00	3982.61	Cardace et al., 2015
Zambales, Philippines	Mainit Falls, MF1	784.00	9.70	100.98	6534.29	11726.09	Cardace et al., 2015
Zambales, Philippines	Manleluag 2, ML2	388.00	10.80	192.59	485.71	813.04	Cardace et al., 2015
Zambales, Philippines	Manleluag 3, ML3	270.00	10.30	200.92	482.86	860.87	Cardace et al., 2015
Zambales, Philippines	Bigbiga well, BB1	428.00	7.00	485.11	280.00	8691.30	Cardace et al., 2015
Zambales, Philippines	Poon Bato 1, PB1	232.00	9.60	99.94	354.29	834.78	Cardace et al., 2015
Zambales, Philippines	Poon Bato 2, PB2	189.00	8.70	927.55	311.43	643.48	Cardace et al., 2015
Cabeco de Vide, Portugal	Maria Rita (b)	n.r.	8.04	181.14	576.57	1208.70	Marques, et al., 2008
Cabeco de Vide, Portugal	Vale Fabiano (sp)	n.r.	7.37	185.51	314.00	508.70	Marques, et al., 2008
Cabeco de Vide, Portugal	Furo da Camara (b)	n.r.	7.54	150.11	259.43	415.65	Marques, et al., 2008
Turkey	YT-0m	n.r.	11.95	83.28	522.86	499.13	Meyer-Dombard et al., 2015
Turkey	YT-S8.8m	n.r.	9.40	302.94	694.57	532.61	Meyer-Dombard et al., 2015
Leka Ophiolite Complex	gw 1	n.r.	9.56	27.00	414.00	429.00	Okland et al., 2012
Leka Ophiolite Complex	gw 2	n.r.	8.58	38.00	519.00	535.00	Okland et al., 2012
Leka Ophiolite Complex	gw 3	n.r.	8.80	38.00	543.00	545.00	Okland et al., 2012
Leka Ophiolite Complex	sw 1	n.r.	7.90	26.00	433.00	440.00	Okland et al., 2012
Cazadero, California, USA	ultrabasic	n.r.	11.54	4.16	1571.43	2173.91	Barnes et al., 2015

Table 2 (cont'd)

New Caledonia	HP11-Site9-W3	n.r.	10.62	1720.00	50580.00	6460.00	Monnin et al., 2014
New Caledonia	HP11-Site9-W4	n.r.	10.46	3820.00	91620.00	44960.00	Monnin et al., 2014
New Caledonia	HP11-Site9-W6	n.r.	9.18	18850.00	380770.00	337760.00	Monnin et al., 2014
New Caledonia	HP11-Site9-W7	n.r.	10.51	4030.00	95840.00	47540.00	Monnin et al., 2014
New Caledonia	La Coulee 1	n.r.	10.80	7.81	628.57	634.78	Barnes et al., 1978
New Caledonia	La Coulee 2	n.r.	10.70	60.38	465.71	1134.78	Barnes et al., 1978
Hakuba Happo	Happo #1	70300.00	10.80	10.00	1770.00	150.00	Suda et al., 2014
Hakuba Happo	Happo #3	48300.00	10.70	10.00	1160.00	130.00	Suda et al., 2014
Lost City Hydrothermal Field	J2-362IGT2	n.r.	10.50	3640.00	541000.00	494000.00	Seyfried et al., 2015
Lost City Hydrothermal Field	J2-362IGT4	n.r.	10.50	3510.00	541000.00	494000.00	Seyfried et al., 2015
Lost City Hydrothermal Field	J2-360IGT2	n.r.	10.40	4120.00	542000.00	491000.00	Seyfried et al., 2015
Lost City Hydrothermal Field	J2-360IGT6	n.r.	10.60	3460.00	541000.00	485000.00	Seyfried et al., 2015
Lost City Hydrothermal Field	J2-360CGTR	n.r.	10.10	5010.00	542000.00	485000.00	Seyfried et al., 2015
Lost City Hydrothermal Field	J2-361IGT5	n.r.	10.50	3990.00	541000.00	495000.00	Seyfried et al., 2015
Lost City Hydrothermal Field	J2-361IGT6	n.r.	10.60	3610.00	543000.00	492000.00	Seyfried et al., 2015
Lost City Hydrothermal Field	J2-361CGTB	n.r.	10.20	6160.00	543000.00	490000.00	Seyfried et al., 2015
Lost City Hydrothermal Field	J2-361CGT-Wu	n.r.	10.50	4240.00	543000.00	493000.00	Seyfried et al., 2015
Lost City Hydrothermal Field	Seawater	n.r.	8.00	28700.00	554000.00	475000.00	Seyfried et al., 2015

Table 3 - CROMO Sulfur Chemistry Reported for all Wells Through Time

Well	Date Sampled	SO_4^{2-} (µM)	HS^- (µM)	pH	Temperature (ºC)	Conductivity (µS/cm)	DO (mg/L)	ORP (mV)
CSW 1.1	March-12	183.64	n.a.	12.38	13.66	4674.00	0.03	-298.90
	June-12	108.27	n.a.	12.30	14.99	5100.00	0.32	-287.90
	August-13	147.08	< 0.10	12.39	16.16	4486.00	0.20	-258.40
	December-13	305.43	n.a.	12.17	14.39	4578.00	0.37	-298.60
	July-14	266.19	12.88	12.32	16.31	4453.00	0.43	-297.00
	August-15	180.46	22.67	11.76	16.71	4206.00	0.17	-243.10
	January-16	340.00	15.49	12.42	14.83	4130.00	0.19	-276.50
	June-16	389.55	3.54	12.06	17.21	3809.00	0.25	-271.60
CSW 1.2	August-13	125.30	< 0.10	9.27	15.62	4174.00	3.55	132.80
	December-13	< 1.56	3.90	8.55	15.38	4278.00	0.30	-55.50
	July-14	191.65	< 0.10	7.76	15.97	4495.00	0.25	-118.50
	June-16	112.43	8.50	8.80	16.90	4627.00	0.41	-97.50
CSW 1.3	August-13	114.90	4.64	10.20	16.51	4708.00	0.14	-246.60
	December-13	135.02	2.64	10.10	15.21	4740.00	0.20	-191.20
	July-14	151.16	< 0.10	10.15	15.64	4842.00	0.16	-204.80
	June-16	174.79	4.20	10.10	18.83	4787.00	0.21	-275.20
CSW 1.4	August-13	222.02	< 0.10	8.04	14.94	1989.00	0.92	336.00
	December-13	393.61	bdl	7.64	15.40	1931.00	2.50	500.00
	July-14	391.94	< 0.10	7.75	15.05	1950.00	2.36	116.20
	June-16	429.42	< 0.10	7.87	17.34	1978.00	4.40	203.00
CSW 1.5	August-13	351.39	33.74	9.95	15.91	4643.00	0.27	-216.40
	December-13	433.37	19.81	9.59	15.29	4632.00	0.43	-290.00
	July-14	317.41	23.75	9.77	15.80	4792.00	0.16	-285.20
	August-15	99.99	27.73	9.39	16.15	4755.00	0.19	-211.60
	June-16	358.21	1.41	9.77	15.69	4780.00	0.49	-206.50
CSW OLD	August-13	47.92	34.21	9.82	18.18	10400.00	0.02	-278.00
	December-13	118.88	0.94	9.69	17.90	11150.00	0.22	-346.00
	July-14	139.29	8.39	9.73	17.43	11529.00	0.26	-279.90
	August-15	96.14	25.63	9.59	17.24	11110.00	0.55	-213.90
	January-16	46.42	bdl	9.87	17.95	11000.00	0.08	-294.90
	June-16	170.21	0.72	9.84	18.45	11290.00	1.42	-356.70
N08-A	August-13	n.a.	3.47	10.42	16.41	5917.00	0.19	-161.10
	December-13	32.27	2.61	10.17	15.34	6444.00	0.07	-229.60
	July-14	40.18	1.14	10.89	16.85	6335.00	0.09	-249.50
	June-16	77.14	3.70	10.82	16.32	6040.00	0.27	-216.10
N08-B	August-13	n.a.	< 0.10	10.98	16.03	3070.00	0.31	-74.60
	December-13	27.48	0.12	10.55	15.03	4350.00	0.10	-117.90
	July-14	27.69	< 0.10	10.68	16.12	3132.00	0.76	-197.60
	June-16	58.30	0.17	10.22	16.87	3047.00	0.15	-78.60
N08-C	August-13	54.53	< 0.10	7.55	14.99	1143.00	0.17	243.90
	December-13	40.70	0.56	9.32	15.08	1307.00	0.10	-164.90
	July-14	51.22	< 0.10	8.46	15.53	1372.00	0.42	-153.10
	June-16	77.45	< 0.10	7.25	16.67	1393.00	0.20	39.80
QV 1.1	August-13	< 10.00	11.53	11.64	16.36	2596.00	0.15	-122.70
	December-13	22.17	0.50	11.54	15.95	6722.00	0.21	-225.40
	July-14	257.13	4.76	11.51	17.52	2854.00	0.28	-233.50
	August-15	17.49	3.53	11.34	17.69	3075.00	0.19	-139.40
	January-16	< 1.56	< 0.10	11.75	15.90	3274.00	0.19	-218.30
	June-16	76.10	0.19	11.41	16.74	3362.00	0.18	-181.00
QV 1.2	August-13	< 10.00	< 0.10	9.07	16.63	2781.00	0.79	-8.50
	December-13	< 1.56	0.21	8.99	15.52	4285.00	0.47	-123.00
	July-14	< 1.56	< 0.10	9.47	17.09	3042.00	0.40	-142.70
	June-16	< 1.56	< 0.10	9.31	16.68	3004.00	0.17	-156.20
QV 1.3	August-13	191.91	4.64	9.63	16.45	6200.00	0.03	-183.40
	December-13	59.96	n.a.	9.58	16.10	6727.00	0.11	-211.50
	July-14	55.69	10.13	9.68	16.60	6507.00	0.26	-223.60
	June-16	72.25	0.99	9.78	16.55	4735.00	0.22	-207.80

n.a. = not analyzed

Table 4 -Thermodynamic Calculations for Select Sulfur Reactions

	Total Delta G (J/L)	CSW 1.1	CSW 1.2	CSW 1.3	CSW 1.4	CSW 1.5	CSW OLD	N08-A	N08-B	N08-C	QV 1.1	QV 1.2	QV 1.3
Sulfate Reduction													
$CH_4 + SO_4^{2-} + H^+ \rightarrow H^{S-} + CO_2 + 2H_2O$		-14.29	-8.27	-7.36	-0.12	-12.81	-6.50	-2.11	-1.33	-0.03	-13.87	-1.21	-2.12
$Acetate + SO_4^{2-} + 5H^+ \rightarrow HS^- + 2CO_2 + 2H_2O$		-93.86	-0.10	-0.13	-0.10	-0.11	-0.12	-0.14	-0.14	-0.11	-0.96	-0.11	-0.90
$4Formate + SO_4^{2-} + 5H^+ \rightarrow HS^- + 4CO_2 + 4H_2O$		-0.72	-0.02	-0.02	-0.02	-0.02	-0.03	-0.03	-0.03	-0.02	-0.03	-0.02	-0.02
$4H_2 + SO_4^{2-} + H^+ \rightarrow HS^- + 4H_2O$		0.00	0.00	-0.07	-0.01	-0.01	0.00	0.00	0.00	-0.01	0.00	-0.01	0.00
Sulfide Oxidation													
$HS^- + 2O_2 \rightarrow SO_4^{2-} + H^+$		-10.31	-0.77	-0.78	-0.78	-1.96	-3.14	-0.86	-0.79	-0.77	-3.80	-0.78	-3.97
$2HS^- + 2O_2 \rightarrow S_2O_3^{2-} + H_2O$		-4.79	-0.36	-0.36	-0.37	-1.85	-2.96	-0.40	-0.37	-0.37	-1.77	-0.37	-3.74
$HS^- + 0.5O_2 \rightarrow S_{(s)} + H_2O$		-2.79	-0.21	-0.10	-0.21	-0.02	-0.01	-0.23	-0.21	-0.21	-1.02	-0.21	-4.34
$HS^- + NO_3^- \rightarrow S_{(s)} + NO_2^- + H_2O$		-1.94	-0.15	-0.16	-0.16	-0.05	-0.29	-0.17	-0.23	-0.16	-0.23	-0.16	-1.21
$5HS^- + 2NO_3^- + 7H^+ \rightarrow 5S_{(s)} + N_2 + 6H_2O$		-0.09	-0.15	-0.14	-0.16	-0.11	-0.68	-0.14	-0.51	-0.15	-0.50	-0.14	-2.78
$5HS^- + 8NO_3^- + 3H^+ \rightarrow SO_4^{2-} + 4N_2 + 4H_2O$		-0.13	-0.72	-0.71	-0.72	-0.13	-0.84	-0.78	0.00	-0.72	0.00	-0.72	-3.46
Thiosulfate Reactions													
$S_2O_3^{2-} + 8NO_3^- + H_2O \rightarrow 10SO_4^{2-} + 4N_2 + 2H^+$		-0.15	-3.92	-3.97	-3.94	-0.14	-3.92	-3.97	-0.79	-3.96	-0.78	-4.00	-3.97
$S_2O_3^{2-} + 2O_2 + H_2O \rightarrow 2SO_{42-} + 2H^+$		-0.86	-0.80	-0.83	-0.81	-0.82	-0.83	-0.84	-0.85	-0.81	-0.85	-0.83	-0.83
$5S_2O_3^{2-} + 4O_2 + H_2O \rightarrow 6SO_4^{2-} + 4S_{(s)} + 2H^+$		-0.33	-0.32	-0.33	-0.33	-0.33	-0.33	-0.33	-0.34	-0.33	-0.33	-0.33	-0.33
$4Formate + S_2O_3^{2-} + 4H^+ \rightarrow 4CO_2 + 2HS^- + 3H_2O$		-0.21	-0.13	-0.15	-0.11	-0.12	-0.15	-0.18	-0.17	-0.13	-0.18	-0.13	-0.12
$S_2O_3^{2-} + H_2O \rightarrow SO_4^{2-} + HS^- + H^+$		-0.06	-0.04	-0.05	-0.04	-0.04	-0.04	-0.06	-0.06	-0.04	-0.05	-0.05	-0.05
$4H_2 + S_2O_3^{2-} \rightarrow 2HS^- + 3H_2O$		-0.03	-0.01	-0.14	-0.01	-0.01	0.00	0.00	0.00	-0.01	-0.01	-0.02	0.00

Calculated Activities	CSW 1.1	CSW 1.2	CSW 1.3	CSW 1.4	CSW 1.5	CSW OLD	N08-A	N08-B	N08-C	QV 1.1	QV 1.2	QV 1.3
aCH_4	-3.23	-3.11	-2.94	-5.40	-2.97	-2.88	-2.90	-3.52	-6.00	-3.54	-3.58	-2.89
aSO_4^{2-}	-3.86	-4.09	-4.20	-3.71	-3.89	-4.34	-4.85	-4.88	-3.94	-3.92	-4.81	-4.68
aH^+	-12.30	-7.80	-10.20	-7.80	-9.80	-9.70	-10.89	-10.68	-8.46	-11.51	-9.47	-9.68
aHS^-	-4.96	-6.16	-6.08	-6.14	-4.71	-5.18	-6.05	-6.07	-6.07	-5.39	-6.07	-5.09
aCO_2	-11.90	-4.40	-7.84	-3.88	-7.03	-7.96	-9.90	-9.37	-5.32	-11.10	-6.43	-6.80
aO_2	-4.89	-5.10	-5.30	-4.13	-5.30	-5.10	-5.52	-4.62	-4.89	-5.05	-4.89	-5.10
aNO_3^-	-6.58	-4.93	-4.54	-4.19	-6.61	-5.83	-5.53	-7.00	-4.19	-7.00	-4.59	-5.21
aNO_2^-	-8.00	-8.00	-8.00	-8.00	-8.00	-8.00	-8.00	-8.00	-8.00	-8.00	-8.00	-8.00
aN_2	-10.00	-10.00	-10.00	-10.00	-10.00	-10.00	-10.00	-10.00	-10.00	-10.00	-10.00	-10.00
$aS_2O_3^{2-}$	-6.25	-6.32	-6.32	-6.22	-6.33	-6.41	-6.37	-6.28	-6.20	-6.26	-6.28	-6.36
aH_2	-5.06	-6.74	-5.53	-6.54	-6.41	-6.81	-6.41	-6.49	-6.58	-5.73	-6.31	-6.76
aFormate	-4.79	-6.08	-6.08	-6.06	-6.08	-6.08	-6.08	-6.08	-6.08	-6.08	-6.08	-6.08
aAcetate	-4.31	-6.08	-6.08	-6.06	-6.08	-6.08	-6.08	-6.08	-6.08	-5.30	-6.08	-5.19

Table 5 - KEGG Accessions and Genes, Transcripts Associated with Metacyc Metabolic Pathways and Respective Metagenome Fragments per Kilobase of Predicted Protein Sequence per Million Mapped Reads (FPKM) for each CROMO Well

	Metabolic Pathway	Gene	KEGG ID	LCY 3862	LCY H08	QV1.1	QV1.1 mt	QV1.2	QV12 mt	N08-B	N08B mt	CSWold	CSWold mt
Sulfate Reduction	dissimilatory sulfate reduction IV (to sulfide)	*sat*	K00956	10.17	6.75	65.06	7.03	176.51	120.99	121.06	10.27	35.76	0.83
	dissimilatory sulfate reduction IV (to sulfide)	*sat*	K00957	35.55	247.90	145.56	6.19	224.29	576.35	241.63	84.02	90.17	2.72
	dissimilatory sulfate reduction IV (to sulfide)	*sat*	K00958	95.74	64.40	0.38	0.00	0.59	29.74	18.60	15.10	72.96	2043.18
	dissimilatory sulfate reduction IV (to sulfide)	*AprA*	K00394	4.63	11.92	65.87	0.65	0.34	35.91	9.85	80.79	10.05	5970.80
	dissimilatory sulfate reduction IV (to sulfide)	*AprB*	K00395	14.66	17.57	21.79	0.00	1.20	65.43	7.53	5.40	6.57	7228.29
	dissimilatory sulfate reduction IV (to sulfide)	*DsrA*	K11180	12.13	9.53	139.56	224.49	1.17	127.06	23.53	47.04	19.81	49.68
	dissimilatory sulfate reduction IV (to sulfide)	*DsrB*	K11181	-	-	98.72	111.89	0.69	25.46	8.15	29.67	3.94	22.94
	dissimilatory sulfate reduction IV (to sulfide)	*DsrK*	K11179	14.74	17.05	105.95	167.95	8.91	313.61	136.28	677.81	132.45	8182.16
Thiosulfate Disproportionation	thiosulfate disproportionation IV (rhodanese)	*sseA*	K01011	66.16	63.06	20.06	0.00	130.71	55.29	86.52	188.53	102.00	71.23
	thiosulfate disproportionation IV (rhodanese)	*glpE*	K02439	14.57	81.70	0.26	0.00	86.86	0.00	0.64	0.00	1.21	0.00
	thiosulfate disproportionation III (quinone)	*phsA*	K08352	0.42	0.00	5.45	73.79	1.23	1.64	21.83	30.84	14.43	0.71
	thiosulfate disproportionation III (quinone)	*phsB*	K08354	-	-	0.00	0.00	2.76	7.15	0.36	0.00	0.00	0.00
Sulfide Oxidation	sulfide oxidation I (sulfide-quinone reductase)	*sqr*	K17218	-	-	193.54	31.97	217.98	395.21	140.38	61.92	109.28	10.61
	sulfide oxidation II (sulfide dehydrogenase)	*fccB*	K17229	-	-	0.13	0.00	1.38	3.67	0.26	0.00	0.27	0.00
	sulfide oxidation II (sulfide dehydrogenase)	*fccA*	K17230	-	-	0.00	0.00	0.13	0.00	0.00	0.00	0.27	0.00

mt = metatranscript
LCY = Lost City
(-) = no sequences were observed meeting the given criteria
KEGG = Kyoto Encyclopedia of Genes and Genomes

Table 6 - Pearson's Correlation Analysis Results

Amplicon Sequence Variant	Enviromental Variable	Correlation	Sign	*p-value*
HWI-M02808_85_AJHNL_1_1108_16168_8446	Bromide (uM)	0.929	+	1.03E-04
Bacteria;Bacteroidetes;Sphingobacteriia;Sphingobacteriales;WCHB1-69;	Fluoride (uM)	0.929	+	1.03E-04
HWI-M02808_85_AJHNL_1_1110_18737_15034	Nitrate (uM)	0.843	+	2.20E-03
Bacteria;Acidobacteria;Acidobacteria;Acidobacteriales;Acidobacteriaceae_(Subgroup_1);	Magnesium (uM)	0.993	+	9.74E-09
HWI-M02808_85_AJHNL_1_1105_21800_25660	Nitrate (uM)	0.842	+	2.23E-03
Bacteria;Verrucomicrobia;OPB35_soil_group;OPB35_soil_group_unclassified;	Magnesium (uM)	0.993	+	9.85E-09
HWI-M02808_85_AJHNL_1_1101_20850_21312	Hydrogen Sulfide (uM)	0.794	+	6.12E-03
Bacteria;Proteobacteria;Betaproteobacteria;Betaproteobacteria_unclassified;				
HWI-M02808_85_AJHNL_1_1101_20642_3370	Well Depth (m)	0.819	+	3.75E-03
Bacteria;Firmicutes;Clostridia;Clostridiales;Family_XIV;Family_XIV_uncultured;	Specific Conductance (uS)	0.785	+	7.16E-03
HWI-M02808_85_AJHNL_1_1107_5134_16942	Nitrate (uM)	0.841	+	2.32E-03
Bacteria;Proteobacteria;Alphaproteobacteria;Sphingomonadales;Erythrobacteraceae;	Magnesium (uM)	0.993	+	1.30E-08
HWI-M02808_85_AJHNL_1_2110_11524_5121				
Bacteria;Firmicutes;Erysipelotrichia;Erysipelotrichales;Erysipelotrichaceae;	Dissolved Hydrogen (uM)	0.918	+	1.79E-04
Erysipelothrix;uncultured_bacterium				
HWI-M02808_85_AJHNL_1_1105_26860_11279	Well Depth (m)	0.917	+	1.84E-04
Bacteria;Firmicutes;Clostridia;Clostridia_Incertae_Sedis;Unknown_Family;	Specific Conductance (uS)	0.825	+	3.29E-03
HWI-M02808_85_AJHNL_1_2105_24061_20363				
Bacteria;Firmicutes;Clostridia;Thermoanaerobacterales;SRB2;	Dissolved Oxygen (uM)	0.794	+	6.07E-03
uncultured_bacterium;uncultured_bacterium_unclassified				
HWI-M02808_85_AJHNL_1_2103_26618_18257	Nitrate (uM)	0.843	+	2.21E-03
Bacteria;Planctomycetes;Phycisphaerae;Phycisphaerales;Phycisphaeraceae;	Magnesium (uM)	0.993	+	1.01E-08
HWI-M02808_85_AJHNL_1_2104_9737_12868				
Bacteria;Bacteroidetes;Bacteroidia;Bacteroidia_Incertae_Sedis;Draconibacteriaceae;	Dissolved Hydrogen (uM)	0.943	+	4.22E-05
Draconibacteriaceae_uncultured;Draconibacteriaceae_unclassified				
HWI-M02808_85_AJHNL_1_1101_17918_2017	Lithium (uM)	0.991	+	2.55E-08
Bacteria;Deinococcus-Thermus;Deinococci;Deinococcales;Trueperaceae;Truepera;	Acetate (uM)	0.980	+	6.40E-07
uncultured_bacterium	Formate (uM)	0.995	+	3.43E-09
HWI-M02808_85_AJHNL_1_2110_14519_22333	Nitrate (uM)	0.842	+	2.26E-03
Bacteria;Planctomycetes;Phycisphaerae;Phycisphaerales;Phycisphaeraceae;SM1A02;	Magnesium (uM)	0.993	+	1.07E-08
HWI-M02808_85_AJHNL_1_1105_18131_5315	Bromide (uM)	0.920	+	1.66E-04
Bacteria;Spirochaetae;Spirochaetes;Spirochaetales;Spirochaetaceae;	Fluoride (uM)	0.920	+	1.66E-04
HWI-M02808_85_AJHNL_1_2111_18984_15162	Nitrate (uM)	0.842	+	2.22E-03
Bacteria;Chlorobi;Chlorobia;Chlorobiales;SJA-28;uncultured_bacterium;	Magnesium (uM)	0.993	+	9.56E-09
HWI-M02808_85_AJHNL_1_2109_4377_21131	Well Depth (m)	0.916	+	1.97E-04
Bacteria;Firmicutes;Clostridia;Clostridiales;Syntrophomonadaceae;Dethiobacter;	Specific Conductance (uS)	0.830	+	2.97E-03
HWI-M02808_85_AJHNL_1_2102_13386_18268				
Bacteria;Proteobacteria;Alphaproteobacteria;Rhizobiales;Methylocystaceae;	Dissolved Hydrogen (uM)	0.967	+	4.74E-06
Methylocystaceae_unclassified;Methylocystaceae_unclassified				
HWI-M02808_85_AJHNL_1_1104_19259_24357	Nitrate (uM)	0.840	+	2.37E-03
Bacteria;Proteobacteria;Alphaproteobacteria;Sphingomonadales;Erythrobacteraceae;	Magnesium (uM)	0.992	+	1.43E-08
HWI-M02808_85_AJHNL_1_1103_15102_15538				
Bacteria;Proteobacteria;Alphaproteobacteria;Rhodobacterales;Rhodobacteraceae;	Calcium (uM)	0.804	+	5.07E-03
Rhodobacter;uncultured_alpha_proteobacterium				
HWI-M02808_85_AJHNL_1_1107_23247_21981	Nitrate (uM)	0.843	+	2.21E-03
Bacteria;Proteobacteria;Betaproteobacteria;Nitrosomonadales;Nitrosomonadaceae;	Magnesium (uM)	0.993	+	9.39E-09
HWI-M02808_85_AJHNL_1_2105_13143_15497	Nitrate (uM)	0.842	+	2.22E-03
Bacteria;Verrucomicrobia;Opitutae;Opitutales;Opitutaceae;Opitutus;uncultured_Opitutus_sp.	Magnesium (uM)	0.993	+	9.78E-09
HWI-M02808_85_AJHNL_1_1103_8071_4949	Nitrate (uM)	0.843	+	2.21E-03
Bacteria;Planctomycetes;Planctomycetacia;Planctomycetales;Planctomycetaceae;	Magnesium (uM)	0.993	+	9.41E-09
HWI-M02808_85_AJHNL_1_1101_17949_2457	Well Depth (m)	0.918	+	1.82E-04
Bacteria;Proteobacteria;Betaproteobacteria;Burkholderiales;Comamonadaceae;	Specific Conductance (uS)	0.825	+	3.28E-03
HWI-M02808_85_AJHNL_1_1107_14145_21318	Bromide (uM)	0.935	+	7.11E-05
Bacteria;Proteobacteria;Alphaproteobacteria;Rhizobiales;Rhizobiaceae;Rhizobium;	Fluoride (uM)	0.935	+	7.14E-05
HWI-M02808_85_AJHNL_1_1101_20048_2184				
Bacteria;Proteobacteria;Betaproteobacteria;Burkholderiales;Comamonadaceae	pH	0.900	+	3.86E-04
Comamonadaceae_unclassified;Comamonadaceae_unclassified				
HWI-M02808_85_AJHNL_1_1101_16854_7369	Well Depth (m)	0.793	+	6.16E-03
Bacteria;Bacteroidetes;Bacteroidia;Bacteroidia_Incertae_Sedis;Draconibacteriaceae;	Specific Conductance (uS)	0.860	+	1.41E-03
Draconibacteriaceae_uncultured;Draconibacteriaceae_unclassified	Chloride (uM)	0.800	+	5.45E-03
HWI-M02808_85_AJHNL_1_1101_7284_6821	Nitrate (uM)	0.843	+	2.21E-03
Bacteria;Chlamydiae;Chlamydiae;Chlamydiales;Simkaniaceae;	Magnesium (uM)	0.993	+	9.40E-09

Table 6 (cont'd)

HWI-M02808_85_AJHNL_1_1101_9105_4721 Bacteria;Firmicutes;Clostridia;Clostridiales;Syntrophomonadaceae;Dethiobacter; uncultured_bacterium	Dissolved Oxygen (uM)	0.795	+	6.02E-03
HWI-M02808_85_AJHNL_1_1106_19311_2988	Nitrate (uM)	0.842	+	2.22E-03
Bacteria;Proteobacteria;Gammaproteobacteria;Xanthomonadales;Xanthomonadaceae;	Magnesium (uM)	0.993	+	9.29E-09
HWI-M02808_85_AJHNL_1_1101_8018_4755 Bacteria;Firmicutes;Clostridia;Clostridiales;Clostridiaceae_4;Clostridiaceae_4_uncultured; uncultured_bacterium	Calcium (uM)	0.823	+	3.41E-03
HWI-M02808_85_AJHNL_1_1101_28097_12743	Well Depth (m)	0.917	+	1.84E-04
Bacteria;Proteobacteria;Alphaproteobacteria;Rhodobacterales;Rhodobacteraceae;	Specific Conductance (uS)	0.825	+	3.29E-03
HWI-M02808_85_AJHNL_1_1101_23196_4273 Bacteria;Proteobacteria;Alphaproteobacteria;Rhizobiales;Bradyrhizobiaceae; Bradyrhizobium;Bradyrhizobium_elkanii	Dissolved Hydrogen (uM)	0.967	+	4.88E-06
HWI-M02808_85_AJHNL_1_1101_23818_10636 Bacteria;Firmicutes;Erysipelotrichia;Erysipelotrichales;Erysipelotrichaceae;Erysipelothrix;	Hydrogen Sulfide (uM)	0.791	+	6.42E-03
HWI-M02808_85_AJHNL_1_2103_22544_20946	Nitrate (uM)	0.843	+	2.22E-03
Bacteria;Proteobacteria;Betaproteobacteria;Nitrosomonadales;Nitrosomonadaceae;	Magnesium (uM)	0.993	+	9.39E-09
HWI-M02808_85_AJHNL_1_1101_7615_8182	Well Depth (m)	0.918	+	1.82E-04
Bacteria;Actinobacteria;Nitriliruptoria;Nitriliruptorales;Nitriliruptoraceae;Nitriliruptor;	Specific Conductance (uS)	0.826	+	3.26E-03
HWI-M02808_85_AJHNL_1_1107_22980_6232 Bacteria;Proteobacteria;Alphaproteobacteria;Rhizobiales;Methylocystaceae; Methylocystaceae_uncultured;uncultured_bacterium	Dissolved Hydrogen (uM)	0.967	+	4.85E-06
HWI-M02808_85_AJHNL_1_1114_20682_21407 Bacteria;Firmicutes;Clostridia;Clostridiales;Family_XII;Fusibacter;uncultured_Fusibacter_sp.	Dissolved Hydrogen (uM)	0.903	+	3.46E-04
HWI-M02808_85_AJHNL_1_1104_20198_4705	Bromide (uM)	0.905	+	3.24E-04
Bacteria;Proteobacteria;Alphaproteobacteria;Caulobacterales;Caulobacteraceae;	Fluoride (uM)	0.904	+	3.24E-04
HWI-M02808_85_AJHNL_1_1101_17192_2407	pH	0.781	+	7.62E-03
Bacteria;Firmicutes;Clostridia;Clostridiales;Syntrophomonadaceae;Dethiobacter;	Potassium (uM)	0.823	+	3.42E-03
HWI-M02808_85_AJHNL_1_1108_20955_13458	Nitrate (uM)	0.843	+	2.18E-03
Bacteria;Proteobacteria;Betaproteobacteria;Rhodocyclales;Rhodocyclaceae;	Magnesium (uM)	0.993	+	9.60E-09
HWI-M02808_85_AJHNL_1_2114_4352_18207	Nitrate (uM)	0.842	+	2.23E-03
Bacteria;Chlorobi;Chlorobia;Chlorobiales;OPB56;uncultured_bacterium;	Magnesium (uM)	0.993	+	1.01E-08
HWI-M02808_85_AJHNL_1_1112_14170_19757	Bromide (uM)	0.918	+	1.79E-04
Bacteria;Proteobacteria;Deltaproteobacteria;Syntrophobacterales;Syntrophaceae;	Fluoride (uM)	0.918	+	1.80E-04
HWI-M02808_85_AJHNL_1_1113_15872_17500	Nitrate (uM)	0.842	+	2.23E-03
Bacteria;Nitrospirae;Nitrospira;Nitrospirales;Nitrospiraceae;Nitrospira;Nitrospira_unclassified	Magnesium (uM)	0.993	+	9.89E-09
HWI-M02808_85_AJHNL_1_1103_10683_9335 Bacteria;Proteobacteria;Alphaproteobacteria;Rhodobacterales;Rhodobacteraceae; Rhodobacteraceae_unclassified;Rhodobacteraceae_unclassified	Dissolved Hydrogen (uM)	0.916	+	1.93E-04
HWI-M02808_85_AJHNL_1_1101_24150_5326	Well Depth (m)	0.917	+	1.84E-04
Bacteria;Firmicutes;Clostridia;Clostridiales;Peptococcaceae;Desulfitispora;uncultured_bacterium	Specific Conductance (uS)	0.825	+	3.29E-03
HWI-M02808_85_AJHNL_1_1104_4942_23661	Nitrate (uM)	0.844	+	2.12E-03
Bacteria;Acidobacteria;Acidobacteria;Subgroup_4;Subgroup_4_uncultured;	Magnesium (uM)	0.993	+	1.06E-08
HWI-M02808_85_AJHNL_1_1101_21249_4130	Well Depth (m)	0.917	+	1.85E-04
Bacteria;Firmicutes;Clostridia;Clostridiales;Syntrophomonadaceae;Dethiobacter;	Specific Conductance (uS)	0.825	+	3.30E-03
HWI-M02808_85_AJHNL_1_1101_22499_5481	Well Depth (m)	0.918	+	1.83E-04
Bacteria;Proteobacteria;Alphaproteobacteria;Rhizobiales;Bradyrhizobiaceae;Salinarimonas;	Specific Conductance (uS)	0.825	+	3.31E-03
HWI-M02808_85_AJHNL_1_1110_2855_18839	Bromide (uM)	0.878	+	8.39E-04
Bacteria;Firmicutes;Clostridia;Clostridiales;Peptococcaceae;Peptococcaceae_uncultured;Peptococcac	Fluoride (uM)	0.878	+	8.41E-04
HWI-M02808_85_AJHNL_1_1101_13289_11050	Well Depth (m)	0.919	+	1.75E-04
Bacteria;Actinobacteria;Acidimicrobiia;Acidimicrobiales;Acidimicrobiales_uncultured;	Specific Conductance (uS)	0.825	+	3.30E-03
HWI-M02808_85_AJHNL_1_1112_20122_9065	Dissolved Oxygen (uM)	0.798	+	5.67E-03
Bacteria;Bacteria_unclassified;Bacteria_unclassified;Bacteria_unclassified;Bacteria_unclassified;				

Correlations ($p<0.05$ and $q<0.05$)

Table 6 (cont'd)

Environmental Variable 1	Environmental Variable 2	Correlation	Sign	*p-value*
Well Depth (m)	Specific Conductance (uS)	0.910	+	2.53E-04
	Sodium (uM)	0.835	+	2.66E-03
pH	Potassium (uM)	0.835	+	2.67E-03
Specific Conductance (uS)	Chloride (uM)	0.852	+	1.77E-03
	Sodium (uM)	0.940	+	5.30E-05
	Dissolved Methane (uM)	0.816	+	3.97E-03
Chloride (uM)	Sodium (uM)	0.956	+	1.51E-05
	Silica (uM)	0.849	+	1.88E-03
	Dissolved Methane (uM)	0.835	+	2.65E-03
Bromide (uM)	Fluoride (uM)	1.00	+	2.96E-27
Nitrate (uM)	Magnesium (uM)	0.873	+	9.66E-04
Lithium (uM)	Acetate (uM)	0.989	+	5.27E-08
	Formate (uM)	0.992	+	1.63E-08
Sodium (uM)	Dissolved Methane (uM)	0.898	+	4.20E-04
Silica (uM)	Dissolved Methane (uM)	0.799	+	5.52E-03
Acetate (uM)	Formate (uM)	0.989	+	5.34E-08

Correlations ($p<0.05$ and $q<0.05$)
uM = micromolar

Table 7 - July 2014 Unique Sequence Variants in >1% Abundance Used in Statistical Analyses

HWI-M02808_85_AJHNL_1_1103_27798_17116	Bacteria;Firmicutes;Clostridia;Clostridiales;Syntrophomonadaceae;Dethiobacter;uncultured_bacterium
HWI-M02808_85_AJHNL_1_1108_16168_8446	Bacteria;Bacteroidetes;Sphingobacteriia;Sphingobacteriales;WCHB1-69;uncultured_Cytophagales_bacterium;uncultured_Cytophagales_bacterium_unclassified
HWI-M02808_85_AJHNL_1_1110_18737_15034	Bacteria;Acidobacteria;Acidobacteria;Acidobacteriales;Acidobacteriaceae_(Subgroup_1);Acidobacteriaceae_(Subgroup_1)_uncultured;uncultured_Acidobacteriaceae_bacterium
HWI-M02808_85_AJHNL_1_1105_21800_25660	Bacteria;Verrucomicrobia;OPB35_soil_group;OPB35_soil_group_unclassified;OPB35_soil_group_unclassified;OPB35_soil_group_unclassified;OPB35_soil_group_unclassified
HWI-M02808_85_AJHNL_1_1101_20850_21312	Bacteria;Proteobacteria;Betaproteobacteria;Betaproteobacteria_unclassified;Betaproteobacteria_unclassified;Betaproteobacteria_unclassified;Betaproteobacteria_unclassified
HWI-M02808_85_AJHNL_1_1101_20642_3370	Bacteria;Firmicutes;Clostridia;Clostridiales;Family_XIV;Family_XIV_uncultured;Family_XIV_unclassified
HWI-M02808_85_AJHNL_1_1106_18337_20397	Bacteria;Proteobacteria;Gammaproteobacteria;Methylococcales;Methylococcaceae;Methylococcaceae_unclassified;Methylococcaceae_unclassified
HWI-M02808_85_AJHNL_1_1103_25473_23195	Bacteria;Proteobacteria;Betaproteobacteria;Burkholderiales;Alcaligenaceae;Alcaligenaceae_uncultured;Alcaligenaceae_unclassified
HWI-M02808_85_AJHNL_1_1107_5134_16942	Bacteria;Proteobacteria;Alphaproteobacteria;Sphingomonadales;Erythrobacteraceae;Porphyrobacter;uncultured_bacterium
HWI-M02808_85_AJHNL_1_2101_12173_12171	Bacteria;Proteobacteria;Betaproteobacteria;Methylophilales;Methylophilaceae;Methylophilaceae_unclassified;Methylophilaceae_unclassified
HWI-M02808_85_AJHNL_1_1108_24510_7557	Bacteria;Firmicutes;Erysipelotrichia;Erysipelotrichales;Erysipelotrichaceae;Erysipelothrix;Erysipelothrix_unclassified
HWI-M02808_85_AJHNL_1_2110_11524_5121	Bacteria;Firmicutes;Erysipelotrichia;Erysipelotrichales;Erysipelotrichaceae;Erysipelothrix;uncultured_bacterium
HWI-M02808_85_AJHNL_1_2113_15368_19109	Bacteria;Proteobacteria;Betaproteobacteria;Burkholderiales;Comamonadaceae;Comamonadaceae_unclassified;Comamonadaceae_unclassified
HWI-M02808_85_AJHNL_1_1105_26860_11279	Bacteria;Firmicutes;Clostridia;Clostridia_Incertae_Sedis;Unknown_Family;Candidatus_Desulforudis;uncultured_bacterium
HWI-M02808_85_AJHNL_1_1106_5301_8438	Bacteria;Firmicutes;Erysipelotrichia;Erysipelotrichales;Erysipelotrichaceae;Erysipelothrix;Erysipelothrix_unclassified
HWI-M02808_85_AJHNL_1_2105_24061_20363	Bacteria;Firmicutes;Clostridia;Thermoanaerobacterales;SRB2;uncultured_bacterium;uncultured_bacterium_unclassified
HWI-M02808_85_AJHNL_1_2103_26618_18257	Bacteria;Planctomycetes;Phycisphaerae;Phycisphaerales;Phycisphaeraceae;Phycisphaeraceae_unclassified;Phycisphaeraceae_unclassified
HWI-M02808_85_AJHNL_1_2104_9737_12868	Bacteria;Bacteroidetes;Bacteroidia;Bacteroidia_Incertae_Sedis;Draconibacteriaceae;Draconibacteriaceae_uncultured;Draconibacteriaceae_unclassified
HWI-M02808_85_AJHNL_1_1105_18048_6511	Bacteria;Firmicutes;Clostridia;Clostridiales;Clostridiaceae_4;Salimesophilobacter;uncultured_bacterium
HWI-M02808_85_AJHNL_1_1101_21442_4297	Bacteria;Firmicutes;Clostridia;Clostridiales;Peptococcaceae;Peptococcaceae_unclassified;Peptococcaceae_unclassified
HWI-M02808_85_AJHNL_1_1101_17918_2017	Bacteria;Deinococcus-Thermus;Deinococci;Deinococcales;Trueperaceae;Truepera;uncultured_bacterium
HWI-M02808_85_AJHNL_1_2110_11654_16963	Bacteria;Proteobacteria;Betaproteobacteria;Rhodocyclales;Rhodocyclaceae;Rhodocyclaceae_uncultured;Rhodocyclaceae_unclassified
HWI-M02808_85_AJHNL_1_2110_14519_22333	Bacteria;Planctomycetes;Phycisphaerae;Phycisphaerales;Phycisphaeraceae;SM1A02;uncultured_bacterium
HWI-M02808_85_AJHNL_1_1105_18131_5315	Bacteria;Spirochaetae;Spirochaetes;Spirochaetales;Spirochaetaceae;Spirochaetaceae_uncultured;uncultured_prokaryote
HWI-M02808_85_AJHNL_1_2111_18984_15162	Bacteria;Chlorobi;Chlorobia;Chlorobiales;SJA-28;uncultured_bacterium;uncultured_bacterium_unclassified
HWI-M02808_85_AJHNL_1_2109_4377_21131	Bacteria;Firmicutes;Clostridia;Clostridiales;Syntrophomonadaceae;Dethiobacter;uncultured_bacterium
HWI-M02808_85_AJHNL_1_2102_13386_18268	Bacteria;Proteobacteria;Alphaproteobacteria;Rhizobiales;Methylocystaceae;Methylocystaceae_unclassified;Methylocystaceae_unclassified
HWI-M02808_85_AJHNL_1_1104_19259_24357	Bacteria;Proteobacteria;Alphaproteobacteria;Sphingomonadales;Erythrobacteraceae;Erythrobacteraceae_uncultured;uncultured_bacterium
HWI-M02808_85_AJHNL_1_1101_19096_11828	Bacteria;Proteobacteria;Alphaproteobacteria;Rhodospirillales;Acetobacteraceae;Roseomonas;Roseomonas_lacus
HWI-M02808_85_AJHNL_1_1103_15102_15538	Bacteria;Proteobacteria;Alphaproteobacteria;Rhodobacterales;Rhodobacteraceae;Rhodobacter;uncultured_alpha_proteobacterium
HWI-M02808_85_AJHNL_1_1107_23247_21981	Bacteria;Proteobacteria;Betaproteobacteria;Nitrosomonadales;Nitrosomonadaceae;Nitrosomonas;Nitrosomonas_unclassified
HWI-M02808_85_AJHNL_1_2105_13143_15497	Bacteria;Verrucomicrobia;Opitutae;Opitutales;Opitutaceae;Opitutus;uncultured_Opitutus_sp.
HWI-M02808_85_AJHNL_1_1103_8071_4949	Bacteria;Planctomycetes;Planctomycetacia;Planctomycetales;Planctomycetaceae;Rhodopirellula;Rhodopirellula_unclassified
HWI-M02808_85_AJHNL_1_1101_4497_8927	Bacteria;Firmicutes;Clostridia;Thermoanaerobacterales;SRB2;uncultured_bacterium;uncultured_bacterium_unclassified
HWI-M02808_85_AJHNL_1_1101_17949_2457	Bacteria;Proteobacteria;Betaproteobacteria;Burkholderiales;Comamonadaceae;Hydrogenophaga;Hydrogenophaga_unclassified
HWI-M02808_85_AJHNL_1_1107_14145_21318	Bacteria;Proteobacteria;Alphaproteobacteria;Rhizobiales;Rhizobiaceae;Rhizobium;Rhizobium_unclassified
HWI-M02808_85_AJHNL_1_1101_20048_2184	Bacteria;Proteobacteria;Betaproteobacteria;Burkholderiales;Comamonadaceae;Comamonadaceae_unclassified;Comamonadaceae_unclassified
HWI-M02808_85_AJHNL_1_1101_16854_7369	Bacteria;Bacteroidetes;Bacteroidia;Bacteroidia_Incertae_Sedis;Draconibacteriaceae;Draconibacteriaceae_uncultured;Draconibacteriaceae_unclassified
HWI-M02808_85_AJHNL_1_1101_7284_6821	Bacteria;Chlamydiae;Chlamydiae;Chlamydiales;Simkaniaceae;Simkaniaceae_unclassified;Simkaniaceae_unclassified
HWI-M02808_85_AJHNL_1_1101_9105_4721	Bacteria;Firmicutes;Clostridia;Clostridiales;Syntrophomonadaceae;Dethiobacter;uncultured_bacterium
HWI-M02808_85_AJHNL_1_1108_13218_15855	Bacteria;Bacteroidetes;Bacteroidia;Bacteroidia_Incertae_Sedis;Draconibacteriaceae;Draconibacteriaceae_uncultured;Bacteroidetes_bacterium_enrichment_culture_clone_VNC3B008
HWI-M02808_85_AJHNL_1_1104_8273_4674	Bacteria;Proteobacteria;Betaproteobacteria;Burkholderiales;Comamonadaceae;Hydrogenophaga;Hydrogenophaga_unclassified
HWI-M02808_85_AJHNL_1_1106_19311_2988	Bacteria;Proteobacteria;Gammaproteobacteria;Xanthomonadales;Xanthomonadaceae;Silanimonas;uncultured_gamma_proteobacterium
HWI-M02808_85_AJHNL_1_1101_8018_4755	Bacteria;Firmicutes;Clostridia;Clostridiales;Clostridiaceae_4;Clostridiaceae_4_uncultured;uncultured_bacterium
HWI-M02808_85_AJHNL_1_1101_28097_12743	Bacteria;Proteobacteria;Alphaproteobacteria;Rhodobacterales;Rhodobacteraceae;Rhodobacteraceae_unclassified;Rhodobacteraceae_unclassified
HWI-M02808_85_AJHNL_1_1101_23196_4273	Bacteria;Proteobacteria;Alphaproteobacteria;Rhizobiales;Bradyrhizobiaceae;Bradyrhizobium;Bradyrhizobium_elkanii
HWI-M02808_85_AJHNL_1_2105_22226_4620	Bacteria;Firmicutes;Clostridia;Clostridiales;Clostridiaceae_4;Salimesophilobacter;uncultured_bacterium
HWI-M02808_85_AJHNL_1_1101_23818_10636	Bacteria;Firmicutes;Erysipelotrichia;Erysipelotrichales;Erysipelotrichaceae;Erysipelothrix;uncultured_low_G+C_Gram-positive_bacterium
HWI-M02808_85_AJHNL_1_1101_8850_3213	Bacteria;Proteobacteria;Gammaproteobacteria;Pseudomonadales;Pseudomonadaceae;Pseudomonas;Pseudomonas_stutzeri
HWI-M02808_85_AJHNL_1_2103_22544_20946	Bacteria;Proteobacteria;Betaproteobacteria;Nitrosomonadales;Nitrosomonadaceae;Nitrosomonas;unidentified
HWI-M02808_85_AJHNL_1_1101_7615_8182	Bacteria;Actinobacteria;Nitriliruptoria;Nitriliruptorales;Nitriliruptoraceae;Nitriliruptor;bacterium_Chibacore_1500
HWI-M02808_85_AJHNL_1_1109_13355_7771	Bacteria;Firmicutes;Clostridia;Thermoanaerobacterales;SRB2;SRB2_unclassified;SRB2_unclassified
HWI-M02808_85_AJHNL_1_1107_22980_6232	Bacteria;Proteobacteria;Alphaproteobacteria;Rhizobiales;Methylocystaceae;Methylocystaceae_uncultured;uncultured_bacterium
HWI-M02808_85_AJHNL_1_2102_14598_23066	Bacteria;Firmicutes;Clostridia;Clostridiales;Syntrophomonadaceae;Dethiobacter;uncultured_bacterium
HWI-M02808_85_AJHNL_1_1114_20682_21407	Bacteria;Firmicutes;Clostridia;Clostridiales;Family_XII;Fusibacter;uncultured_Fusibacter_sp.
HWI-M02808_85_AJHNL_1_1101_8931_5002	Bacteria;Firmicutes;Clostridia;Clostridiales;Syntrophomonadaceae;Dethiobacter;uncultured_bacterium
HWI-M02808_85_AJHNL_1_1104_20198_4705	Bacteria;Proteobacteria;Alphaproteobacteria;Caulobacterales;Caulobacteraceae;Phenylobacterium;Phenylobacterium_unclassified
HWI-M02808_85_AJHNL_1_1112_21164_19133	Bacteria;Firmicutes;Clostridia;Clostridiales;P._palm_C-A_51;uncultured_bacterium;uncultured_bacterium_unclassified
HWI-M02808_85_AJHNL_1_1109_20613_22006	Bacteria;Firmicutes;Clostridia;Clostridiales;Peptococcaceae;Desulfitispora;uncultured_bacterium
HWI-M02808_85_AJHNL_1_1101_17192_2407	Bacteria;Firmicutes;Clostridia;Clostridiales;Syntrophomonadaceae;Dethiobacter;uncultured_bacterium
HWI-M02808_85_AJHNL_1_1108_20955_13458	Bacteria;Proteobacteria;Betaproteobacteria;Rhodocyclales;Rhodocyclaceae;Denitratisoma;uncultured_soil_bacterium
HWI-M02808_85_AJHNL_1_2114_4352_18207	Bacteria;Chlorobi;Chlorobia;Chlorobiales;OPB56;uncultured_bacterium;uncultured_bacterium_unclassified
HWI-M02808_85_AJHNL_1_1103_16857_24687	Bacteria;Proteobacteria;Betaproteobacteria;Burkholderiales;Comamonadaceae;Comamonadaceae_unclassified;Comamonadaceae_unclassified
HWI-M02808_85_AJHNL_1_1101_16532_7035	Bacteria;Chloroflexi;Anaerolineae;Anaerolineales;Anaerolinaceae;Bellilinea;Bellilinea_unclassified
HWI-M02808_85_AJHNL_1_1112_14170_19757	Bacteria;Proteobacteria;Deltaproteobacteria;Syntrophobacterales;Syntrophaceae;Smithella;Smithella_unclassified
HWI-M02808_85_AJHNL_1_1104_11682_21160	Bacteria;Proteobacteria;Alphaproteobacteria;Rhizobiales;Methylocystaceae;Methylocystaceae_unclassified;Methylocystaceae_unclassified
HWI-M02808_85_AJHNL_1_1106_10033_4103	Bacteria;Firmicutes;Clostridia;Clostridiales;P._palm_C-A_51;P._palm_C-A_51_unclassified;P._palm_C-A_51_unclassified
HWI-M02808_85_AJHNL_1_1113_15872_17500	Bacteria;Nitrospirae;Nitrospira;Nitrospirales;Nitrospiraceae;Nitrospira;Nitrospira_unclassified
HWI-M02808_85_AJHNL_1_1103_10683_9335	Bacteria;Proteobacteria;Alphaproteobacteria;Rhodobacterales;Rhodobacteraceae;Rhodobacteraceae_unclassified;Rhodobacteraceae_unclassified
HWI-M02808_85_AJHNL_1_1101_24150_5326	Bacteria;Firmicutes;Clostridia;Clostridiales;Peptococcaceae;Desulfitispora;uncultured_bacterium
HWI-M02808_85_AJHNL_1_1107_6126_6665	Bacteria;Proteobacteria;Alphaproteobacteria;Rhizobiales;Rhizobiales_Incertae_Sedis;Phreatobacter;uncultured_bacterium
HWI-M02808_85_AJHNL_1_1109_22908_21284	Bacteria;Proteobacteria;Gammaproteobacteria;Methylococcales;Methylococcaceae;Methylomonas;Methylomonas_unclassified
HWI-M02808_85_AJHNL_1_1104_4942_23661	Bacteria;Acidobacteria;Acidobacteria;Subgroup_4;Subgroup_4_uncultured;Subgroup_4_unclassified;Subgroup_4_unclassified
HWI-M02808_85_AJHNL_1_1110_17696_7989	Bacteria;Proteobacteria;Alphaproteobacteria;Caulobacterales;Caulobacteraceae;Brevundimonas;Brevundimonas_alba
HWI-M02808_85_AJHNL_1_1101_10693_7658	Bacteria;Firmicutes;Clostridia;Clostridiales;Syntrophomonadaceae;Dethiobacter;uncultured_bacterium
HWI-M02808_85_AJHNL_1_1103_21100_6722	Bacteria;Bacteroidetes;Bacteroidetes_unclassified;Bacteroidetes_unclassified;Bacteroidetes_unclassified;Bacteroidetes_unclassified;Bacteroidetes_unclassified
HWI-M02808_85_AJHNL_1_1101_21249_4130	Bacteria;Firmicutes;Clostridia;Clostridiales;Syntrophomonadaceae;Dethiobacter;Dethiobacter_unclassified
HWI-M02808_85_AJHNL_1_1113_19158_10121	Bacteria;Firmicutes;Clostridia;Clostridiales;Family_XIII;Family_XIII_unclassified;Family_XIII_unclassified
HWI-M02808_85_AJHNL_1_1101_22499_5481	Bacteria;Proteobacteria;Alphaproteobacteria;Rhizobiales;Bradyrhizobiaceae;Salinarimonas;Salinarimonas_unclassified
HWI-M02808_85_AJHNL_1_1110_2855_18839	Bacteria;Firmicutes;Clostridia;Clostridiales;Peptococcaceae;Peptococcaceae_uncultured;Peptococcaceae_unclassified
HWI-M02808_85_AJHNL_1_1101_13289_11050	Bacteria;Actinobacteria;Acidimicrobiia;Acidimicrobiales;Acidimicrobiales_uncultured;Acidimicrobiales_unclassified;Acidimicrobiales_unclassified
HWI-M02808_85_AJHNL_1_1112_20122_9065	Bacteria;Bacteria_unclassified;Bacteria_unclassified;Bacteria_unclassified;Bacteria_unclassified;Bacteria_unclassified;Bacteria_unclassified

Table 8 - PhyloPythiaS+ Assigned Taxonomy for each Contig Encoding a Sulfur Gene and Calculated Abundance of each Contig in each Metagenome and Metatranscriptome

gene	KEGG ID	Contig	CSW1.1	QV1.1	CSW1.3	QV1.2	N08-A	N08-B	N08-C	CSWold	CSW1.4	QV1.1 mt	CSWold mt	N08-B mt	QV1.2 mt	Domain	Phyla	Class	Order	Family	Genus	Genus, Species
aprA	K00394	c_000000997749	0.00	0.00	0.00	0.00	0.00	0.00	0.00	69.82	1.04	0.00	10384.23	0.00	42.48	Bacteria	Proteobacteria	Deltaproteobacteria				
aprAB	K00394, K00395	c_000000283170	0.00	0.00	0.00	0.00	0.00	0.00	0.00	145.54	0.00	0.00	487114.56	0.00	0.00	Bacteria	Firmicutes	Clostridia	Clostridiales	Syntrophomonadaceae		
aprAB	K00394, K00395	c_000000848240	0.00	0.00	0.00	2.57	2.22	70.53	0.00	27.90	0.00	0.00	4033.03	2821.95	2090.42	Bacteria	Firmicutes	Clostridia	Clostridiales			
aprAB	K00394, K00395	c_000000000009	57.78	24241.81	1137.75	59.40	243.88	98.03	15.19	205.54	72.88	5438.98	32.15	56.76	82.56	Bacteria						
aprAB	K00394, K00395	c_000000423537	36.51	18.61	13.55	60.36	23.18	22.81	7.87	13.31	75.38	2.04	0.42	7.42	7.77	Bacteria	Proteobacteria	Betaproteobacteria	Hydrogenophilales	Hydrogenophilaceae	Thiobacillus	Thiobacillus denitrificans
aprAB	K00394, K00395	c_000000706742	4.54	4.37	5.73	11.66	21.70	5.89	31.82	2.29	24.58	0.00	301.48	0.00	12.48	Bacteria	Proteobacteria	Betaproteobacteria	Rhodocyclales	Rhodocyclaceae	Dechloromonas	Dechloromonas aromatica
aprB	K00395	c_000000337380	0.00	0.00	0.00	0.00	0.00	0.00	0.00	42.12	0.00	0.00	16553.58	0.00	0.00							
dsrA	K11180	c_000000631759	64.30	7.74	13.56	30.02	86732.15	4792.45	0.00	7907.83	215.43	0.00	0.00	11766.11	17213.37	Bacteria	Proteobacteria	Betaproteobacteria	Rhodocyclales	Rhodocyclaceae	Azoarcus	
dsrA	K11180	c_000000491049	33.69	16.21	14.21	30.46	67908.42	9546.10	28.35	8183.20	106.85	0.00	0.00	8793.94	23854.45	Bacteria	Proteobacteria	Betaproteobacteria	Burkholderiales	Comamonadaceae		
dsrAB	K11180, K11181	c_000000000103	22.98	12.08	12.78	20.62	3.13	14.03	7.06	6.01	56.41	0.00	0.00	2.95	0.00	Bacteria	Proteobacteria	Betaproteobacteria	Hydrogenophilales	Hydrogenophilaceae	Thiobacillus	Thiobacillus denitrificans
dsrAB	K11180, K11181	c_000000284787	0.00	0.00	0.00	0.00	0.00	24.71	0.00	9.61	3.56	0.00	0.00	0.00	401.05	Bacteria	Proteobacteria					
dsrAB	K11180, K11181	c_000000563986	3.41	4.93	4.32	3.19	702.07	119.29	32.33	90.34	31.21	0.00	76.92	44.12	167.93	Bacteria	Proteobacteria	Betaproteobacteria				
dsrAB	K11181, K11180	c_000000285367	0.00	0.00	0.00	2.82	0.00	58.76	0.00	36.50	2.26	0.00	4743.09	1980.40	2596.92	Bacteria	Proteobacteria	Deltaproteobacteria				
dsrAB	K11181, K11180	c_000000774717	83.04	24355.88	1137.08	73.39	206.18	88.78	19.68	191.18	81.19	6924.59	684.59	62.67	103.89	Bacteria	Firmicutes	Clostridia	Clostridiales	Syntrophomonadaceae		
sat	K0057	c_000000398317	28.82	14.10	10833.90	7.23	10.64	17.61	16.21	10.34	26.12	0.00	4.59	0.00	1.48	Bacteria	Proteobacteria	Betaproteobacteria	Burkholderiales	Comamonadaceae	Acidovorax	Acidovorax sp. KKS102
sat	K00956	c_000000977096	84526.58	19876.01	11205.54	72.78	49003.63	50882.12	57.91	6675.43	153.67	9740.85	0.00	10862.14	16924.84	Bacteria	Proteobacteria	Betaproteobacteria	Burkholderiales		Rubrivivax	Rubrivivax gelatinosus
sat	K00956	c_000001130468	54531.37	288.35	224.00	2.70	18.46	29068.37	1.62	3.64	0.54	980.42	0.00	0.00	0.93	Bacteria	Proteobacteria	Betaproteobacteria	Burkholderiales	Comamonadaceae	Acidovorax	Acidovorax sp. KKS102
sat	K00956	c_000000706657	266.54	46.89	0.91	1.01	822.41	543.77	3.89	123.25	2.61	0.00	1.56	1455.56	13515.27	Bacteria	Proteobacteria	Gammaproteobacteria	Methylococcales	Methylococcaceae	Methylomonas	Methylomonas methanica
sat	K00956	c_000000844528	11.47	6.15	3.43	11.39	0.93	5.93	36.45	0.00	2.60	0.00	79.45	0.00	0.64	Bacteria	Proteobacteria	Betaproteobacteria	Rhodocyclales	Rhodocyclaceae	Dechloromonas	Dechloromonas aromatica
sat	K00956, K00957	c_000000901007	14921.21	4163.72	2365.59	18.99	15539.69	8876.58	16.98	2228.88	76.28	2538.42	4.56	980.61	2958.11	Bacteria	Proteobacteria	Betaproteobacteria	Burkholderiales	Comamonadaceae		
sat	K00956, K00957	c_000000706934	20.52	15.59	16.84	21.72	6.00	23.58	21.07	0.78	0.36	0.00	2.67	0.00	0.09	Bacteria	Proteobacteria	Betaproteobacteria	Methylophilales	Methylophilaceae	Methylovorus	
sat	K00956, K00957	c_000000988584	79.20	9142.45	17068.56	6.29	8.43	45.63	5.46	2.79	42.66	2354.78	0.00	0.00	30.35	Bacteria	Firmicutes	Clostridia	Clostridiales	Syntrophomonadaceae	Dethiobacter	Dethiobacter alkaliphilus
sat	K00956, K00957	c_000000283369	433.91	8466.31	11.35	9.29	9066.61	359.80	3.94	361.66	27.97	1356.55	1.11	240.51	0.00	Bacteria	Firmicutes	Clostridia	Clostridiales			
sat	K00956, K00957	c_000001130590	7.82	8.77	13.27	8426.91	1.34	4.59	0.93	0.47	817.90	0.00	0.00	0.00	581.92	Bacteria	Bacteroidetes	Cytophagia	Cytophagales	Cyclobacteriaceae	Belliella	Belliella baltica
sat	K00957	c_000000918750	125814.64	38594.52	18683.03	99.12	108815.23	74943.16	34.18	12715.45	414.81	1085.08	0.00	15617.41	2041.07	Bacteria	Proteobacteria	Betaproteobacteria	Burkholderiales	Comamonadaceae		
sat	K00957	c_000000706203	8.09	0.00	1811.77	797.88	6.46	136.22	210.66	0.00	3.02	0.00	113.62	311.45	46465.63	Bacteria	Proteobacteria	Alphaproteobacteria	Rhizobiales	Methylocystaceae	Methylocystis	Methylocystis sp. SC2
sat	K00957	c_000000423398	0.00	0.00	327.65	1.36	0.00	0.00	0.00	1.60	1.19	33.54	0.00	0.00	34644.73	Bacteria	Proteobacteria	Alphaproteobacteria				
sat	K00957	c_000000289758	0.00	11.84	2449.62	2755.79	29.48	0.00	13.80	43.41	174.15	0.00	0.00	0.00	2076.87	Bacteria	Proteobacteria	Gammaproteobacteria				
sat	K00957	c_000000493173	0.00	0.00	241.42	3525.73	16.07	0.00	180.56	15.22	25865.78	0.00	0.00	511.00	44.29	Bacteria	Proteobacteria	Gammaproteobacteria	Xanthomonadales	Xanthomonadaceae	Pseudoxanthomonas	Pseudoxanthomonas suwonensis
sat	K00957	c_000000564124	9.15	5.75	3.30	3.32	16.94	3.63	20972.95	0.36	0.00	0.00	0.00	0.00	0.00	Bacteria						
sat	K00957	c_000000486621	0.00	0.00	18.37	4.07	0.00	0.00	2.44	0.00	10342.90	0.00	0.00	0.00	0.00	Bacteria	Proteobacteria	Alphaproteobacteria	Rhizobiales			
sat	K00957	c_000000707125	0.00	0.77	9.41	484.47	0.00	0.00	0.00	3.22	7795.69	0.00	0.00	0.00	0.00	Bacteria	Proteobacteria					
sat	K00958	c_000000997109	0.00	0.00	0.00	0.00	0.00	56.90	0.00	44.28	0.00	0.00	13589.05	4758.88	4230.45	Bacteria	Proteobacteria	Deltaproteobacteria				
sat	K00958	c_000000564734	0.00	0.00	0.00	0.00	0.00	0.00	0.00	102.82	0.00	0.00	91198.10	0.00	0.00	Bacteria						
sat	K00958	c_000000283222	21.37	10.66	12.23	79.51	0.61	12.36	11.57	13.09	91.58	0.00	0.00	0.00	1.97	Bacteria	Proteobacteria	Betaproteobacteria	Hydrogenophilales	Hydrogenophilaceae	Thiobacillus	Thiobacillus denitrificans
sat	K00958	c_000000988663	20.77	10.98	6.69	11.09	4.56	10.38	6.40	4.31	41.02	0.00	0.00	0.00	0.00	Bacteria	Proteobacteria	Betaproteobacteria	Hydrogenophilales	Hydrogenophilaceae	Thiobacillus	Thiobacillus denitrificans
sat	K00958	c_000000995678	0.00	0.00	0.00	0.00	0.00	0.00	0.00	12469.00	0.00	0.00	203.96	0.00	0.00	Bacteria	Actinobacteria	Actinobacteria	Actinomycetales			
sat	K00958	c_000000706642	9.35	2.71	0.00	1.76	10.52	7.89	11341.59	0.00	0.00	0.00	0.00	0.00	0.00	Archaea	Thaumarchaeota		Nitrosopumilales	Nitrosopumilaceae		
sat	K00958	c_000000853757	0.00	0.00	0.00	0.00	0.00	0.00	0.00	9.24	0.00	0.00	10183.02	0.00	21.09	Bacteria	Proteobacteria	Deltaproteobacteria				
sat, aprA	K00958, K00394	c_000000988818	19.19	13.12	12.75	19.06	2.56	12.44	5.40	3.64	85.97	0.00	2.91	0.00	0.58	Bacteria	Proteobacteria	Betaproteobacteria	Hydrogenophilales	Hydrogenophilaceae	Thiobacillus	Thiobacillus denitrificans
sat, aprA	K00958, K00394	c_000000848590	0.00	0.00	0.00	0.00	0.00	58.23	0.00	5.66	35.64	0.00	0.00	0.00	300.05	Bacteria	Proteobacteria	Deltaproteobacteria				
sat, sseA	K01011, K00956, K00957	c_000001130721	48.12	28.05	158.09	39949.88	13.37	38.06	63.15	1.89	15.71	0.00	1.25	0.00	2152.07	Bacteria	Proteobacteria	Betaproteobacteria	Rhodocyclales	Rhodocyclaceae	Dechloromonas	Dechloromonas aromatica
phsA	K008352	c_000000706397	0.00	0.00	0.00	2.40	4114.25	742.20	8.65	427.61	23.91	0.00	0.00	2652.94	0.00	Bacteria	Deinococcus-Thermus	Deinococci	Deinococcales	Trueperaceae	Truepera	Truepera radiovictrix
phsA	K08352	c_000000712386	19.15	5804.73	4.04	0.00	434.45	43.43	0.00	71.38	21.47	73203.83	0.00	246.68	6.49	Bacteria	Proteobacteria	Gammaproteobacteria				
phsA	K08352	c_000000002143	182.72	831.40	1574.87	0.00	808.11	123.31	0.00	156.50	7.46	37888.28	114.24	800.17	22.45	Bacteria	Firmicutes	Clostridia	Clostridiales	Syntrophomonadaceae	Dethiobacter	Dethiobacter alkaliphilus
sseA	K01011	c_000000988440	2.30	1.11	0.97	1.61	606.80	313.25	3.87	81.83	0.86	27.97	2.12	4738.30	34224.89	Bacteria	Proteobacteria	Gammaproteobacteria	Methylococcales	Methylococcaceae	Methylomonas	Methylomonas methanica
sseA	K01011	c_000000988355	0.00	0.00	0.00	924.97	0.00	0.00	7.39	0.00	3.59	0.00	6.37	0.00	11236.07	Bacteria	Proteobacteria	Betaproteobacteria	Rhodocyclales	Rhodocyclaceae	Thauera	
sseA	K01011	c_000001130720	43.40	27.72	169.50	40932.68	15.68	35.43	71.76	1.51	21.31	0.00	1.54	0.00	4212.05	Bacteria	Proteobacteria	Betaproteobacteria	Rhodocyclales	Rhodocyclaceae	Dechloromonas	Dechloromonas aromatica
sseA	K01011	c_000000670881	0.00	0.00	29.41	2981.63	0.00	0.00	0.00	21.05	23826.74	0.00	0.00	0.00	0.00	Bacteria	Proteobacteria					
sseA	K01011	c_000000563829	4.41	3.30	76.06	3380.51	1.82	2.86	32.02	26.35	19868.45	0.00	2.09	0.00	2.12	Bacteria	Proteobacteria	Betaproteobacteria	Burkholderiales	Comamonadaceae		
sseA	K01011	c_000000007983	17790.20	6391.00	22.17	18.11	379.74	9555.44	2.70	127.75	48.58	5806.54	0.00	22453.38	167.66	Bacteria	Proteobacteria	Deltaproteobacteria	Myxococcales			
sseA	K01011	c_000000423185	81.89	17.23	21362.15	1.15	25.51	54.84	1.49	1.34	1.98	0.00	0.00	0.00	3.95	Bacteria	Firmicutes					
sseA	K01011	c_000000706442	3.58	5.15	2.26	5.01	15.72	4.64	20849.28	1.80	0.00	0.00	1.71	0.00	0.00	Archaea	Thaumarchaeota					
sseA	K01011	c_000000847966	3.60	5.20	6.06	20.11	0.00	4.67	4.04	4.50	37.63	0.00	0.00	0.00	0.00	Bacteria	Proteobacteria	Betaproteobacteria	Hydrogenophilales	Hydrogenophilaceae	Thiobacillus	Thiobacillus denitrificans
sseA	K01011	c_000000989118	11.30	3.59	2.64	3.28	24.10	7.61	19601.26	0.40	0.00	0.00	0.37	0.00	0.00	Archaea	Thaumarchaeota		Nitrosopumilales	Nitrosopumilaceae		
sseA	K01011	c_000000848504	18.38	12.64	6.65	7.36	14.69	11.91	19365.54	0.00	0.00	0.00	0.00	0.00	0.00	Archaea	Thaumarchaeota		Nitrosopumilales	Nitrosopumilaceae		
sseA	K01011	c_000000072116	22.66	21.81	0.00	0.00	18.11	14.68	17752.16	0.00	0.00	0.00	0.00	0.00	0.00	Archaea	Thaumarchaeota		Nitrosopumilales	Nitrosopumilaceae		
sseA	K01011	c_000000425171	0.00	5.30	3.10	3.43	4058.11	541.06	8.24	369.30	16.47	0.00	0.00	839.09	0.00	Bacteria	Deinococcus-Thermus	Deinococci	Deinococcales	Trueperaceae	Truepera	Truepera radiovictrix
sseA	K01011	c_000000140882	0.00	0.00	0.00	0.00	0.00	0.00	0.00	15840.65	2.54	0.00	233.62	0.00	0.00	Bacteria	Actinobacteria	Actinobacteria	Actinomycetales			
sseA	K01011	c_000001130348	0.00	0.00	7.41	0.00	1.75	0.00	0.00	5.53	11442.87	0.00	0.00	0.00	0.00	Bacteria	Proteobacteria	Alphaproteobacteria				
sseA	K01011	c_000000993730	54.84	4.58	4.01	3.55	0.00	22.21	26.69	0.00	3.58	0.00	117.75	0.00	0.00	Bacteria	Proteobacteria	Betaproteobacteria	Rhodocyclales	Rhodocyclaceae	Dechloromonas	Dechloromonas aromatica
sseA	K01011	c_000000988651	38.32	10.91	10766.41	10.43	7.82	21.79	20.86	20.32	37.17	0.00	5.77	185.50	7.90	Bacteria	Proteobacteria	Betaproteobacteria	Burkholderiales	Comamonadaceae	Polaromonas	
sseA	K01011	c_000000002451	4.90	0.00	0.00	0.00	0.00	9.19	10378.67	0.00	0.00	0.00	0.00	0.00	0.00	Archaea	Thaumarchaeota		Nitrosopumilales	Nitrosopumilaceae	Nitrosopumilus	Nitrosopumilus maritimus
sseA	K01011	c_000000282673	23.74	14.48	9807.09	21.81	12.44	15.40	55.90	91.22	107.40	0.00	7.30	130.64	9.76	Bacteria	Proteobacteria	Betaproteobacteria	Burkholderiales	Comamonadaceae	Acidovorax	Acidovorax sp. KKS102
sseA	K01011	c_000000000140	0.00	0.00	5.51	416.76	0.73	0.00	0.51	3.44	7049.61	0.00	0.00	0.00	0.00	Bacteria	Proteobacteria	Alphaproteobacteria	Rhodobacterales			
sseA	K01011	c_000000328761	0.00	3.03	0.00	11.76	0.00	0.00	7.06	0.00	0.00	0.00	12.01	0.00	0.00	Bacteria	Proteobacteria	Betaproteobacteria				
sqr	K17218	c_000000581008	0.00	0.00	0.00	0.00	0.00	0.00	0.00	13433.39	0.00	0.00	218.76	0.00	0.00	Bacteria	Actinobacteria	Actinobacteria	Actinomycetales	Nocardioidaceae		
sqr	K17218	c_000000140824	65032.49	19877.86	10964.38	142.00	94048.06	42273.69	36.48	10542.71	305.12	3247.87	0.00	4368.36	5662.39	Bacteria	Proteobacteria	Betaproteobacteria	Burkholderiales	Comamonadaceae	Polaromonas	
sqr	K17218	c_000000459937	12009.32	2729.13	2388.33	90.36	78010.96	10452.47	32.71	7869.74	271.75	1684.04	4.66	2377.53	17985.21	Bacteria	Proteobacteria	Betaproteobacteria	Burkholderiales	Comamonadaceae	Polaromonas	
sqr	K17218	c_000000000017	60.43	24400.52	1128.18	63.06	155.95	79.74	21.98	207.90	79.64	8105.34	72.77	231.47	149.80	Bacteria	Firmicutes	Clostridia	Clostridiales	Syntrophomonadaceae		
sqr	K17218	c_000000706490	0.00	3.58	51.03	3078.38	0.00	0.00	1.04	27.23	27054.57	0.00	0.00	0.00	2.00	Bacteria	Proteobacteria					
sqr	K17218	c_000000988639	29.87	9.66	15.09	25.01	5.17	20.57	19.83	0.24	0.35	0.00	7.15	0.00	0.68	Bacteria	Proteobacteria	Betaproteobacteria	Methylophilales	Methylophilaceae	Methylovorus	
sqr	K17218	c_000000285577	16.66	0.00	986.35	1118.55	8.88	168.61	227.23	11.20	8.30	154.26	121.94	0.00	23397.80	Bacteria	Proteobacteria	Alphaproteobacteria	Rhizobiales	Methylocystaceae	Methylocystis	Methylocystis sp. SC2
sqr	K17218	c_000000461334	0.00	0.00	2123.69	1523.21	0.00	0.00	0.00	15.40	17.06	0.00	0.00	0.00	1425.64	Bacteria	Proteobacteria	Alphaproteobacteria	Caulobacterales	Caulobacteraceae		
sqr	K17218	c_000000141364	10180.24	3145.86	1258.00	17.01	12908.74	6532.75	6.83	2087.76	67.28	103.21	0.00	481.90	946.26	Bacteria	Proteobacteria	Betaproteobacteria	Burkholderiales	Comamonadaceae	Polaromonas	
sqr	K17218	c_000000433572	0.00	0.00	0.00	875.77	0.00	0.00	0.00	0.00	11.33	0.00	14.53	0.00	1786.88	Bacteria	Proteobacteria	Gammaproteobacteria				
sqr	K17218	c_000000847661	0.00	0.65	0.00	1.26	4299.42	568.53	2.27	378.73	23.60	0.00	0.00	1793.18	0.00	Bacteria	Deinococcus-Thermus	Deinococci	Deinococcales	Trueperaceae	Truepera	Truepera radiovictrix
sqr	K17218	c_000000564250	0.00	0.00	1.38	0.00	610.70	407.95	4.93	96.32	1.30	5.06	1.64	3993.35	15502.00	Bacteria	Proteobacteria	Gammaproteobacteria				
sqr	K17218	c_000000283007	30.11	11.94	10.99	23.77	4.18	16.12	5.14	8.58	58.19	0.00	0.00	0.00	1.39	Bacteria	Proteobacteria	Betaproteobacteria	Hydrogenophilales	Hydrogenophilaceae	Thiobacillus	Thiobacillus denitrificans
sqr	K17218	c_000000282745	11.32	8.47	6.22	11.56	2.83	6.42	12.26	7.09	62.60	0.00	0.00	0.00	3.05	Bacteria	Proteobacteria	Betaproteobacteria	Hydrogenophilales	Hydrogenophilaceae	Thiobacillus	Thiobacillus denitrificans
sqr	K17218	c_000000847790	10.93	3.56	4.29	4.21	15.54	7.62	17421.41	0.25	0.00	0.00	0.00	0.00	0.00	Bacteria	Actinobacteria	Actinobacteria				
sqr	K17218	c_000000283105	9.92	8.30	9.66	13.51	3.47	8.71	5.89	4.06	38.21	0.00	0.00	0.00	0.00	Bacteria	Proteobacteria	Betaproteobacteria	Hydrogenophilales	Hydrogenophilaceae	Thiobacillus	Thiobacillus denitrificans
sqr	K17218	c_000000448349	73055.51	16991.27	1174.83	78.17	6809.68	38999.13	23.56	719.20	86.27	5221.91	0.00	0.00	3522.51	Bacteria	Actinobacteria	Actinobacteria	Actinomycetales			
fccB	K17229	c_000000283845	45.45	10.94	9.59	0.00	8.72	22.09	3.19	0.00	21.23	0.00	0.00	0.00	0.00	Bacteria	Proteobacteria	Betaproteobacteria	Rhodocyclales	Rhodocyclaceae	Dechloromonas	Dechloromonas aromatica
fccB	K17229	c_000000564232	16.32	10.16	9.31	20.10	4.60	11.20	4.31	2.42	42.30	0.00	0.00	0.00	0.00	Bacteria	Proteobacteria	Betaproteobacteria	Hydrogenophilales	Hydrogenophilaceae	Thiobacillus	Thiobacillus denitrificans
fccB	K17229	c_000000141967	0.00	4.05	1.77	421.29	0.00	0.00	0.00	8.08	7458.79	0.00	0.00	0.00	0.00	Bacteria	Proteobacteria	Alphaproteobacteria	Sphingomonadales	Sphingomonadaceae		

Table 9 - dsrAB Phylogenetic Tree Data

ID (PROKKA)	Contig	Site	# aa
#PROKKA_06633_sulfite_reductase_dissimilatory-type_beta_subunit	c_000000000103	CROMO	356
#PROKKA_06634_sulfite_reductase_dissimilatory-type_alpha_subunit	c_000000000103	CROMO	433
#PROKKA_135376_dsrA_sulfite_reductase_dissimilatory-type_beta_subunit	c_000000155579	CROMO	85
#PROKKA_150636_dsrA_DsrA:_sulfite_reductase_dissimilatory-type_subunit_alpha	c_000000176231	CROMO	68
#PROKKA_15420_sulfite_reductase_dissimilatory-type_alpha_subunit	contig-25435000000	LCY 3862	394
#PROKKA_16556_sulfite_reductase_dissimilatory-type_beta_subunit	contig-42395000000	LCY H08	61
#PROKKA_17090_dissimilatory_sulfite_reductase_subunit_B	contig-46854000000	LCY H08	55
#PROKKA_192588_sulfite_reductase_dissimilatory-type_alpha_subunit	c_000000282889	CROMO	432
#PROKKA_192589_sulfite_reductase_dissimilatory-type_beta_subunit	c_000000282889	CROMO	357
#PROKKA_196276_dsrA_sulfite_reductase_dissimilatory-type_subunit_alpha	c_000000282982	CROMO	431
#PROKKA_196277_sulfite_reductase_dissimilatory-type_beta_subunit	c_000000282982	CROMO	357
#PROKKA_210993_dsrA_dissimilatory-type_sulfite_reductase_subuit_alpha	c_000000284787	CROMO	402
#PROKKA_210994_dsrB_dissimilatory-type_sulfite_reductase_subuit_beta	c_000000284787	CROMO	356
#PROKKA_213122_sulfite_reductase_dissimilatory-type_beta_subunit	c_000000285367	CROMO	395
#PROKKA_213123_sulfite_reductase_dissimilatory-type_alpha_subunit	c_000000285367	CROMO	474
#PROKKA_21789_dsrA_dissimilatory-type_sulfite_reductase_subuit_alpha	contig-2000003	LIG	402
#PROKKA_21790_dsrB_dissimilatory-type_sulfite_reductase_subuit_beta	contig-2000003	LIG	356
#PROKKA_224266_sulfite_reductase_dissimilatory-type_beta_subunit	c_000000290566	CROMO	295
#PROKKA_225542_dsrA_dissimilatory_sulfite_reductase_alpha_subunit	c_000000291373	CROMO	68
#PROKKA_232924_sulfite_reductase_dissimilatory-type_alpha_subunit	c_000000297434	CROMO	236
#PROKKA_24745_DsrA_protein	contig-1323000001	LCY H08	195
#PROKKA_32198_dissimilatory_sulfite_reductase_alpha_subunit	c_000000006519	CROMO	260
#PROKKA_32600_sulfite_reductase_dissimilatory-type_alpha_subunit	contig-14191000001	LCY H08	111
#PROKKA_326785_dsrB_dissimilatory_sulfite_reductase_subunit_B	c_000000449980	CROMO	122
#PROKKA_330124_sulfite_reductase_dissimilatory-type_beta_subunit	c_000000455538	CROMO	357
#PROKKA_330125_dissimilatory_sulfite_reductase_alpha_subunit	c_000000455538	CROMO	413
#PROKKA_339325_sulfite_reductase_dissimilatory-type_alpha_subunit	c_000000475836	CROMO	105
#PROKKA_344146_dsrA_sulfite_reductase_dissimilatory-type_subunit_alpha	c_000000491049	CROMO	181
#PROKKA_349922_sulfite_reductase_dissimilatory-type_beta_subunit	c_000000516947	CROMO	82
#PROKKA_357997_sulfite_reductase_dissimilatory-type_beta_subunit	c_000000563866	CROMO	358
#PROKKA_357998_dsrA_sulfite_reductase_dissimilatory-type_subunit_alpha	c_000000563866	CROMO	431
#PROKKA_359047_dsrA_sulfite_reductase_dissimilatory-type_alpha_subunit	c_000000563943	CROMO	433
#PROKKA_359048_dsrB_sulfite_reductase_dissimilatory-type_subunit_beta	c_000000563943	CROMO	356
#PROKKA_42087_sulfite_reductase_dissimilatory-type_subunit_alpha	contig-14436000005	LIG	437
#PROKKA_42088_sulfite_reductase_dissimilatory-type_beta_subunit	contig-14436000005	LIG	382
#PROKKA_436008_sulfite_reductase_dissimilatory-type_subunit_alpha	c_000000631759	CROMO	157
#PROKKA_444110_sulfite_reductase_dissimilatory-type_beta_subunit	c_000000669909	CROMO	44
#PROKKA_451956_sulfite_reductase_beta_subunit	c_000000706274	CROMO	197
#PROKKA_458890_sulfite_reductase_dissimilatory-type_alpha_subunit	c_000000706678	CROMO	387
#PROKKA_458891_dsrB_dissimilatory_sulfite_reductase_subunit_B	c_000000706678	CROMO	354
#PROKKA_473929_sulfite_reductase_dissimilatory-type_beta_subunit	c_000000706981	CROMO	392
#PROKKA_473930_sulfite_reductase_dissimilatory-type_alpha_subunit	c_000000706981	CROMO	478
#PROKKA_498107_dissimilatory_sulfite_reductase_alpha_subunit	c_000000711526	CROMO	397
#PROKKA_498108_dissimilatory_sulfite_reductase_beta_subunit	c_000000711526	CROMO	357
#PROKKA_539296_dissimilatory_sulfite_reductase_beta_subunit	c_000000774717	CROMO	352
#PROKKA_539297_sulfite_reductase_dissimilatory-type_alpha_subunit	c_000000774717	CROMO	395
#PROKKA_539303_hydrogensulfite_reductase	c_000000774717	CROMO	368
#PROKKA_579882_sulfite_reductase_dissimilatory-type_alpha_subunit	c_000000850202	CROMO	474
#PROKKA_587390_hydrogensulfite_reductase	c_000000853312	CROMO	368
#PROKKA_61903_dissimilatory_sulfite_reductase_alpha_subunit	c_000000042697	CROMO	144
#PROKKA_64417_dsrA_dissimilatory_sulfite_reductase_alpha_subunit	c_000000048840	CROMO	68
#PROKKA_655163_sulfite_reductase_dissimilatory-type_alpha_subunit	c_000000988828	CROMO	434
#PROKKA_674702_dissimilatory_sulfite_reductase_alpha_subunit	c_000000993551	CROMO	387
#PROKKA_700089_sulfite_reductase_dissimilatory-type_alpha_subunit	c_000001017955	CROMO	150
#PROKKA_723091_dsrA_Sulfite_reductase_dissimilatory-type_subunit_alpha	c_000001090005	CROMO	88
#PROKKA_733294_dsrA_sulfite_reductase_dissimilatory-type_subunit_alpha	c_000001130442	CROMO	431
#PROKKA_81017_sulfite_reductase_dissimilatory-type_beta_subunit	c_000000121447	CROMO	353
#PROKKA_81018_dsrA_sulfite_reductase_dissimilatory-type_subunit_alpha	c_000000121471	CROMO	431
#PROKKA_95979_dsrA_sulfite_reductase_dissimilatory-type_alpha_subunit	c_000000141084	CROMO	432

Predicted protein length cutoff value:	40
Longest sequence (number of amino acids)	478
aa = amino acids	

REFERENCES

REFERENCES

Albert, D. B. & Martens, C. S. Determination of low-molecular-weight organic acid concentrations in seawater and pore-water samples via HPLC. *Mar. Chem.* **56,** 27–37 (1997).

Alcalá, F. J. & Custodio, E. Using the Cl/Br ratio as a tracer to identify the origin of salinity in aquifers in Spain and Portugal. *J. Hydrol.* **359,** 189–207 (2008).

Amend, J. P., McCollom, T. M., Hentscher, M. & Bach, W. Catabolic and anabolic energy for chemolithoautotrophs in deep-sea hydrothermal systems hosted in different rock types. *Geochim. Cosmochim. Acta* **75,** 5736–5748 (2011).

Barnes, I., Oneil, J. R. & Trescases, J. J. Present Day Serpentinization in New-Caledonia, Oman and Yugoslavia. *Geochim. Cosmochim. Acta* **42,** 144–145 (1978).

Barnes, I., Lamarche, V. C. & Himmelberg, G. Geochemical Evidence of Present-Day Serpentinization. **156,** 830–832 (2015).

Beller, H. R. *et al.* The genome sequence of the obligately chemolithoautotrophic, facultatively anaerobic bacterium Thiobacillus denitrificans. *J. Bacteriol.* **188,** 1473–1488 (2006).

Blank, J. G. *et al.* An alkaline spring system within the Del Puerto Ophiolite (California, USA): A Mars analog site. *Planet. Space Sci.* **57,** 533–540 (2009).

Boisvert, S., Raymond, F., Godzaridis, E., Laviolette, F. & Corbeil, J. Ray Meta: scalable de novo metagenome assembly and profiling. *Genome Biol.* **13,** R122 (2012).

Boschetti, T. & Toscani, L. Springs and streams of the Taro-Ceno Valleys (Northern Apennine, Italy): Reaction path modeling of waters interacting with serpentinized ultramafic rocks. *Chem. Geol.* **257,** 76–91 (2008).

Brazelton, W. J., Mehta, M. P., Kelley, D. S. & Baross, J. A. Physiological differentiation within a single-species biofilm fueled by serpentinization. *MBio* **2,** 1–9 (2011).

Brazelton, W. J., Morrill, P. L., Szponar, N. & Schrenk, M. O. Bacterial communities associated with subsurface geochemical processes in continental serpentinite springs. *Appl. Environ. Microbiol.* **79,** 3906–3916 (2013).

Brazelton, W. J., Nelson, B. & Schrenk, M. O. Metagenomic evidence for H2 oxidation and H2 production by serpentinite-hosted subsurface microbial communities. *Front. Microbiol.* **2,** 1–16 (2012).

Callahan, B. J., McMurdie, P. J. & Holmes, S. P. Exact sequence variants should replace operational taxonomic units in marker gene data analysis. *ISME J.* 113597 (2017). doi:doi:10.1038/ismej.2017.119

Cardace, D. *et al.* Establishment of the Coast Range ophiolite microbial observatory (CROMO): Drilling objectives and preliminary outcomes. *Sci. Drill.* 45–55 (2013). doi:10.5194/sd-16-45-2013

Cardace, D. & Hoehler, T. M. Serpentinizing Fluids Craft Microbial Habitat. *Northeast. Nat.* **4,** 133–144 (2009).

Cardace, D., Meyer-Dombard, D. R., Woycheese, K. M. & Arcilla, C. A. Feasible metabolisms in high pH springs of the Philippines. *Front. Microbiol.* **6,** 10 (2015).

Carpenter, A. B., Origin and chemical evolution of brines in sedimentary basins. *Oklahoma Geologic Survey Circular 79*, 60-76. (1978).

Caspi, R. *et al.* The MetaCyc database of metabolic pathways and enzymes and the BioCyc collection of pathway/genome databases. *Nucleic Acids Res.* **44,** D471–D480 (2016).

Chavagnac, V., Monnin, C., Ceuleneer, G., Boulart, C. & Hoareau, G. Characterization of hyperalkaline fluids produced by low-temperature serpentinization of mantle peridotites in the Oman and Ligurian ophiolites. *Geochemistry, Geophys. Geosystems* **14,** 2496–2522 (2013).

Chivian, D. *et al.* Environmental Genomics Reveals a Single-Species Ecosystem Deep Within Earth. *Science (80-.).* **322,** 275–278 (2008).

Choi, S. H., Shervais, J. W. & Mukasa, S. B. Supra-subduction and abyssal mantle peridotites of the Coast Range ophiolite, California. *Contrib. to Mineral. Petrol.* **156,** 551–576 (2008).

Cipolli, F., Gambardella, B., Marini, L., Ottonello, G. & Zuccolini, M. V. Geochemistry of high-pH waters from serpentinites of the Gruppo di Voltri (Genova, Italy) and reaction path modeling of CO2 sequestration in serpentinite aquifers. *Appl. Geochemistry* **19,** 787–802 (2004).

Cline, J. D. Spectrophotometric determination of hydrogen sulfide in natural waters. *Limnol. Oceanogr.* 454–458 (1969). doi:10.4319/lo.1969.14.3.0454

Crespo-Medina, M. *et al.* Insights into environmental controls on microbial communities in a continental serpentinite aquifer using a microcosm-based approach. *Front. Microbiol.* **5,** 604 (2014).

Crespo-Medina, M. *et al.* Methane Dynamics in a Tropical Serpentinizing Environment: The Santa Elena Ophiolite, Costa Rica. *Front. Microbiol.* **8,** 1–14 (2017).

Culkin, F. & Cox, R. A. Sodium, potassium, magnesium, calcium and strontium in sea water. *Deep Sea Res.* **13,** 789–804 (1966).

Darling, A. E. *et al.* PhyloSift: phylogenetic analysis of genomes and metagenomes. *PeerJ* **2,** e243 (2014).

Delacour, A., Früh-Green, G. L., Bernasconi, S. M., Schaeffer, P. & Kelley, D. S. Carbon geochemistry of serpentinites in the Lost City Hydrothermal System (30N, MAR). *Geochim. Cosmochim. Acta* **72,** 3681–3702 (2008).

Dilek, Y. & Furnes, H. Ophiolite genesis and global tectonics: Geochemical and tectonic fingerprinting of ancient oceanic lithosphere. *Bull. Geol. Soc. Am.* **123,** 387–411 (2011).

Edgar, R. C., Haas, B. J., Clemente, J. C., Quince, C. & Knight, R. UCHIME improves sensitivity and speed of chimera detection. *Bioinformatics* **27,** 2194–2200 (2011).

Etiope, G., Schoell, M. & Hosgörmez, H. Abiotic methane flux from the Chimaera seep and Tekirova ophiolites (Turkey): Understanding gas exhalation from low temperature serpentinization and implications for Mars. *Earth Planet. Sci. Lett.* **310,** 96–104 (2011).

Glass, E. M. & Meyer, F. The Metagenomics RAST Server: A Public Resource for the Automatic Phylogenetic and Functional Analysis of Metagenomes. *Handb. Mol. Microb. Ecol. I Metagenomics Complement. Approaches* **8,** 325–331 (2011).

Hanson, N. W., Konwar, K. M. & Hallam, S. J. LCA∗: An entropy-based measure for taxonomic assignment within assembled metagenomes. *Bioinformatics* **32,** 3535–3542 (2016).

Hem, J. D. *Study and Interpretation of the Chemical Characteristics of Natural Water*. (United States Geological Survey, 1985).

Hobbie JE Jasper S, D. R. J. Use of nuclepore filter counting bacteria by fluoroscence microscopy. *Appl. Environ. Microbiol.* **33,** 1225–1228 (1977).

Huot, F. & Maury, R. C. The Round Mountain serpentinite mélange, northern Coast Ranges of California: An association of backarc and arc-related tectonic units. *Bull. Geol. Soc. Am.* **114,** 109–123 (2002).

Hyatt, D. *et al.* Prodigal: prokaryotic gene recognition and translation initiation site identification. *BMC Bioinformatics* **11,** 119 (2010).

Johnson, J. W., Oelkers, E. H. & Helgeson, H. C. *SUPCRT92: a soft- ware package for calculating the standard molal thermodynamic properties ofminerals, gases, aqueous species, and reactions from 1 bar to 5000 bar and 0Cto 1000C*. *Computers and Geosciences* **18,** (1992).

Joye, S. B. *et al.* The anaerobic oxidation of methane and sulfate reduction in sediments from Gulf of Mexico cold seeps. *Chem. Geol.* **205,** 219–238 (2004).

Katz, B. G., Eberts, S. M. & Kauffman, L. J. Using Cl/Br ratios and other indicators to assess potential impacts on groundwater quality from septic systems: A review and examples from principal aquifers in the United States. *J. Hydrol.* **397,** 151–166 (2011).

Kelley, D. S. *et al.* A Serpentinite-Hosted Ecosystem: The Lost City Hydrothermal Field. *Science (80-.).* **307,** 1428–1434 (2005).

Kelly, D. P., Shergill, J. K., Lu, W. P. & Wood, A. P. Oxidative metabolism of inorganic sulfur compounds by bacteria1. Kelly DP, Shergill JK, Lu WP, Wood AP. Oxidative metabolism of inorganic sulfur compounds by bacteria. Antonie Van Leeuwenhoek. 1997;71(1-2):95-107.. *Antonie Van Leeuwenhoek* **71,** 95–107 (1997).

Kohl, A. L., Cumming, E., Cox, A., Rietze, A. & Morrissey, L. Exploring the metabolic potential of microbial communities in ultra-basic, reducing springs at The Cedars, CA, US: Experimental evidence of microbial methanogenesis and heterotrophic acetogenesis. (2016). doi:10.1002/2015JG003233

Kozich, J. J., Westcott, S. L., Baxter, N. T., Highlander, S. K. & Schloss, P. D. Development of a dual-index sequencing strategy and curation pipeline for analyzing amplicon sequence data on the miseq illumina sequencing platform. *Appl. Environ. Microbiol.* **79,** 5112–5120 (2013).

Kuhar, C. W. In the Deep End: Pooling Data and Other Statistical Challenges of Zoo and Aquarium Research. *Zoo Biol.* **25,** 339–352 (2006).

Lang, S. Q. *et al.* Microbial utilization of abiogenic carbon and hydrogen in a serpentinite-hosted system. *Geochim. Cosmochim. Acta* **92,** 82–99 (2012).

Langmead, B. & Salzberg, S. L. Fast gapped-read alignment with Bowtie 2. *Nat. Methods* **9,** 357–359 (2013).

Li, H. & Durbin, R. Fast and accurate short read alignment with Burrows-Wheeler transform. *Bioinformatics* **25,** 1754–1760 (2009).

Li, Z. X. A. & Lee, C. T. A. Geochemical investigation of serpentinized oceanic lithospheric mantle in the Feather River Ophiolite, California: Implications for the recycling rate of water by subduction. *Chem. Geol.* **235,** 161–185 (2006).

Lin, C. & Stahl, D. A. Taxon-specific probes for the cellulolytic genus Fibrobacter reveal abundant and novel equine-associated populations. *Appl. Environ. Microbiol.* **61,** 1348–1351 (1995).

Ludwig, K. A., Kelley, D. S., Butterfield, D. A., Nelson, B. K. & Früh-Green, G. Formation and evolution of carbonate chimneys at the Lost City Hydrothermal Field. *Geochim. Cosmochim. Acta* **70,** 3625–3645 (2006).

Macgregor, B. J. *et al.* Crenarchaeota in Lake Michigan sediment . Crenarchaeota in Lake Michigan Sediment †. *Appl. Environ. Microbiol.* **63,** 1178–1181 (1997).

Marques, J. M. *et al.* Origins of high pH mineral waters from ultramafic rocks, Central Portugal. *Appl. Geochemistry* **23,** 3278–3289 (2008).

Mayhew, L. E., Ellison, E. T., McCollom, T. M., Trainor, T. P. & Templeton, A. Hydrogen generation from low-temperature water-rock reactions. *Nat. Geosci.* **6,** 478–484 (2013).

McCaffrey, M. A., Lazar, B. & Holland, H. D. The evaporation path of seawater and the coprecipitation of Br- and K+ with halite. *J. Sediment. Petrol.* **57,** 928–938 (1987).

McCollom, T. M. & Seewald, J. S. A reassessment of the potential for reduction of dissolved CO2 to hydrocarbons during serpentinization of olivine. *Geochim. Cosmochim. Acta* **65,** 3769–3778 (2001).

McCollom, T. M. & Seewald, J. S. Serpentinites, hydrogen, and life. *Elements* **9,** 129–134 (2013).

McCollom, T. M. & Shock, E. L. Geochemical constraints on chemolithoautotrophic metabolism by microorganisms in seafloor hydrothermal systems. *Geochim. Cosmochim. Acta* **61,** 4375–4391 (1997).

McMurdie, P. J. & Holmes, S. Phyloseq: An R Package for Reproducible Interactive Analysis and Graphics of Microbiome Census Data. *PLoS One* **8,** (2013).

Mei, N. *et al.* Fermentative hydrogen production by a new alkaliphilic Clostridium sp. (strain PROH2) isolated from a shallow submarine hydrothermal chimney in Prony Bay, New Caledonia. *Int. J. Hydrogen Energy* **39,** 19465–19473 (2014).

Ménez, B., Pasini, V. & Brunelli, D. Life in the hydrated suboceanic mantle. *Nat. Geosci.* **5,** 133–137 (2012).

Meyer-Dombard, D. R. *et al.* High pH microbial ecosystems in a newly discovered, ephemeral, serpentinizing fluid seep at Yanartas (Chimera), Turkey. *Front. Microbiol.* **6,** 1–13 (2015).

Miller, H. M. *et al.* Modern water/rock reactions in Oman hyperalkaline peridotite aquifers and implications for microbial habitability. *Geochim. Cosmochim. Acta* **179,** 217–241 (2016).

Monnin, C. *et al.* Fluid chemistry of the low temperature hyperalkaline hydrothermal system of Prony bay (New Caledonia). *Biogeosciences* **11,** 5687–5706 (2014).

Morrill, P. L. *et al.* Geochemistry and geobiology of a present-day serpentinization site in California: The Cedars. *Geochim. Cosmochim. Acta* **109,** 222–240 (2013).

Nandasena, K. *et al.* Complete genome sequence of Mesorhizobium ciceri bv. biserrulae type strain (WSM1271 T). *Stand. Genomic Sci.* **9,** 462–472 (2014).

Neal, C. & Shand, P. Spring and surface water quality of the Cyprus ophiolites. *Hydrol. Earth Syst. Sci.* **6,** 797–817 (2002).

Ogata, H., Goto, S., Sato, K., Fujibuchi, W. & Bono, H. KEGG: Kyoto Encyclopedia of Genes and Genomes. *Kanehisa Lab.* **27,** 29–34 (2017).

Okland, I., Huang, S., Dahle, H., Thorseth, I. H. & Pedersen, R. B. Low temperature alteration of serpentinized ultramafic rock and implications for microbial life. *Chem. Geol.* **318–319,** 75–87 (2012).

Oze, C. & Sharma, M. Have olivine, will gas: Serpentinization and the abiogenic production of methane on Mars. *Geophys. Res. Lett.* **32,** 1–4 (2005).

Patil, K. R., Roune, L. & McHardy, A. C. The phyloPythiaS web server for taxonomic assignment of metagenome sequences. *PLoS One* **7,** (2012).

Peters, E. K. D-18O enriched waters of the Coast Range Mountains, northern California: Connate and ore-forming fluids. *Geochim. Cosmochim. Acta* **57,** 1093–1104 (1993).

Proskurowski, G. *et al.* Abiogenic hydrocarbon production at lost city hydrothermal field. *Science* **319,** 604–7 (2008).

Pruesse, E., Peplies, J. & Glöckner, F. O. SINA: Accurate high-throughput multiple sequence alignment of ribosomal RNA genes. *Bioinformatics* **28,** 1823–1829 (2012).

Quéméneur, M. *et al.* Spatial distribution of microbial communities in the shallow submarine alkaline hydrothermal field of the Prony Bay, New Caledonia. *Environ. Microbiol. Rep.* **6,** 665–674 (2014).

Ravot, G., Magot, M., Fardeau, M., Patel, B. K. C. & Ollivierl, B. Anaerobic , Thiosulfate-Reducing Bacterium From an Oil-Producing Well. **47,** 1141–1147 (2016).

Rempfert, K. R. *et al.* Geological and geochemical controls on subsurface microbial life in the Samail Ophiolite, Oman. *Front. Microbiol.* **8,** in press (2017).

Rizopoulos, D. ltm : An R Package for Latent Variable Modeling and Item Response Theory Analyses. *J. Stat. Softw.* **17,** (2006).

Robinson, M. D., McCarthy, D. J. & Smyth, G. K. edgeR: A Bioconductor package for differential expression analysis of digital gene expression data. *Bioinformatics* **26,** 139–140 (2009).

Sanchez-Murillo, R. *et al.* Geochemical evidence for active tropical serpentinization in the Santa Elena Ophiolite, Costa Rica: An analog of a humid early Earth? *Geochemistry Geophys. Geosystems* **18,** 1–16 (2014).

Scambelluri, M. *et al.* High salinity fluid inclusions formed from recycled seawater in deeply subducted alpine serpentinite. *Earth Planet. Sci. Lett.* **148,** 485–499 (1997).

Schloss, P. D. & Westcott, S. L. Assessing and improving methods used in operational taxonomic unit-based approaches for 16S rRNA gene sequence analysis. *Appl. Environ. Microbiol.* **77,** 3219–3226 (2011).

Schloss, P. D. *et al.* Introducing mothur: Open-source, platform-independent, community-supported software for describing and comparing microbial communities. *Appl. Environ. Microbiol.* **75,** 7537–7541 (2009).

Schrenk, M. O., Brazelton, W. J.,. & Lang, S. Q. Serpentinization, Carbon, and Deep Life. *Rev. Mineral.* **75,** 575–606 (2013).

Schrenk, M. O., Kelley, D. S., Delaney, J. R. & Baross, J. A. Incidence and diversity of microorganisms within the walls of an active deep-sea sulfide chimney. *Appl. Environ. Microbiol.* **69,** 3580–3592 (2003).

Schwarzenbach, E. M., Gill, B. C., Gazel, E. & Madrigal, P. Sulfur and carbon geochemistry of the Santa Elena peridotites: Comparing oceanic and continental processes during peridotite alteration. *Lithos* **252–253,** 92–108 (2016).

Scribano, V. *et al.* Origin of salt giants in abyssal serpentinite systems. *Int. J. Earth Sci.* **0,** 1–14 (2017).

Seemann, T. Prokka: Rapid prokaryotic genome annotation. *Bioinformatics* **30,** 2068–2069 (2014).

Seyfried, W. E., Foustoukos, D. I. & Fu, Q. Redox evolution and mass transfer during serpentinization: An experimental and theoretical study at 200C, 500 bar with implications for ultramafic-hosted hydrothermal systems at Mid-Ocean Ridges. *Geochim. Cosmochim. Acta* **71,** 3872–3886 (2007).

Seyfried, W. E., Pester, N. J., Tutolo, B. M. & Ding, K. The Lost City hydrothermal system: Constraints imposed by vent fluid chemistry and reaction path models on subseafloor heat and mass transfer processes. *Geochim. Cosmochim. Acta* **163,** 59–79 (2015).

Shervais, J. W. & Kimbrough, D. L. Geochemical evidence for the tectonic setting of the Coast Range ophiolite: a composite island arc-oceanic crust terrane in western California. *Geology* **13,** 35–38 (1985).

Shervais, J. W. *et al.* Multi-Stage Origin of the Coast Range Ophiolite, California: Implications for the Life Cycle of Supra-Subduction Zone Ophiolites. *Int. Geol. Rev.* **46,** 289–315 (2004).

Sievers, F. *et al.* Fast, scalable generation of high-quality protein multiple sequence alignments using Clustal Omega. *Mol. Syst. Biol.* **7,** 539–539 (2014).

Sleep, N. H., Meibom, a, Fridriksson, T., Coleman, R. G. & Bird, D. K. H2-rich fluids from serpentinization: geochemical and biotic implications. *Proc. Natl. Acad. Sci. U. S. A.* **101,** 12818–12823 (2004).

Sorokin, D. Y., Tourova, T. P., Lysenko, A. M. & Muyzer, G. Diversity of culturable halophilic sulfur-oxidizing bacteria in hypersaline habitats. *Microbiology* **152,** 3013–3023 (2006).

Suda, K. *et al.* Origin of methane in serpentinite-hosted hydrothermal systems: The CH4-H2-H2O hydrogen isotope systematics of the Hakuba Happo hot spring. *Earth Planet. Sci. Lett.* **386,** 112–125 (2014).

Suzuki, S. *et al.* Microbial diversity in The Cedars, an ultrabasic, ultrareducing, and low salinity serpentinizing ecosystem. *Proc. Natl. Acad. Sci. U. S. A.* **110,** 15336–15341 (2013).

Suzuki, S. *et al.* Physiological and genomic features of highly alkaliphilic hydrogen-utilizing Betaproteobacteria from a continental serpentinizing site. *Nat. Commun.* **5,** 3900 (2014).

Tamura, K., Stecher, G., Peterson, D., Filipski, A. & Kumar, S. MEGA6: Molecular evolutionary genetics analysis version 6.0. *Mol. Biol. Evol.* **30,** 2725–2729 (2013).

Thorup, C. & Schramm, A. Disguised as a Sulfate Reducer : Growth of the Deltaproteobacterium Desulfurivibrio alkaliphilus by Sulfide Oxidation with Nitrate. **8,** 1–9 (2017).

Tiago, I. & Veríssimo, A. Microbial and functional diversity of a subterrestrial high pH groundwater associated to serpentinization. *Environ. Microbiol.* **15,** 1687–1706 (2013).

Twing, K. I. *et al.* Serpentinization-influenced groundwater harbors extremely low diversity microbial communities adapted to high pH. *Front. Microbiol.* **8,** 308 (2017).

Twing, K. I. Microbial Diversity and Metabolic Potential of the Serpentinite Subsurface Environment. (Ph.D. Thesis). Order No. 3739219 Michigan State University. Ann Arbor: *ProQuest* (2015).

Vannini, C. *et al.* Sulphide oxidation to elemental sulphur in a membrane bioreactor: Performance and characterization of the selected microbial sulphur-oxidizing community. *Syst. Appl. Microbiol.* **31,** 461–473 (2008).

Wakabayashi, J. Subducted sedimentary serpentinite melanges: Record of multiple burial-exhumation cycles and subduction erosion. *Tectonophysics* **568–569,** 230–247 (2012).

Weber, H. S., Thamdrup, B. & Habicht, K. S. High Sulfur Isotope Fractionation Associated with Anaerobic Oxidation of Methane in a Low-Sulfate, Iron-Rich Environment. *Front. Earth Sci.* **4,** 1–14 (2016).

White, D. Saline waters of sedimentary rocks. 342–366 (1965).

CHAPTER 3

Biologically-catalyzed Methane Oxidation in Serpentinite-Hosted Groundwater[2]

Abstract

Ultramafic ocean crust uplifted onto continents in the form of ophiolites can become hydrated and altered through a process known as serpentinization. For the first time in an ophiolitic serpentinizing system, a comprehensive analysis of biogeochemical gradients (i.e. sulfate, methane, DIC, pH, conductivity, etc.) in the standing water column of a monitoring well, CSW1.1, at the Coast Range Ophiolite Microbial Observatory (CROMO) was successfully performed. Geochemical and microbiological samples were collected from four discrete depths at the top of the well equal to 100%, 50%, 15%, and 0% of atmospheric oxygen concentrations, and bioenergetic calculations were performed for a suite of methane cycling reactions. Microcosm experiments inoculated with $^{13}CH_4$, thiosulfate or ferric iron, and constructed with water from the 15% oxygen level or from the well bottom were monitored over the course of 190 days for incorporation into ^{13}DIC. Microcosm results indicate the most growth in the combination of $^{13}CH_4$ + thiosulfate amended bottles and notably, biogenic ^{13}DIC was produced from the $^{13}CH_4$ and $^{13}CH_4$ + thiosulfate inoculated bottles. Results from the profile work indicate at the top of the well, aerobic methane oxidation to CO_2 is favorable for microbial metabolisms here as expected, however the anaerobic oxidation

[2] The work described in this chapter is currently in preparation for submission to the Geochemistry, Geophysics, Geosystems Journal (G^3) for publication: Mary C. Sabuda, Tori M. Hoehler, Michael D. Kubo, Dawn Cardace, Lindsay I. Putman, and Matthew O. Schrenk Methane Oxidation from Environmental Gradients in Serpentinite-Hosted Groundwater (in Prep)

of methane (AOM) coupled to sulfate and thiosulfate are also exergonic in the column. Decreases in methane and sulfate are observed in chemical data between the 50% and 15% depths, and an increase in methane and continued decrease in sulfate between 15% and 0% oxygen. The sample suite was collected from the base of CSW1.1 and other CROMO wells to gain perspective into how the seawater- and serpentinization-influenced groundwaters influence biogeochemistry throughout the site. Bacterial community compositions throughout CSW1.1 indicate a dominance of the families Trueperaceae and Comamonadaceae, with appearances of sulfur-cycling SRB-2 and *Dethiobacter.* Increased diversity is observed at 50% and 0% oxygen levels, where the oxic-anoxic interface occurs, and where the well becomes uncased, respectively. Isotope Ratio Mass Spectrometry $^{13}CH_4$ microcosm results reveal separation between ^{13}DIC in biotic and abiotic trials, which shows promise for identifying relationships between organisms capable of methane and sulfur metabolisms within the serpentinite subsurface environment. The combined profile and microcosm results presented here help elucidate the intriguing relationship between habitability, microbial diversity, and chemical fluctuations in serpentinite-hosted groundwater.

Introduction

Water-Rock Interactions

Serpentinization is the process of hydrating ultramafic rocks such as peridotite, dunite, or lherzolite composed primarily of olivine, pyroxenes, and minor plagioclase. As hydrothermal fluids interact with these primitive rock types, the three hydrated minerals composing serpentinite (lizardite, antigorite and chrysotile) crystallize and replace the original minerals. In this process, secondary magnetite and brucite can form with the release of hydrogen gas. (Seyfried et al., 2007; Evans, 2010; Mayhew et al., 2013). The geologic setting and degree to which serpentinization occurs can control mineral composition and impact the surrounding water chemistry, as described below.

Along the ocean floor, hydrothermal vent systems such as the Lost City Hydrothermal Field (LCHF) located along the Mid-Atlantic Ridge, are powered by crust-mantle interactions and extensive fluid mixing between cold ocean water and hydrothermal fluids. In shallow marine locations, such as the Prony hydrothermal field (PHF) in New Caledonia, continental meteoric high pH fluids discharge into shallow seawater creating energy-rich chemical gradients (Monnin et al., 2014). These seafloor hydrothermal systems and the unique environments that develop as a result have been studied in detail for their similarity to early Earth conditions and prospective locations for the origin of life (Sleep et al., 2004; Lang et al., 2012; Frost et al., 2013; McCollom et al., 2013). Chemosynthetic bacteria and archaea can take advantage of the H_2 and CH_4 rich fluids and thermodynamic disequilibrium that results from the mixing of end member fluids to obtain energy (Brazelton et al., 2006).

Similar to hydrothermal vents, continental serpentinite-hosted groundwaters within ophiolite sequences are becoming well-studied throughout the world, in locations such as Oman (Chavagnac et al., 2013; Miller et al., 2016), Italy (Schwarzenbach et al., 2012; Chavagnac et al., 2013), Portugal (Marques et al., 2008), the Philippines (Cardace et al., 2015; Meyer-Dombard et al., 2015), and Costa Rica (Sanchez-Murillo et al., 2014; Schwarzenbach et al., 2016) for various environmental (Baes III et al., 1987; Aloupi et al., 2012; Visioli et al., 2013), astrobiological (Szponar et al., 2013; McKay et al., 2014), and economic (Holloway et al., 2009) purposes. Gradient work (temperature, pH, ORP, DO, etc.) along a lateral transect of a serpentinizing fluid seep ecosystem from the Philippines examined how deeply sourced fluids and associated microbial communities had responded to surface mixing along the outflow channel (Woycheese et al., 2015). This work provided insight into how microbial communities within a serpentinite-hosted aquifer could adapt to surficial conditions downstream, as decreased diversity was observed with distance from the source and organisms included an abundance of hydrogen oxidizing bacteria (Woycheese et al., 2015).

Previous work at CROMO has clearly shown that Betaproteobacteria and Clostridiales are dominant members of this system. Microcosm experiments inoculated with CROMO fluids, hydrogen atmosphere, a suite of carbon sources (CO_2, CH_4, acetate, formate) showed growth when provided with methane or acetate. The addition of nutrients or electron acceptors had no significant effect on the growth (Crespo-Medina et al., 2014). The exception to this are microcosms amended with sulfur compounds, where community compositions changed to favor *Dethiobacter* and Comamonadaceae. An analysis of methane isotopologues within natural CROMO

groundwater revealed both thermogenic and microbial sources for methane (Wang et al., 2015). Similarly, recent work by Twing et al., 2017 showed pH, CO, and CH_4 best explained the variability in bacterial community composition across the site, with significant positive correlations between both *Dethiobacter* and Comamonadaceae to methane. This foundational work helps to elucidate which factors control community composition and the importance of sulfur and carbon in this system.

In this study, we investigate the distribution and activities of microorganisms in the context of environmental gradients (pH, conductivity, methane, sulfate, DIC, etc.) with depth at CROMO to gain insight into how fluctuations in chemistry impact the extremophiles able to thrive within this challenging environment. Microbes in these locations likely work in tandem with other species to obtain enough energy for survival in the high pH, low-oxygen fluids, and thus it is important to understand how these communities shift in response to chemical variances. This is the first study to date that has combined aqueous geochemical measurements, microbiological characterization, and thermodynamic calculations to develop a comprehensive depth profile of a terrestrial serpentinite-hosted groundwater well.

Background

Ultramafic Peridotite Alteration to Serpentinite

Along the ocean floor at various tectonic settings, ultramafic rocks can be uplifted which allows seawater to infiltrate to extensive depths and interact with primitive basement rock such as basalt, gabbro, and peridotite. During this process, water can hydrate the olivine and pyroxene minerals that comprise peridotite, dunite, etc. and alter it to become the serpentine minerals, lizardite, antigorite, and chrysotile (Proskurowski et al., 2008; Frost et al., 2013; McCollom et al., 2013). This process can happen in low-temperature environments (50-300°C) where the serpentine mineral, lizardite, dominates, or in high temperature settings where antigorite is the predominant form (Evans et al., 2010). In addition to the formation of serpentine minerals this process produces magnesium-iron hydroxides in the form of brucite, magnetite, and aqueous hydrogen (Mayhew et al., 2013). During this process, water reacts with carbon dioxide in solution to produce methane and hydrogen (McCollom and Seewald, 2013). Reduced iron in olivine can also react with water and contribute high concentrations of hydrogen (Suda et al., 2014). Iron and nickel accessory components such as oxides and sulfides can also be produced and contribute to the overall production of organic compounds (McCollom and Seewald, 2013). These serpentine-hosted metals are also studied extensively to understand mobility and chemical interactions for environmental toxicity and human safety purposes (Becquer et al., 2003; Morrison et al., 2015).

Gases Produced, Carbon Cycling

Methane, in particular, is a widespread greenhouse gas produced by serpentinization (Barnes et al., 1978; Etiope and Sherwood Lollar, 2013; Etiope et al., 2013; Schrenk et al., 2013) that can be generated from hydrogen reacting with carbon dioxide via Fischer-Tropsch type (FTT) reactions (Proskurowski et al., 2008; Suda et al., 2014). As reducing conditions become more prevalent with depth, carbon dioxide (CO_2) or carbon monoxide (CO) can be reduced to hydrocarbons such as methane (CH_4) (McCollom et al., 2001; Oze et al., 2005; Proskurowski et al., 2006; Brazelton et al., 2011; Brazelton et al., 2013; McCollom et al., 2013). Methane flux due to serpentinization at mid-ocean ridges was calculated to be 0.4 Megatons per kilometer of ridge axis (Cannat et al., 2010). The Chimaera gas seep in Turkey releases greater than 50 tons/year of a gas mixture, half of which is abiogenic methane influenced by low-temperature serpentinization (Hosgormez et al., 2008). The Teikrova ophiolites overall exhume 150-190 tons/year of methane (Etiope et al., 2011). Microbial consumption of methane can aid in regulating the concentrations released to the atmosphere (Reeburgh, 2007). Earlier work at CROMO and other serpentinization-influenced sites has generated confounding interpretations of the origins of methane due to thermogenic and microbial sources and sinks (Proskurowski et al., 2008; Brazelton et al., 2011; Wang et al., 2015).

Understanding the origins and fate of methane can provide essential information about carbon cycling, redox reactions, and microbial activity. Aerobic methanotrophic bacteria, methanogenic archaea, or anaerobic methanotrophic archaea (ANME) can facilitate methane cycling (Knittel et al., 2009). ANME-2, specifically, are known to be

capable of performing reverse methanogenesis (Hoehler et al., 1994; Orphan et al., 2002). The anaerobic oxidation of methane (AOM) is a topic discussed throughout a wide variety of environmental sites, where oxic surface waters interact with anoxic conditions at depth (Orphan et al., 2002; Jørgensen et al., 2004; Stadnitskaia et al., 2008; Beal et al., 2016). To date, an understanding of the relationship between AOM coupled to various electron acceptors (nitrate, iron, manganese, sulfate) in redox reactions for a terrestrial serpentinizing system has yet to be determined, and isolates of ANME organisms have yet to be obtained and characterized. To this end, it is important to understand the processes that control carbon concentrations in serpentinizing systems, including chemical gradient development with depth and microbial metabolisms.

Serpentinite-Influenced Biogeochemistry

Natural gradients in water chemistry develop as serpentinization reactions occur, and as end-member fluids mix. Measured serpentine waters range from circumneutral pH 7.5 to hyperalkaline pH 12.5 and above due to an influence of hydroxides. In marine settings, the ions associated with seawater can interact with the ultrabasic waters associated with serpentinization, creating complex mixtures of compounds and therefore unique environments to sustain life. Similarly, in ophiolite complexes, meteoric water can percolate into the groundwater and mix with ultrabasic serpentinite-and-seawater fluids. Hydrogen and carbon monoxide concentrations have been the focus of other studies at CROMO (e.g. Crespo-Medina et al., 2014; Twing et al., 2017), and due to minimal concentrations identified in the profile it is important to focus on the

abundance of and relationships between sulfate and methane detected here. Similarly, nitrate and nitrite are below detection or are in minimal concentration through the system. For this reason, sulfate and methane will be the focus of this study with hydrogen, CO, nitrate, and nitrite reported for consistency and comparison.

Terminal electron accepting processes (TEA) are limiting in serpentinite-hosted ecosystems due to extensive water-rock interactions. Additionally, inorganic carbon is precipitated as carbonates in the form of calcite or aragonite, depending on pressure conditions, which leaves a scarce amount of available electron donors for microbes. Life on Earth requires energy generation from chemical gradients and disequilibria (Möller et al., 2017) and thus it is important to quantify oxygen concentrations and accurately measure nitrate, iron, and sulfur speciation along interfaces to further elucidate the metabolic potential and activity of organisms capable of withstanding these challenging habitats.

CROMO Site Description

The Coast Range Ophiolite Microbial Observatory (CROMO) is located at N38°51' 42.624" W122°24'51.408", on the Donald and Sylvia McLaughlin Natural Reserve, near Lower Lake, California, USA (Fig. 6). The Reserve's geology is complex, with serpentinite, gabbro, metasediment, and peridotite influence (Cardace et al., 2013). To explore the geology, geochemistry, microbiology, hydrology, and geophysical characteristics of the hydrothermally altered serpentinite subsurface, a total of 8 wells were drilled in 2011 and are monitored seasonally. The Reserve and twelve respective CROMO wells (including heritage wells) are located on and drilled into the mélange of

the northern Coast Range Ophiolite (CRO) of mid to late Jurassic age (Shervais et al., 1985; Huot and Maury, 2002). The Coast Range Ophiolite extends north from San Francisco to the Klamath Mountains and beyond Oregon's Coast Range, and west from the eastern end of the Franciscan Complex to the Great Valley of California as fragments of ophiolite scattered throughout the area (Shervais et al., 2004). The CRO is tectonically altered and overlain by the Jurassic-Cretaceous Great Valley Sequence and is in contact with the younger Jurassic-Paleogene Franciscan Complex (Shervais et al., 1985; Shervais et al., 2004).

Two well clusters, Quarry Valley (QV) and Core Shed Wells (CSW) encompass CROMO, with six of these wells at the QV location, three of which (N08-A, N08-B, N08-C) were drilled by the Homestake Mining Company Inc. and another three wells, QV1.1, QV1.2, and QV1.3 were drilled as part of the establishment of the CROMO in 2011. Located 1.2 km east and downslope of Quarry Valley, is the Core Shed area, which include the remaining six monitoring wells. The main well, CSW1.1, is drilled to 21m, and cased only to 5m. The other surrounding wells, CSW1.2 - CSW1.5 and CSWold are drilled from 9m to 72m depth, which lends insight into the lithologic and biogeochemical variability of the site. From prior work at the site (i.e. Crespo-Medina et al., 2014; Twing et al., 2017, and Chapter 1), it is known that with depth, waters exhibit dilute seawater chemistries mixed with hyperalkaline fluids.

The monitoring wells at CROMO sample a variety of water sources, as detailed in Ortiz et al., (submitted). Perched water tables, deep water sources, and shallow meteoric waters host unique water chemistries which lends variability to the site (Fig. 5; Table 10). As this subsurface water recharges the wells post-pumping, it interacts and

equilibrates with atmospheric conditions at the water table. Natural gradients in water chemistry develop with time, and microbes can take advantage of disequilibrium in the system for metabolic processes and energy generation. With this idea in mind, a comprehensive depth profile of CSW1.1, the most extreme well at CROMO, was completed to understand how chemical disequilibrium within energy limited, serpentinite hosted waters influences microbial community composition.

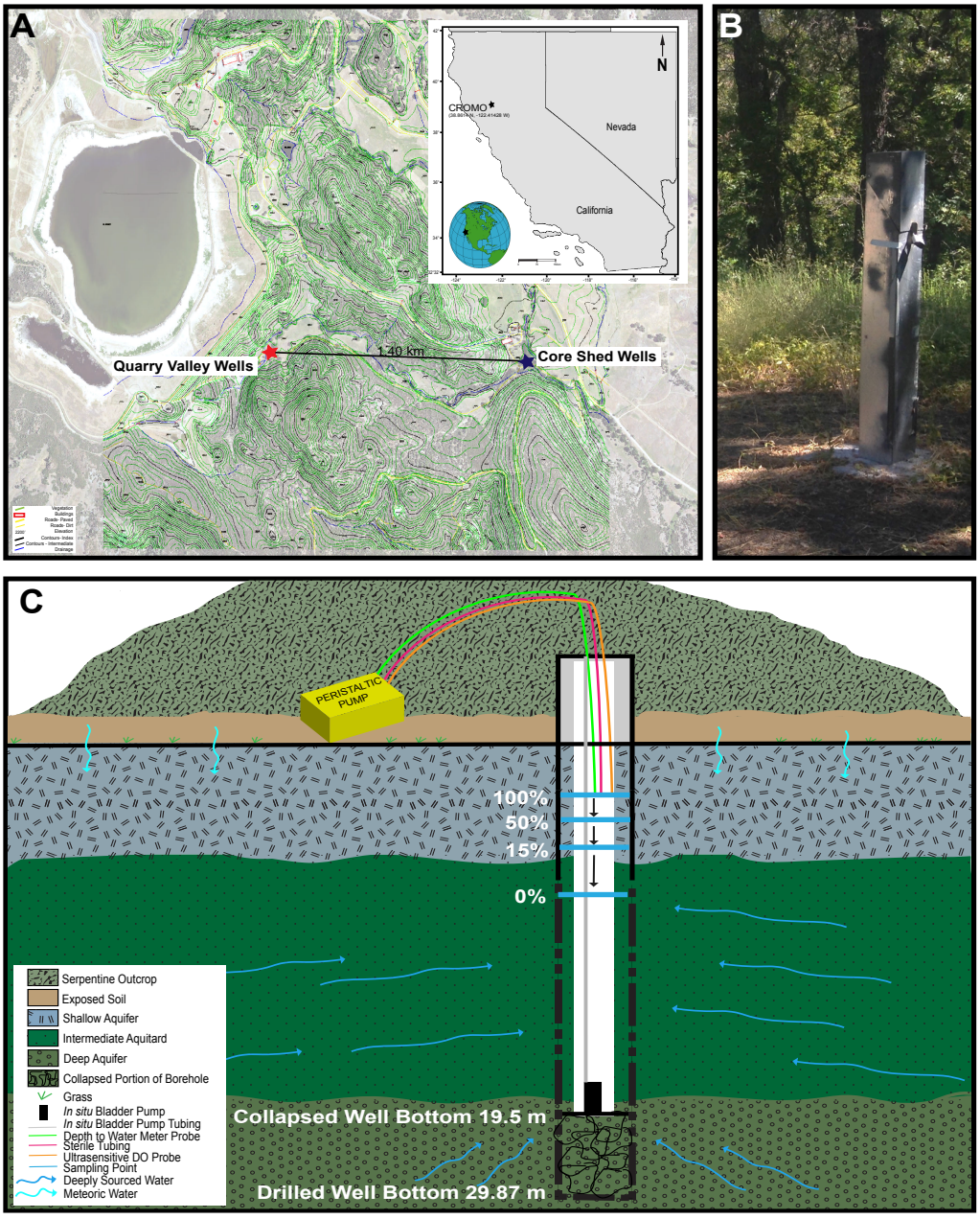

Figure 6 - Depth Profile Schematic. (A) Location of CROMO in northern California. (B) Field image of CSW1.1. (C) Cross section of CSW 1.1, with lithologies estimated after Ortiz et al., (submitted). Note the peristaltic pump (yellow box) at the ground surface was used to pump water for the profile, and the bladder pump (black rectangle, well base) was used to pump the CSW1.1 well bottom. Black horizontal line denotes ground level, and the outcrop in the background denotes serpentine rock. Profile samples were taken at depths of 2.81m, 3.21 m, 3.41 m, and 5.91 m depth for 100%, 15%, 50%, and 0% air saturation, respectively. Note the 0% air saturation sampling point is located in the uncased portion of the well (cased to 5m depth - uncased portion indicated by dashed lines).

Serpentinization Influenced Microbiology

Microbial communities vary throughout the CROMO fluids with changes in pH, dissolved oxygen, nutrient composition, and dissolved gases. Cell abundances are on the order of 10^5 cells/mL with a dominance of Proteobacteria (Betaproteobacteria) Firmicutes, Bacteroidetes, and other members of Proteobacteria (Alpha-, Gamma-, Delta-) varying in abundance throughout the site. In the circumneutral, shallow wells, CSW1.4, CSW1.2, QV1.2, and N08-A, diversity and cell abundance are the greatest, as nutrients and lower pH levels create less extreme living conditions. The wells drilled to intermediate and deeper depths are more heavily influenced by hyperalkaline fluids, contain less DO, lower ORP, higher conductivity, and increased methane and hydrogen.

The site is generally characterized by low microbial diversity, with a predominance of Betaproteobacteria and Clostridia. Sulfur cycling organisms are prominent at CROMO and reported at other terrestrial serpentinizing locations (Tiago and Veríssimo, 2012; Brazelton et al., 2017; Crespo-Medina et al., 2017; Chapter 1). Twing et al., 2015 statistically distinguished taxa based on if they were fluid-, soil- or core- enriched at CROMO. Fluid-enriched taxa include Betaproteobacteria and Clostridia, while core-enriched taxa contain organisms from Phyla such as Actinobacteria, Proteobacteria, Firmicutes, Chlorobi, Chloroflexi, Planctomycetes. Soil taxa include members of Acidobacteria, Actinobacteria, Bacteroidetes, Chloroflexi, Gemmatimonadetes, Planctomycetes, Proteobacteria, and Verrucomicrobia.

Archaea are generally present in low abundances throughout CROMO. Groups of these organisms were detected in core material, including methanogens in the deeper sections of QV (Twing, 2015), yet this Domain has been virtually undetectable in

the fluids, until the May 2016 field campaign, where qPCR revealed an abundance of Archaea in CSW1.1 well fluid. 16S rRNA gene sequencing will aid in determining whether the Archaea play a role in the cycling of methane and contribute to the portion of biogenic methane detected by Wang et al., (2015) Interestingly, previous culturing work at CROMO reveals methane can stimulate the growth of microbes without the concomitant presence of Archaea (Crespo-Medina et al., 2014), and methane may in part be utilized by bacteria.

Methods

Profile Sampling

Due to the complex hydrogeology, isolated nature of the waters in proximity to these wells, and long recharge rates, the stagnant water column of CSW 1.1 was characterized in May 2016 for its aqueous geochemistry and microbiology at four distinct depths according to oxygen concentrations. Predetermined oxygen levels of 100%, 50%, 15% and 0% air saturation were used as a depth indicator using an ultrasensitive Orion Dissolved Oxygen Probe for Lab or Field (ThermoScientific), and sterile Tygon tubing (Sigma-Aldrich), which allowed samples to be extracted from these discrete depths once reached. . These four air saturation concentrations of DO were chosen to identify the oxic-anoxic transition zone within the column, which is outlined in detail below. Due to cord length limits on the YSI probe, the ultrasensitive probe was a necessary alternative for the creation of this profile. An ethanol-sterilized water level meter (Solinst, Georgetown, ON) was simultaneously lowered in to monitor water table

levels, and all three devices were zip tied together and sterilized before being lowered into the well. The interior PVC tubing radius of the CSW1.1 well (0.051m), was used in calculations of the maximum water volume extractable without disturbance to the remaining deeper column samples. Tubing was attached to a peristaltic pump resting on the ground near the well opening, which allowed water to flow from each interval and be preserved using the methods detailed below. As each DO concentration was reached using the ultrasensitive DO probe, 60 mL of water was collected for measurement on a digital YSI probe to obtain estimates for pH, oxidation-reduction potential, specific conductance, and temperature (Table 8). Dissolved oxygen limit of detections for the ultrasensitive probe are 0.002 mg/L and 0.157 for the YSI meter, as calculated using June 2016 data. Well fluids at each interval were collected for anions, cations, hydrogen sulfide, dissolved iron, organic acids, dissolved inorganic carbon, and dissolved gases. Additionally, cell abundance and 16S rRNA samples were collected at each depth using the methods detailed below.

16S rRNA Gene Amplicon Sequencing and Data Analysis

At each sampling interval, water was pumped through the tubing using a portable peristaltic pump at the ground surface near the well head. Water samples were collected immediately for 16S rRNA sequencing (400mL) using Sterivex filters (Millipore, Billerica, MA) attached directly to the Tygon tubing. The filter was immediately capped and stored in liquid nitrogen until shipped to the lab at Michigan State University, where they were stored at -80°C until DNA extractions. Total genomic DNA was extracted using freeze/thaw cycles and lysozyme/Proteinase K treatment to

lyse cells, followed by purification with phenol-chloroform, precipitation using ethanol as previously described, and purified using QiaAmp (Qiagen, Hilden, Germany) columns according to manufacturer instructions (Brazelton et al., 2017; Crespo-Medina et al., 2017; Twing et al., 2017). A Qubit 2.0 fluorometer (ThermoFisher) was used to quantify extracted DNA using a Qubit® dsDNA High Sensitivity Assay kit.

Bacterial and archaeal samples were amplified via quantitative Polymerase Chain Reaction (qPCR) on a BioRad C1000 instrument with a CFX96 Optics Module using the SsoAdvanced Universal SybrGreen assay, and domain-specific primers targeting the V6 region of the 16S rRNA gene. 958F and 1048R major and minor mix archaeal primers, and the 967F and 1046R bacterial primers were used (Sogin et al., 2006). Gene copy numbers were obtained by plotting quantification values from environmental samples onto standard curves generated by *Escherichia coli* and *Methanocaldococcus jannaschii* for bacteria and archaea respectively with the domain-specific primers. Thermal cycling for denaturation (98°C, 2 min., 15 sec.), annealing (57°C, 30 sec.), and extension (65°C, 10 sec.), was run for 30 cycles total.

Purified 16S rRNA samples were submitted to the Genomics Core Facility at Michigan State University for bacterial analysis and processed using an Illumina MiSeq instrument to amplify the V4 region of the bacterial 16S rRNA gene (515F/806R primers) using dual indexed Illumina fusion primers (Kozich et al., 2013). Products were normalized and pooled using an Invitrogen SequalPrep DNA Normalization Plate where it was then loaded on an Illumina MiSeq v2 flow cell and sequenced using a standard 500 cycle reagent kit after library quality control and quantitation was performed. Illumina Real Time Analysis (RTA) software v1.18.54 performed base calling, and using

Illumina Bcl2fastq (v1.8.4), the RTA output was demultiplexed and converted to FastQ files.

Paired-end sequence reads were filtered and merged using USEARCH 8 (Edgar et al., 2010) with additional quality filtering in Mothur (Schloss et al., 2008) to remove sequences with ambiguous bases and more than 8 homopolymers. Chimaeras were removed with Mothur's implementation of UCHIME (Edgar et al., 2011) before sequences were pre-clustered with the Mothur command recluse (diffs=1), which reduced from 402,702 to 253,866, which removes rare sequences most likely created by sequencing errors (Schloss et al., 2011).

The SILVA SSURef alignment (v119) was used to align sequences, and taxonomy was assigned using Mothur (Pruesse et al., 2007; Schloss et al., 2009), as described in Twing et al., 2017. Rather than binning Operational Taxonomic Units (OTUs) by the 3% distance threshold in mothur, June 2016 CROMO sequences were binned into Amplicon Sequence Variants (ASVs) as described in Chapter 1 and by Brazelton et al. (2017).

Cell Abundance

Unfiltered water for cell abundance analyses were collected in 15 mL Falcon tubes (Fisher Scientific) and fixed in 3.7% formaldehyde. Triplicate samples were preserved and stored at 4 degrees Celsius until analysis. Cells were collected on black polycarbonate filters (Millipore, Billerica, MA, USA) and a 1 µg/mL 4',6-diamidino-2-phenylindole (DAPI) stain was applied. An Olympus epifluorescence microscope was

used to count cells according to previously published protocols (Hobbie et al., 1977; Schrenk et al., 2003).

Aqueous Geochemistry

In addition to the CSW1.1 profile, water was pumped from all CROMO wells (CSW, QV, N08) for geochemical analyses in June 2016 as described in Chapter 1, with the few deviations explained here. Briefly, fluids were pumped from the bottom of each well via a pre-installed Teflon bladder pump (Geotech Environmental Equipment, Denver, CO, USA) and sterile tubing, where samples were collected anoxically at the surface for fluid chemistry. A digital YSI mulitprobe was utilized to collect pH, ORP, DO, specific conductance, and temperature measurements after dissolved oxygen stabilized.

Fluids were preserved for anion (Br^-, Cl^-, NO_2^-, NO_3^-, and SO_4^{2-}) analysis via ion chromatography using 0.2µm Sterivex syringe filters and collected in 25 mL HDPE bottles before storing at 4 ºC. Triplicate samples were measured on a Dionex ICS-2100 Ion Chromatography System (ThermoScientific).

Cations (Fe, S, Si, Cr, Ni) were collected in 25 mL HDPE bottles washed in 10% trace metal grade nitric acid. For every 9 mL of well fluid, 1 mL of the trace metal grade nitric acid was used to preserve cations. Samples were sent to the Geochemical Analytical Laboratory at the University of New Mexico for inductively coupled plasma optical emission spectrometry (ICP-OES), and inductively coupled plasma mass spectrometry (ICP-MS) for S, Si, and Cr, Ni, Fe respectively.

Organic acid samples were collected in duplicate by filtering 15 mL of bubble-free well fluid through a 0.2 µM syringe filter (Whatman Puradisc 25 mm PES sterile packed, GE Healthcare Life Sciences, Pittsburgh, PA) into acid washed and ashed 20 mL I-Chem vials with PTFE lined caps. Samples were then analyzed in duplicate injections by High Performance Liquid Chromatography with UV/VIS detection, followed by derivatization with 2-nitrophenylhydrazide (Albert and Martens, 1997; Crespo-Medina et al., 2014).

Dissolved gases were extracted in the field by vigorously shaking a known volume of anoxic sample fluid with a known volume of N_2 gas in a 60 mL syringe attached to a stopcock. The headspace gas was added via needle to a 15 mL tube completely filled with 200 ppt sodium chloride solution. Immediately after field sampling, gases were analyzed for H_2 and CO via a Trace Analytical RGA3 Reduced Gas Analyzer, and methane was analyzed with a SRI 8610C GC-FID.

Fluids for DIC samples were collected by filtration through a 0.2 µM syringe filter into a pre-calibrated and nitrogen flushed 125 mL glass serum bottle (Wheaton Industries, Inc., Millville, NJ) fitted with a 20 mm thick blue butyl stopper (Chemglass Life Sciences, Vineland, NJ) with a vent needle inserted to allow excess nitrogen headspace to escape. Samples were acidified within the sealed vials in the field using 3 mL concentrated phosphoric acid. Quantification was performed by measuring the concentration of liberated CO_2 in the headspace by GC-FID (SRI8610) following passage through a “methanizer,” which catalyzes the in-line conversion of CO and CO_2 to methane in the presence of H_2 over a heated Ni catalyst (380 ºC), which allows

sensitive detection of these species by flame ionization detector following their separation by gas chromatography (Twing et al., 2017).

Hydrogen sulfide was determined via spectrophotometry according to the methylene blue method (Cline, 1969; Joye et al., 2004; Weber et al., 2016; etc.). 45 mL fluid samples from each well were preserved immediately in the field using 2.0 mL of a 0.05M zinc acetate solution for every 0.5 mL of sample in order to preserve the volatile sulfide as zinc sulfide. In lab, the 2.5 mL triplicate aliquots of this solution were placed into individual 2 mL centrifuge tubes (Sigma-Aldrich) and vortexed. Prior to analysis, 0.2 mL of the appropriate diamine reagent (0-3 μM, 3-40 μM, 40-250 μM, or 250-1000 μM, respectively) was added to each tube to develop the characteristic blue color. For each diamine reagent used, a standard curve was created using the same method of preservation and 50 μM or 500 μM stock solutions of hydrogen sulfide, depending on the diamine reagent range being analyzed. After a 20-minute allotted time for fixation, samples and standards were immediately run in parallel to an 18 mΩ water, 0.22 μm syringe filtered, zinc acetate-preserved, 0-3 μM diamine-reacted blank on an Ultraviolet-1800 Shimadzu UV spectrophotometer at 670 nm.

Samples for total organic carbon (DOC) quantification were filtered into a 30 mL Nalgene bottle using 0.2 μM Sterivex filter cartridges. Samples were kept cold in the field and immediately frozen at -20 ºC back in lab. Non-purgeable Organic Carbon (NPOC) were analyzed using a Shimadzu TOC-L total organic carbon analyzer using the 720ºC combustion catalytic oxidation method (LOD 0.1 mg/L NPOC) at Michigan State University.

Dissolved iron (total, ferrous) was quantified in triplicate by collecting well fluids in a 60 mL bubble free syringe and filtering through a 0.2 μM syringe filter into a sterile bubble-free 60 mL syringe via stopcock. A syringe with 100 μL of trace metal grade concentrated HCl per sample was injected into the syringe with filtered well fluids for anoxic preservation of any ferrous iron. Fluids were then added in 2.5 mL volumes into a 10 mL HCl acid washed I-Chem vial. In the field, 1.0 mL of a 0.1% 1,10-Phenanthroline monohydrate color reagent was added to the vials, followed by 0.5 mL of an ammonium acetate buffer solution (62.5 g ammonium acetate, 37.5 mL 18 mΩ water, 175 mL glacial acetic acid) and 1.0 mL of 18 mΩ water to analyze Fe (II). Total iron was similarly analyzed with an addition of hydroxylamine hydrochloride reagent before addition of other reagents, in the order described above. Standards of 0, 0.5, 1.0, 2.0, and 4.0 ppm Fe concentrations were prepared simultaneously for both total and ferrous iron and run in parallel to samples at the 510 nm wavelength on an Ultraviolet-1800 Shimadzu UV spectrophotometer.

Gibbs Free Energy Calculations

Gibbs free energy calculations were performed for reactions involving the oxidation of methane coupled to the reduction of various oxidants (O_2, SO_4^{2-} , $S_2O_3^{2-}$, Fe^{3+}). Conservative estimates (1 μM) of thiosulfate for the system were used in the calculations, as data were available for only some components of the fluid. The activity of dissolved species for each sample fluid was manually determined via speciation calculations for ions using the theoretical Debye-Hückel equation (Langmuir, 1997), and for CO_2 using the equation:

$$\left(\frac{[H^+]^2}{[H^+]^2} + K_1[H^+] + K_1K_2\right) * \mathrm{DIC} \qquad (1)$$

Wherein K_1 is the first dissociation constant for the transformation of carbonic acid to hydrogen and bicarbonate, and K_2 is the second dissociation constant for the conversion of carbonate and hydrogen to bicarbonate (Langmuir, 1997), H+ is calculated from the fluid pH, and DIC is factored in from measured concentrations. These activities were compared to previous CROMO activity calculations (Chapter 1) to ensure consistency. In equation 2 below, ΔG^0 is the Gibbs energy of reaction (J/mol). ΔG_r^0 is the standard Gibbs energy (J/mol), R is the universal gas constant (J/mole*K), T is the temperature (Kelvin), and Q is the reaction quotient of the compounds involved in the respective reaction. The reaction quotient was calculated using the activities established by the fluid speciation calculations. ΔG_r^0 values for the selected reactions were cited from the work of Amend & Shock (2001), or manually calculated using their ΔG^0 values for components of the reaction when the ΔG_r^0 was not available from their work. These constituents were then used in the given equation below to calculate a total ΔG (J/L) for the respective reaction by accounting for the concentration of the limiting reactant (McCollom and Shock, 1997).

$$\Delta G^0 = \Delta G_r^0 + \mathrm{RTlnQ} \qquad (2)$$

Microcosm Experiments

A 36-bottle microcosm experiment selecting for the enrichment of methanotrophs was run in parallel to the depth profiles in order to test for evidence of methane oxidation within the native microbial communities. At the 15% O_2 air saturation level, water was pumped through sterile tubing via a peristaltic pump into 9 stoppered, 500mL

Pyrex bottles, pre-flushed with N_2 gas. A set of 9 controls was assembled at this time, with the addition of a 0.2μm Sterivex (EMD Millipore, Billerica, MA) filter added to the end of the pump tubing. An identical set of 9 microcosms and 9 controls (0.2μm syringe filter) were assembled via water pumped from 19.5m depth in the well using the pre-existing tubing and bladder pump resting at the well bottom. All microcosms were completely filled with zero gas headspace in the bottles during transport from the field and amendment preparation.

At NASA Ames Research Center, all bottles were inoculated with 50 mL of methane gas with a composition of 80% $^{12}CH_4$ and 20% $^{13}CH_4$. The oxic bottles received 2mL of O_2 at each sampling point in order to maintain the oxygen level within the microcosms. The displaced volume of water in the bottles from the gases was removed using a 4-inch-long needle attached to an anoxic syringe for sampling the initial time point (T0, day 1), before amendments were added and before injected gases could equilibrate with the microcosms. One-third of each oxic and anoxic set were injected with either 16mM iron oxyhydroxide or 2mM thiosulfate to ensure electron flow was consistent between amendments. All amendments and gases were autoclaved or 0.2 μm filter-sterilized to avoid contamination. All bottles were sampled for cell counts at each of the 5 time points. 16S rRNA and Isotope Ratio Mass Spectrometry (IRMS) analyses were carried out as described above. Multiple sampling points were taken close together at the start of the experiment and time between sampling was extended as the experiment progressed in order to catch any initial activity and also monitor change over time (Fig. 10).

IRMS vials were prepared by adding 1 mL of 85% phosphoric acid to 12 mL septum capped vials (Exetainers, Labco, High Wycombe, UK), which were then flushed with nitrogen gas and placed under vacuum. Sample fluid from the microcosms was then injected directly into the vials until equilibrium was achieved to prevent inflow of atmospheric gas. Samples were sent to the Stable Isotope Facility at the University of California Davis, where they were analyzed for ^{13}C- labeled Dissolved Inorganic Carbon (DIC) using a GasBench II system interfaced to a Delta V Plus IRMS (Thermo Scientific, Bremen, Germany), as described by the UC Davis facility. Briefly, sample analysis included injection of a double-needle sampler into the vial to remove evolved CO_2 and transport it to a helium carrier steam, where it is sampled and passed through to the IRMS via a Poroplot Q GC column. Sample isotope ratios were compared to standard gases injected before and after samples on the IRMS. A reference CO_2 peak was calculated and adjusted for instrumental drift to provide final del^{13}C values. Final values are represented as relative to the Vienna PeeDee Belmenite (V-PDB) international standard. Limit of quantification is approximately 150 nanomoles, with a standard deviation of 0.1 $^{0}/_{00.}$

Results

CSW1.1 Profile

The profile results from CSW1.1 show the occurrence of both geochemical and microbiological patterns with depth in the well (Fig. 8). The 100% atmospheric oxygen concentration level was extracted from 2.81m depth. During the time it took to complete

preservation of field samples for the 50% air saturation level at 3.41m depth, slight water recharge was observed. This placed the depth to water measurement for the 15% air saturation level at 3.21m. While this recharge caused water table measurements to rise, water still maintained an oxygen concentration of 15 +/- 1% air saturation while all samples at this interval were taken, revealing the irrelevance of true depth in the well, and the importance of oxygen as the identifier for each sampling point.

Geochemistry

As oxygen decreased through the well profile, an interface of water chemistry parameters is evident between each of the four depths. From 100% to 50% air saturation, pH decreased, and temperature, oxidation reduction potential, and conductivity increased. Between the 50% and 15% levels, the opposite pattern was observed. The 15% to 0% range indicates pH slightly increased, temperature slightly decreased, and that ORP and conductivity increased.

Anion results indicate nitrate and nitrite are below detection limits of 1.0 μM, and bromide quickly drops below detection at 50% air saturation (Table 8). Due to high concentrations of chloride in the waters, dilutions were necessary to run the fluids through the freshwater ion chromatograph column. This process potentially reduced concentrations of nitrite, the next compound to elute after chloride, to undetectable quantities. Chemically stripping chloride from solution may yield more accurate nitrite values from this technique, though nitrate would still fall below detection, as it elutes much later than nitrite. Nutrient analyses in work by Crespo-Medina et al., 2014 report concentrations of other nitrogen species (i.e. ammonia) in greater detail from earlier

sampling work, though NO_2^- and NO_3^- concentrations from these analyses still reveal low abundances. Fluoride fluctuates between below detection limits and up to 40 μM at 15% oxygen. Dissolved iron remains below detection levels as well, likely due to the instability of dissolved iron at high pH. Sulfide similarly remains below detection levels, due to the oxic conditions at the top of the well and microbial sulfide oxidation processes. Chloride concentrations range from 3.4 mM to 2.9 mM, and sulfide and DIC range within 200 and 800 μM, respectively. Sulfate and DIC both increase to the 50% air saturation level, but decrease through the remainder of the profile. Hydrogen concentrations remain steady around 0.04 μM, but carbon monoxide slightly increases with depth. This is likely due to the flux of gases out of the borehole and dilution of deeply sourced groundwater with meteoric input. Cell abundance and pH mirror DIC concentrations. Methane concentrations increase with depth, with the exception of the region from 50% - 15% oxygen.

Gibbs Free Energy

Carbon cycling is an important component of serpentinizing systems, where the carbonate groundwaters act as a sink for CO_2. With Ca^{2+} that is released abiotically in this environment and the DIC present in the groundwater, insoluble calcium carbonate actively precipitates (Suzuki et al., 2013). Organisms such as the candidate genus ‘Serpentinomonas’ are adapted to thrive in these Ca-OH rich waters (Suzuki et al., 2013). Thermodynamic calculations for Gibbs free energy indicate that the aerobic oxidation of methane is extremely favorable in the profile of CSW1.1. With decreasing dissolved oxygen levels as depth increases, energy availability decreases. Interestingly,

the anaerobic oxidation of methane (AOM) coupled to sulfate reduction remains favorable, and AOM coupled to thiosulfate reduction also has a net energy yield above the -20 kJ/mol minimum needed to be considered biologically useful (Schink 1997; Hoehler et al., 2001). AOM coupled to ferric iron reduction is an endothermic reaction yielding no free energy. Similarly, nitrate and nitrite values are below detection levels, which eliminates this reaction from being favorable in the CSW1.1 well. With minimal concentrations of nitrate throughout and a rapid decrease in oxygen with depth, sulfate reduction quickly becomes an attractive choice for ATP generation. Due to extremely low recharge rates on the order of weeks, and the complex hydrology described above, the stagnant water within CSW1.1 was sampled for its profile. The timespan between the prior sampling campaign (January 2016) and June 2016 allowed the development of a complex redox gradient, setting the stage for coordinated analyses of microbiology and geochemistry within the standing well system.

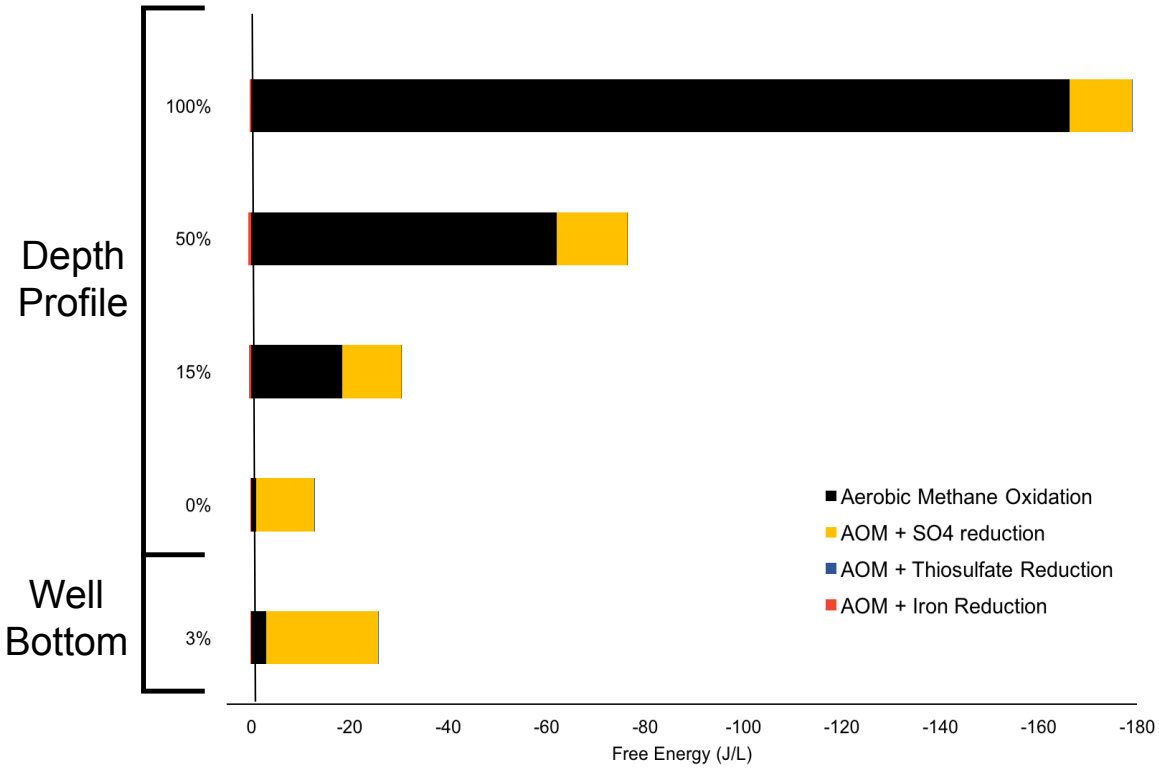

Figure 7 - Thermodynamic Free Energy Calculations. Free energy yields (J/L) calculated using water chemistries (Table 8) from each depth in the CSW1.1 profile and CSW1.1 well bottom for aerobic methane oxidation (AOM), AOM + sulfate reduction, AOM + thiosulfate reduction, and AOM + iron reduction (Table 9).

Microbiology

Bacterial communities throughout the profile have extremely low diversity and cell abundances, and interesting combinations of organisms have developed at each depth. Inverse Simpson diversity index values, representing Alpha-diversity, indicate low diversity throughout all samples (2.03, 2.89, 3.06, etc.). Increases in the index match fluctuations in cell abundance through the profile. Throughout CSW1.1, Trueperaceae, Comamonadaceae, SRB-2, and Xanthomonadaceae dominate. In addition to these at the top of the well, Syntrophomonadaceae (specifically *Dethiobacter* genus) a sulfate-reducing member of the Firmicutes Phyla is noted. At the 50% oxygen level, Burkholderiaceae (Betaproteobacteria), Verrucomicrobiaceae (Verrucomicrobia), Corynebacteraceae, Dietziaceae, Intrasporangiaceae, and Micrococcaceae from the Actinobacteria class are enriched. This increase in diversity matches the appearance of the oxic-anoxic interface and the gradient of mixing meteoric and serpentinite-influenced waters. At 15% air saturation, microbial diversity decreases, and Trueperaceae, Comamonadaceae, Xanthomonadaceae, SRB-2, and Syntrophomonadaceae become the only abundant members. With increasing depth, cell abundances decrease, with the exception of the 15% air saturation level, where cells increased slightly. In addition to the sulfate reducers, Trueperaceae, and Comamonadaceae, three Actinobacteria families Actinomycetaceae, Bifidobacteriaceae, and Dietziaceae were detected at 0% (Fig. 9).

Strikingly, archaea have not been detected in CROMO fluids prior to the June 2016 field campaign (Crespo-Medina et al., 2014; Twing et al., 2017). Archaeal qPCR results indicate archaea are present at 100%, 50%, 15% and the CSW1.1 well bottom

(Table 12). Ongoing efforts for determining this novel archaeal community at CROMO through 16S rRNA analyses will aid in discerning community dynamics.

Profile Compared to CSW1.1 Well Bottom

At 19.5m depth, waters become more extreme in chemistry as sulfate concentrations nearly double that of the 0% air saturation level to 389.6 µM, chloride slightly decreases to 2466 µM, and conductivity increases to 3820 µS/cm (Table 8). Nitrate, nitrite, and dissolved iron remain below detection levels. Sulfide concentrations increase above detection limits to 3.54 µM. Cell abundance increases, while community diversity decreases to a select group capable of withstanding pH 12 (Fig. 8). Fluids near the bottom of the well have more negative ORP values and higher conductivities, which signifies a more reducing and saline aquifer with depth. With fluctuating chemistries throughout CSW1.1 with depth, microbial communities shift in response.

Comamonadaceae thrive in these hyperalkaline waters, with their population extending to 49% of the community abundance in CSW1.1 (Fig. 8). Trueperaceae, a family isolated from hot spring runoff on São Miguel in the Azores, contain the alkaliphilic and facultatively halophilic *T. radiovictrix* species capable of extreme radiation resistance (Albuquerque et al., 2005) and comprise 48% of the population at 19.5m depth. Additionally, bacteria from Xanthomonadaceae contribute 2%, and the sulfate reducers SRB-2 and Syntrophomonadaceae represent the remaining portion of the community. To streamline the data while maintaining the majority of species present, an ‘other’ category was created for families with abundances comprising less than 0.05% of the total abundance in the wells (Fig. 9).

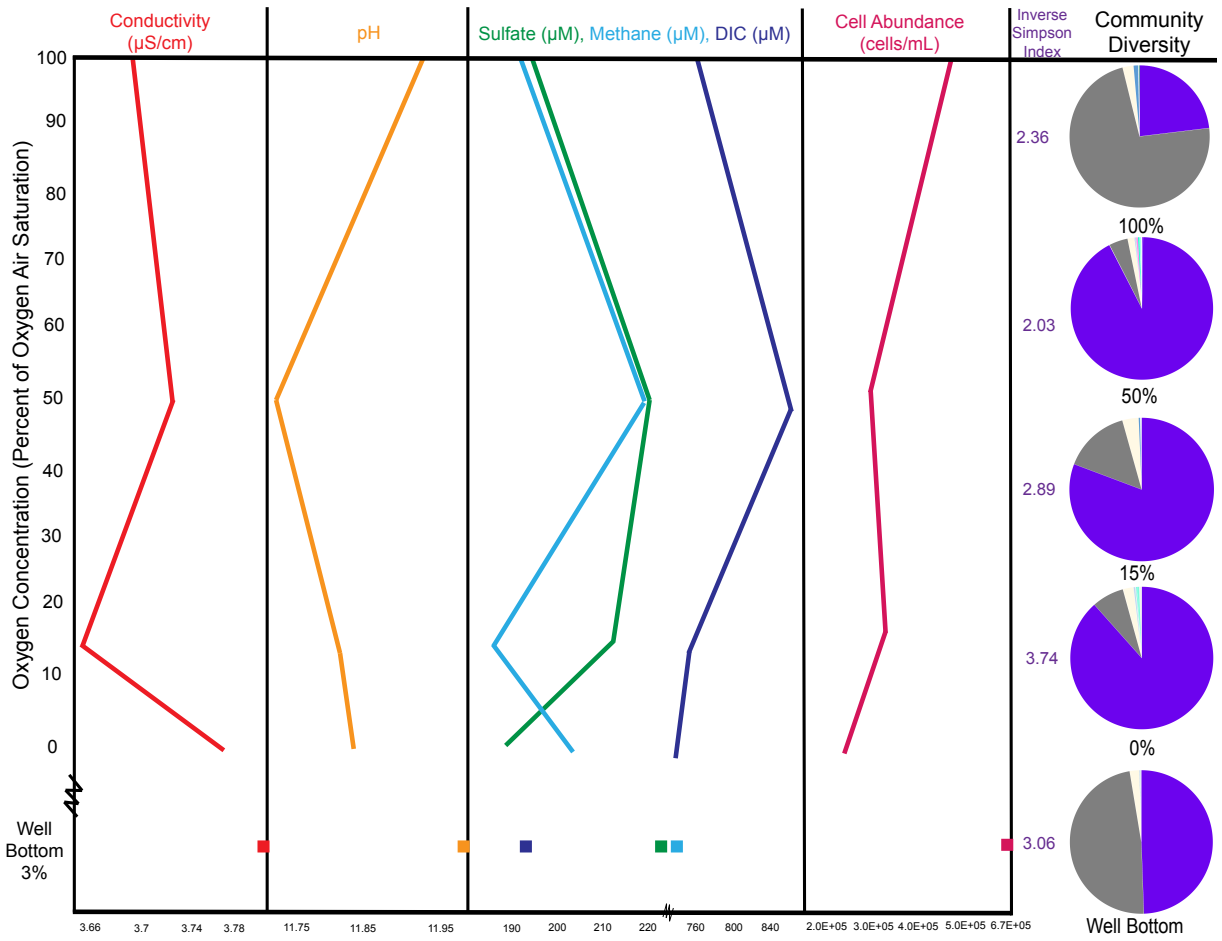

Figure 8 - CSW1.1 Profile Chemistry and Bacterial Families. Conductivity, pH, sulfate, methane, DIC, and cell abundances are shown next to their respective microbial community pie chart and Inverse Simpson diversity index. Clostridiaceae (purple), Trueperaceae (dark grey), and Xanthomonadaceae (light yellow) dominate the communities throughout, with appearances of Verrucomicrobiaceae (pink) SRB2 (light blue), Methylobacteriaceae (green). Organisms comprising less than 1% of the total well abundance were grouped into the <1% category (light grey), and those listed as unclassified or uncultured were grouped into an Unclassified category (lighter grey). The full phylogeny for the profile and all CROMO wells analyzed here is listed in Table 11.

Profile Compared to Other Wells

A comparison of the aqueous chemistry and microbiology from the water column study to the remaining shallow, medium, and deep CROMO wells was completed to gain perspective into how this data-rich profile fits within the complex serpentinite subsurface waters. Generally, CROMO organisms are influenced by a wide range of chemical parameters, however CSW 1.1 organisms are strongly influenced by organic acids, pH, and conductivity (Twing et al., 2017). Shallow wells at CROMO (CSW1.4, N08-C, QV1.2, and CSW1.2) are the least reducing, have the lowest pH, and have the highest concentrations of nitrate (up to 75 μM), while intermediate wells (CSW1.1, QV1.1, CSW1.3, and N08-B) exhibit a relative drop in ORP, increase in conductivity, nitrate levels predominantly below detection, and an increase in pH. Deep wells (CSW1.5, QV1.3, N08-A, and CSWold) have extremely high conductivities and chloride values, pH levels approximately 10.0, a minimal amount of nitrate, and the most negative ORP values overall (Table 10).

The CSW1.1 profile most similarly reflects intermediate well conditions, in terms of pH, ORP, conductivity, and nitrate levels. However, chemistries fluctuate enough that distinctions can be made between each depth in the profile. Other CROMO wells show higher microbial diversities compared to CSW 1.1 (Fig. 9; Twing et al., 2017). Biologically, the profile compares most strongly to data from the base of CSW1.1, and though CSW1.1 is more oxic near the top, it does not reflect conditions or community diversity characteristic of the shallow well group (Fig. 9).

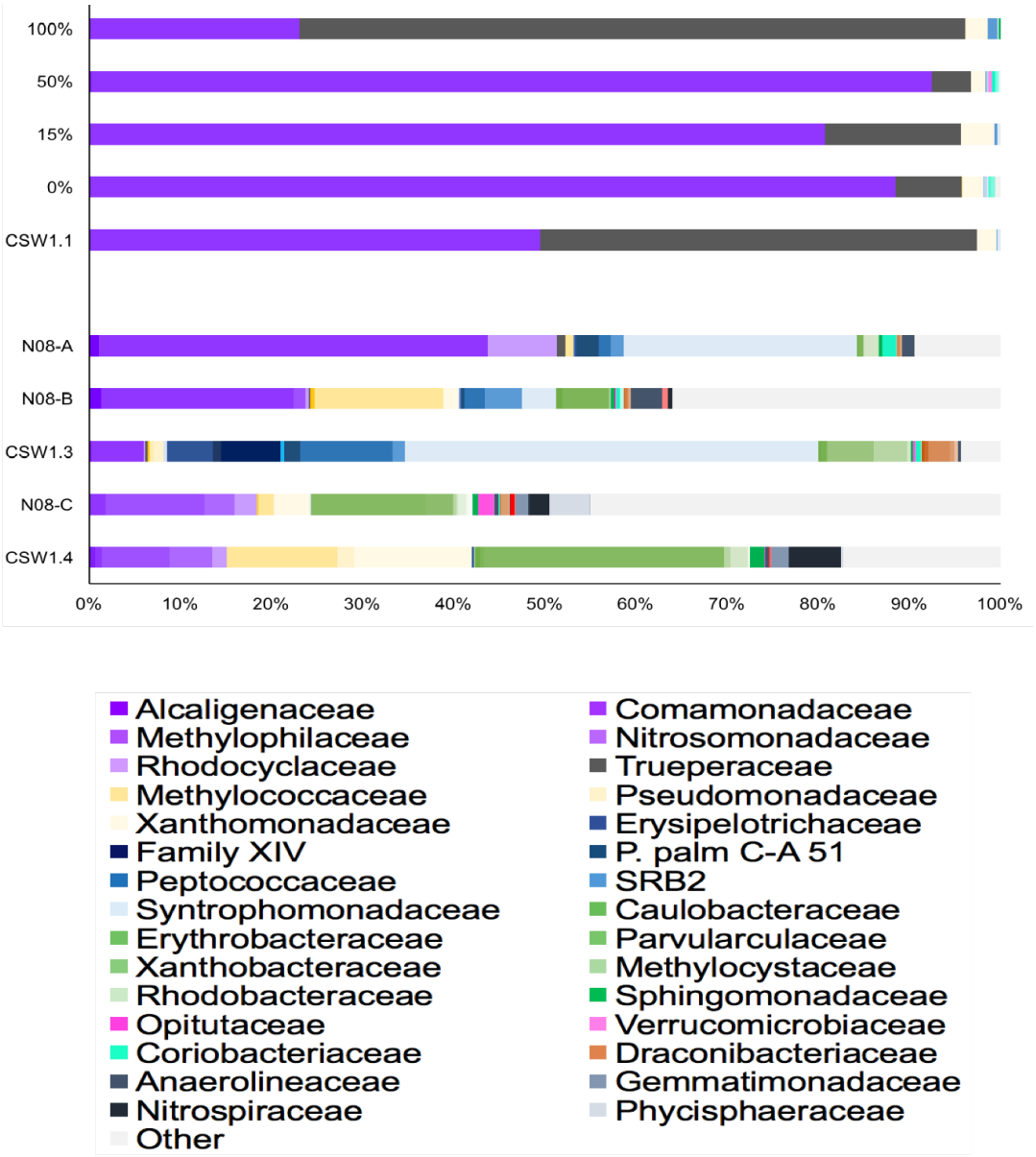

Figure 9 - Community Compositions from 16S rRNA sequences. Microbial communities from the profile and wells listed above were assembled into amplicon sequence variants (ASVs) in Mothur using the average-neighbor algorithm. Note that filtered fluids were limited to 400 mL per depth in the profile, and 4 liters in all other samples. Color blocks indicate Phylum/Class, and specific colors indicate ASVs. Truepera (grey), Betaproteobacteria (purple), Firmicutes (blue), Alphaproteobacteria (green), Gammaproteobacteria (yellow), Actinobacteria (Teal), Bacteroidetes (orange), Verrucomicrobiae (pink), and for Phyla/Classes with only one member observed, shades of blue-grey (0-50% transparency) were assigned. These include Nitrospirae, Gemmatimonadetes, Chloroflexi, and Planctomycetes. ASVs with calculated abundances <0.05% of the total dataset for each well. Groups greater than 1% abundance are listed in the legend; the full taxonomic description for the data is listed in Table 11.

Microcosms

Results from the 190-day microcosm experiment reveal an overall increase in cell abundance through time. $^{13}CH_4$ + thiosulfate amended bottles from the anoxic well bottom revealed the highest growth overall (3.37×10^5 cells/mL; Fig. 10), with $^{13}CH_4$ amended anoxic bottles just below these concentrations. Oxic bottles for these two amendments revealed slightly fewer cells. $^{13}CH_4$ + iron inoculated bottles showed the least amount of growth, though the concentrations in the anoxic $^{13}CH_4$ + iron bottles remained steady overall.

16S rRNA analyses extracted at the 190-day mark reveal an extremely low diversity of organisms. An abundance of Truepera is evident under all conditions, and Comamonadaceae is apparent in smaller quantities than in the well profile of CSW1.1. Anoxic methane bottles reveal the least diversity, with abundances of only Trueperaceae and Comamonadaceae detected. Oxic methane bottles additionally host small quantities of Xanthomonadaceae and Bradyrhizobiaceae. Thiosulfate oxic bottles reveal Alphaproteobacteria Sphingomonadaceae (SRB-2), and KCM-B-15, and Actinobacteria YNPFFP1, Planctomycetaceae, and Acidobacteriaceae. Thiosulfate anoxic bottles selected for RB41, and two Actinobacteria families, in addition to Truepera and Comamonadacecae. Oxic iron bottles reveal no additional groups than the dominant members, while anoxic iron bottles show a large diversity of families of the Gammaproteobacteria, Truepera, Firmicutes, Betaproteobacteria, Bacilli, and Actinobacteria.

The most confounding results from these microcosms lies in the del ^{13}DIC data (Fig. 10C). Separation from experiments and controls from Day 0 to Day 190 is

observed in both thiosulfate treatments and both methane treatments. Anoxic thiosulfate bottles revealed the greatest separation (i.e. the highest biologic ^{13}DIC production), followed by oxic thiosulfate, oxic methane, and anoxic methane treatments. Iron control bottles for both oxic and anoxic sets show more ^{13}DIC than the experimental bottles.

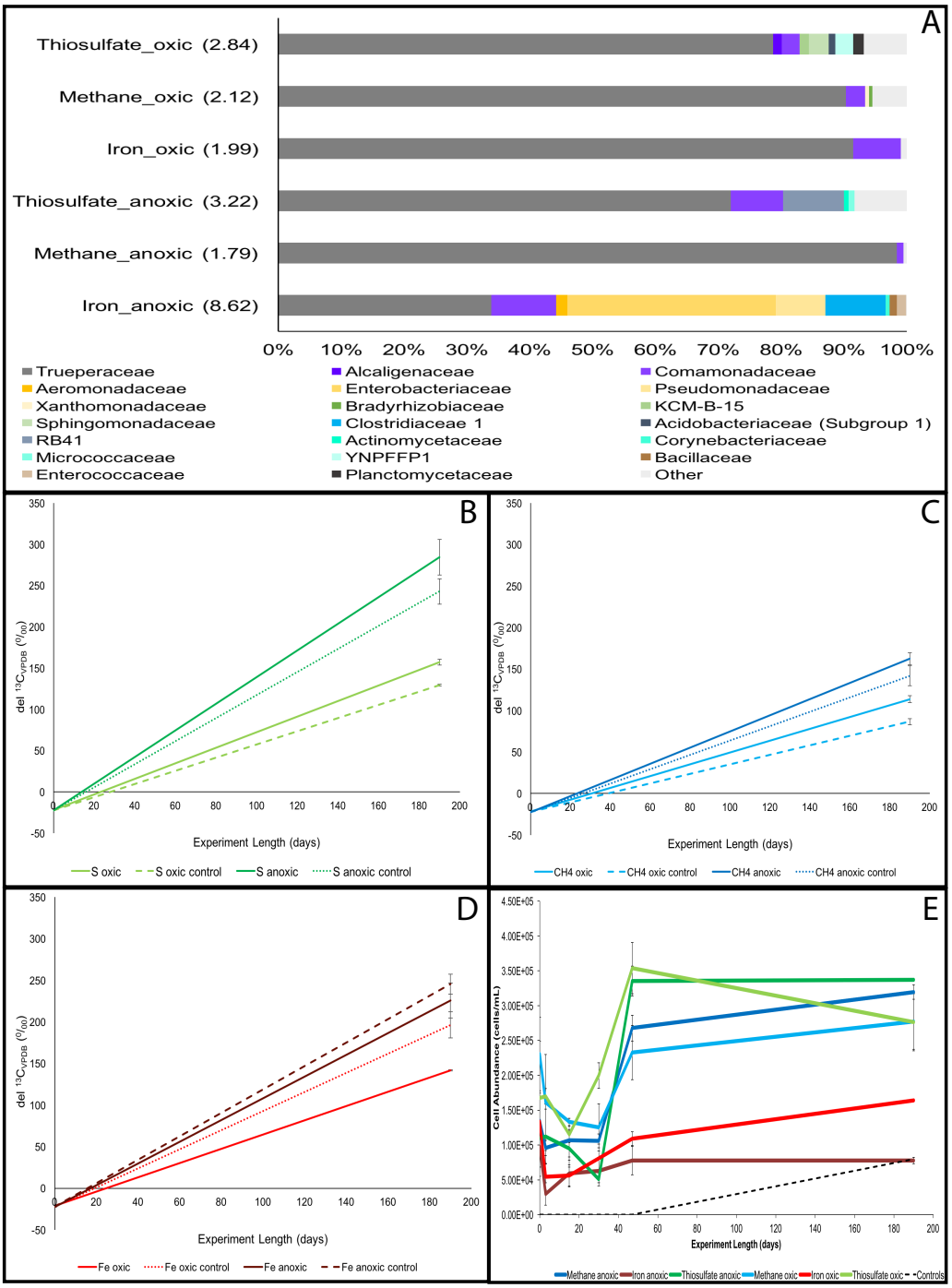

Figure 10 - Depth Profile Microcosm Results. (A) Microcosm 16S rRNA end-point bacterial community composition. Phyla/Class are represented by individual colors, and ASVs are identified by individual shades. Colors are the same as in Figures 8 and 9 with the addition of Bacilli (brown). (B-D) ^{13}DIC separation is observed between experiments and controls from the duration of the experiment, except in iron experiments. $^{13}CH_4$ was consumed and ^{13}DIC was created. (E) Cell abundances throughout the 190-day experiment for each amendment. Contamination was observed in the final time point for the anoxic set of controls, represented by the dashed line.

Discussion

The exploration of small scale processes associated with the unique serpentinite microbiology in a location such as the Coast Range Ophiolite Microbial Observatory in northern California as it can lend important insight into how these extreme organisms take advantage of chemical gradients that develop over time to gain energy. Aqueous chemistry data coupled to thermodynamic free energy calculations, archaeal qPCR, bacterial 16S rRNA data, and microcosm results reveal relationships between abiotic and biotic components of this system, and provide multiple lines of evidence for methane oxidation in the subsurface ecosystem.

CSW1.1 Gradient Identification via Depth Profile

The CSW1.1 well is drilled into complex subsurface lithologies consisting of three predominant sections, as described in detail by Ortiz et al., (submitted), and discussed here briefly (Fig. 6). Meteoric water that falls predominantly during the wet season is stored in the upper 3.5m of the subsurface at CROMO. This circumneutral water can mix with the deeper serpentinite influenced fluids and host a more habitable environment for organisms. As the two end members mix, dissolved ions in solution can interact, leading to thermodynamic disequilibrium and the development of chemical gradients. Due to field equipment restraints (i.e. DO probe length), this study was unable to explore trends throughout the middle portion of the well. Below this shallow section, intermittent aquicludes and perched aquifers permit the isolation of microbial communities that may remain largely unexplored owing to these sampling restrictions. The deeper subsurface (>20m depth) hosts medium storativity serpentinite aquifers that

are extremely saline relative to other continental serpentinizing systems (Chapter 2), and a community of microbes that have adapted to the hyperalkaline groundwaters (Crespo-Medina et al., 2014; Twing et al., 2017).

From the results of Chapter 2, while CSW1.1 was drilled to 31m depth, it is only cased with PVC to 5m depth and as a result a 10-meter collapse of the borehole during drilling was observed, placing it with the medium depth wells. Rather than extracting waters only from 19.5m depth, CSW1.1 hosts chemistries less representative of the deeply sourced wells, and has some influence from shallower layers. This lends insight into mixing within the well and an understanding of how the water stored within the serpentine gravel, magnetite-bearing serpentinite, and (deeper) serpentinite-altered mafic rock layers impact the water chemistry when compared to surrounding cased wells.

Aqueous chemistry within the CSW1.1 profile shows abundant concentrations of methane, sulfate, DIC, and chloride. Once oxygen becomes a limiting factor, sulfate becomes the dominant electron acceptor in this system due to nitrate, nitrite, (Table 8) and previously determined manganese (Chapter 1, Table 1) quantities that fall below detection. With nitrate concentrations below detection, methane and sulfate relationships became the focus of this study. Concentrations of CH_4 and SO_4^{2-} increase at first with depth, but at the 50% oxygen interface, both slightly decrease, indicating a shift from aerobic methane oxidation to anaerobic processes (Fig. 8). Conditions above this point are more oxidizing, and below here transition more reducing, allowing sulfate to be consumed abiotically or by sulfate reducing organisms.

It is evident from thermodynamic calculations that aerobic methane oxidation is one of the most energetically favorable processes for organisms to perform in this system, with free energies as high as -123 J/L (Fig 7; Table 10). Where oxygen levels are greater than 50% air saturation, this process transforms methane and oxygen into CO_2 and water. As oxygen quickly becomes a limiting factor with depth and delta G values decrease in response, anaerobic methane oxidation (AOM) reactions become favorable alternatives, as observed at the 15% depth where aerobic methane oxidation free energies fall below the favorability for AOM coupled to sulfate reduction. AOM coupled to thiosulfate reduction was calculated to understand how the striking relationships observed in Chapter 1 between thiosulfate and metabolic activity transitions to this water column study. From these calculations AOM coupled to thiosulfate oxidation is less favorable, yet is still an exergonic process.

In the water column, microbial community compositions indicate a dominance of Trueperaceae, Comamonadaceae, SRB-2 (Clostridia), Syntrophomonadaceae, and Xanthomonadaceae throughout. At the top of the profile, Trueperaceae are the dominant family, with few Comamonadaceae and SRB-2. *T. radiovictrix,* the only species yet to be named from the Truepera Phyla, does not grow below 20°C or above approximately pH 11.2 (Albuquerque et al., 2005). Because Trueperaceae clearly dominates the CROMO fluids at pH 12, 15°C, and anoxic conditions, it is likely the species here is a native group of the system adapted to the extreme conditions present in these fluids (Fig. 8). These organisms play a key role in this system that requires further exploration through culturing.

At the 50% level, organisms capable of oxidizing hydrogen with a variety of electron acceptors (Comamonadaceae) become the dominant family, and in addition, the sulfate reducing SRB-2 and *Dethiobacter* groups are detected. This is the only depth where Burkholderiaceae, a family known to inhabit oxygen-mixing zones and have aerobic H_2- fueled capabilities, are detected (Twing et al., 2017). The candidate genus 'Serpentinomonas' of the Comamonadaceae family was reported to grow optimally at pH 11 and utilize hydrogen and calcite. While the three isolates were all capable of utilizing oxygen, A1 could transform thiosulfate and B1 and H1 used nitrate (Suzuki et al., 2014).

Serpentine soil bacteria Actinobacteria and Verrucomicrobiaceae take advantage of the chemical gradient and thrive here. Specifically, *Dietzia natronolimnaea* is an alkaliphilic organism isolated from an African soda lake identified at this depth. At 15%, diversity decreases potentially due to a decrease in DIC, methane, and other chemical components, and only Trueperaceae and Comamonadaceae remain abundant.

The 0% air saturation level is the most confounding of all four profile depths examined. A spike in chloride, conductivity, ORP, pH, and methane, and a decrease in sulfate and oxygen (Fig 8; Table 8) are observed here as the system attempts to reach equilibrium. While the goal was to extract water only from the stagnant water column, due to the drilling decision to shorten well casings for CSW1.1 and QV1.1, water was additionally pulled from the adjacent aquifer at the 0% air saturation level, as evidenced by the surge of soil- hosted bacteria identified here (as depicted in Fig. 6 by the dashed well outline at depth; Fig. 9). This allows a glimpse into the niches present within the low diversity hyperalkaline serpentinite subsurface. In the shallow CSW1.1 core material,

Acidobacteria, Actinobacteria, Bacteroidetes, Chloroflexi, Gemmatimonadetes, and Planctomycetes, Proteobacteria, and Verrucomicrobia were identified as the groups significantly distinct from fluid- or core-enriched taxa (Twing et al., 2015). In addition to the Firmicutes and Betaproteobacteria, (fluid-enriched taxa; Twing et al., 2015) documented in this study, soil-enriched taxa include 3 families within Actinobacteria, and core-enriched taxa include one family within Gammaproteobacteria.

In this region where the oxic-anoxic interface exists, microbes increase in abundance and are likely performing a consortia of methane metabolic reactions to obtain energy, including aerobic methane oxidation, anaerobic oxidation of methane coupled to sulfate reduction, and potentially AOM coupled to thiosulfate reduction. Because oxygen is decreasing in the profile, organisms become increasingly reliant on anaerobic metabolisms, and communities shift toward those capable of facilitating anaerobic processes. While groups such as SRB-2 and *Dethiobacter* are capable of sulfate reduction, archaea are currently the only organisms known to be capable of facilitating AOM when coupled to sulfur cycling (Knittel et al., 2009). However, bacteria capable of facilitating AOM coupled to nitrogen cycling were recently identified, indicating more organisms may be capable of performing these reactions solo than are currently known (Ettwig et al., 2010)

Because archaea were detected in CROMO well fluids via qPCR for the first time during this study, ongoing efforts for sequencing these organisms are in progress. Previous studies of core material at CROMO reveal Methanosarcinales within the Euryarchaeota phyla are abundant in QV1.1, and Euryarchaeota, Crenarchaeota, and Thaumarchaeota are enriched in CSW1.1 (Twing et al., 2015). With these results in

mind, it is likely soil archaea (Thaumarchaeota) were detected in CSW1.1, though ongoing 16S rRNA analyses will aid in determining archaeal community composition.

With the striking chemistry, thermodynamic, and microbiological results, particle-associated archaea in saturated serpentine pore spaces should be the focus moving forward to further unravel methane cycling mechanisms in the serpentinite subsurface. If known AOM participants are absent in these fluids, microaerophilic methane oxidation processes may be contributing to the signals observed while releasing formaldehyde intermediate products (Ettwig et al., 2010) through organisms from Phyla such as Verrucomicrobia or Actinobacteria. Ongoing stable isotope culturing work with CROMO fluids under conditions selecting for AOM processes will further aid in the identification of any active AOM organisms.

Comparison to Bottom of CSW1.1

To understand how this top-down profile of CSW1.1 relates spatially within the serpentinite subsurface, fluid biogeochemistry was compared to the bottom of CSW1.1, where seasonal sampling routinely occurs. Where lithologies transition to more intact serpentine bedrock at the base of CSW1.1, water chemistries exhibit higher pH levels, higher conductivities, and dissolved oxygen concentrations around 3% of oxygen air saturation. This slight peak in oxygen may be due to a combination of discrepancies between DO probes used (ultrasensitive DO probe at top, YSI probe at bottom), and mixing processes. Additionally, June 2016 falls just after the wet season (Ortiz et al., in submission), where fluids have potential to mix more than during the dry season.

At the bottom of CSW1.1 where pH reaches a site-wide maximum of 12.0, organisms are divided almost evenly between Trueperaceae and Comamonadaceae. The Gammaproteobacteria Xanthomonadaceae family (unclassified organism from the genus *Silanimonas*) comprises the remaining few percent of the community. This sampling point is a window into the true extremophiles of the system. From many studies, it is evident Betaproteobacteria dominates deeply sourced serpentinite fluids (Brazelton et al., 2012; Brazelton et al., 2013; Schrenk et al., 2013). Comamonadaceae are a well-known family harboring the *Serpentinomonas* genus, and utilize the hydrogen, calcium carbonate, and oxygen to generate energy in these waters (Suzuki et al., 2013). Xanthomonadaceae are less abundant, but are to date only known to be strictly aerobic, non-spore forming organisms withstanding pH values up to 10.0 (*S. lenta*) and 12.0 (*S. mangrovi*) (Lee et al., 2005; Srinivas et al., 2013). Trueperaceae are by far the confounding family here, as the only member characterized to date is known for its extreme ionizing radiation resistance capabilities (Albuquerque et al., 2005). While this alkaliphilic, slightly thermophilic and halophilic group may be simply surviving within this environment, they can potentially utilize the organic acids, amino acids, and other carbon compounds in the system. It is likely they are native members of the system as they comprise almost 50% of the population at 19.5m depth where *in situ* experiments have not been performed.

Comparison to Other CROMO Wells

The CSW1.1 profile hosts oxygen concentrations that range from 9.4 mg/L DO to 0.075 mg/L. Due to the abundance of oxygen, community diversity at the top of the well

should be most similar to shallow wells N08-C and CSW1.4. However, because pH is ~11.8 in the profile, different groups are observed. CSW1.3, N08-B, and N08-A reveal higher pH values (~10) than the shallow wells (~7.5), but host a wider diversity of organisms (Fig. 9), indicating fluid chemistries and pH tolerance play a key role in determining community composition. In the deepest well represented in this study, N08-A, abundant populations of Comamonadaceae (Betaproteobacteria) and Firmicutes such as Syntrophomonadaceae, SRB-2, Peptococcaceae, and Clostridiaceae (known sulfur cyclers) are present. Organismal abundance is CSW1.1 is considerably less than even this deeply sourced groundwater well.

Microcosms

Thirty-six 500mL microcosms created from the top of the CSW1.1 profile (15% oxygen air saturation; 18 bottles) and the bottom of the well (19.5m; 18 bottles) were all inoculated with $^{13}CH_4$ and monitored at incubation-end for evolution to ^{13}DIC. In 6 bottles from the top and bottom of the well respectively, 2mM thiosulfate was amended. Similarly, iron oxyhydroxide was amended to another 6 from each set. The remaining 6 from each set received only $^{13}CH_4$. Bottles from the top of the well received 2mL oxygen gas in order to maintain their “oxic” status.

Evidence for methane cycling is apparent in both the thiosulfate + $^{13}CH_4$ and $^{13}CH_4$-only inoculated experiments, while iron-amended bottles reveal minimal results in terms of ^{13}DIC concentrations. Biologic aerobic methane oxidation is apparent in the oxic methane set of cultures in terms of cell growth and end point ^{13}DIC concentrations (Fig. 10). Bacterial families Xanthomonadaceae, Bradyrhizobiaceae, Trueperaceae, and

Comamonadaceae were detected in these cultures, which signifies their potential role in this process.

Iron- amended bottles reveal little to no cell growth throughout the experiment and higher ^{13}DIC concentrations in control bottles above those of the set's experimental values at the end of the incubation time indicate biologic methane oxidation coupled to iron reduction is not an active process in these cultures. Oxic iron bottles reveal no additional groups than the dominant members, while anoxic iron bottles show a large diversity of families from the Gammaproteobacteria, Truepera, Firmicutes, Betaproteobacteria, Bacilli, and Actinobacteria groups. Though a greater amount of diversity was identified here, evidence for methane oxidation coupled to iron reduction is not evident in the CSW1.1 fluid.

In contrast to the lack of results in iron-amended bottles, thiosulfate- amended cultures reveal not only the highest cell growth, but the highest measured biologic ^{13}DIC production of all treatments. This is striking evidence for methane cycling at CROMO and potentially for the anaerobic oxidation of methane coupled to thiosulfate. While neither an organism capable of facilitating this entire reaction nor an ANME organism have been isolated and characterized, it is apparent sulfate-reducing and thiosulfate-utilizing bacteria are present in both the experiment and the CSW1.1 fluids. Thiosulfate anoxic bottles selected for bacterial families RB41, Trueperaceae, Comamonadacecae, and two Actinobacteria families.

It is clear Truepera and Comamonadaceae are two groups that are ubiquitous throughout these cultures, and while Comamonadaceae are known to be endemic to serpentine systems, Trueperaceae require further investigation to understand if their

role in this system is purely survival, or if they are active contributors to the biologic ^{13}DIC quantities observed. Due to their abundant presence at the bottom of CSW1.1 during regular sampling in the June 2016 field campaign, it is likely they are also endemic to the CROMO system.

Ongoing work to classify the archaeal community at CROMO via 16S rRNA analysis and to isolate the organisms in this experiment will help to determine those responsible for the biologic isotopic variations. These results are promising for future stable isotope culturing work involving intermediate sulfur species and AOM within serpentinizing systems.

Conclusions

This novel profile study is a detailed look into how fluid within serpentinite hosted wells equilibrates with the more deeply seated aquifers post-pumping, and how small chemical gradients impact microbial community dynamics. Combined, this lends new insight into how life thrives within these waters and helps to understand the relationship between chemical gradients, microbial populations, and energy availability. Fluctuating concentrations of sulfate and methane, energetically favorable AOM thermodynamic calculations, and evidence of microbes capable of facilitating sulfate reduction and methane cycling reactions implicate the execution of aerobic methane oxidation near the top of the profile, and reveal potential for AOM at the oxic-anoxic interface and well bottom at CROMO. Bacterial populations identified at CROMO are capable of utilizing methane, which provides intermediate carbon compounds for sulfate reduction. For the first time, qPCR shows archaeal populations are present in CSW1.1 fluids that may be

contributing to the cycling of methane, and ongoing culturing and 16S rRNA sequencing work will help to determine this extent. Together, this study reveals the key role methane and sulfur cycling have in guiding community diversity in this serpentinite-hosted environment.

APPENDIX

Table 10 - CSW1.1 Depth Profile Biogeochemical Measurements

	% Air Saturation	DO (mg/L)	Depth Sampled	pH	T (℃)	ORP (mV)	Conductivity (µS/cm)	Fe	Fe^{2+}	HS^-	SO_4^{2-}	Cl^-	Br^-	F^-	NO_3^-	NO_2^-	DIC	H_2	CO	CH_4	Cell Abundance (cells/mL)	Qubit (ng/mL)
top of well	100%	9.20	2.81	11.95	15.01	-224.00	3706.00	1.51	0.79	0.01	196.84	3381.8	1.40	16.56	< 1.00	< 1.00	774.14	0.03	0.24	194.19	4.70E+05	2.28
	50%	4.66	3.41	11.76	15.20	-228.10	3738.00	3.19	1.15	0.01	223.23	3423.8	< 1.00	< 1.00	< 1.00	< 1.00	875.09	0.04	0.24	221.67	3.08E+05	5.18
	15%	1.40	3.21	11.84	15.04	-213.80	3667.00	1.42	1.04	0.03	214.59	2931.7	< 1.00	36.12	< 1.00	< 1.00	764.82	0.04	0.26	188.78	3.37E+05	48.80
	0%	0.07	5.91	11.86	15.00	-226.60	3778.00	1.31	0.52	0.05	191.11	3398.6	< 1.00	< 1.00	< 1.00	< 1.00	748.13	0.05	0.31	205.22	2.64E+05	3.25
bottom of well	3%	0.23	19.50	12.00	18.71	-261.70	3820.00	0.91	0.54	3.54	389.55	2466.36	30.91	15.79	<1.61	< 1.45	195.00	0.20	0.02	620.00	6.66E+05	16.30

look at all time data to see if bottom is normal DO

collapsed well depth = 19.5 meters
drilled well depth = 31.09 meters
peristaltic pump used to pump water from top of well
bladder pump pre-installed at well bottom used to pump well bottom fluids
% Air Saturation = oxygen level relative to the concentration of atmospheric oxygen
DO = dissolved oxygen; DTW = depth to water; DIC = dissolved inorganic carbon
n.a. = not analyzed

Table 11 - Thermodynamic Data for Select Methane Oxidation Reactions in CSW1.1

	% Air Saturation	Total △G (J/L)	**Aerobic Methane Oxidation** $CH_4 + 2O_2 \rightarrow CO_2 + 2H_2O$	**AOM + Sulfate Reduction** $CH_4 + SO_4^{2-} + H^+ \rightarrow HS^- + CO_2 + H_2O$	**AOM + Thiosulfate Reduction** $CH_4 + S_2O_3^{2-} \rightarrow 2HS^- + 2H^+ + CO_2$	**AOM + Iron Reduction** $CH_4 + Fe^{3+} + 2H_2O \rightarrow Fe^{2+} + 8H^+ + CO_2$	**AOM + Nitrate Reduction** $CH_4 + NO_3^- \rightarrow CO_2 + NO_2^-$
Top of Well	100%		-166.26	-12.61	-0.18	0.40	0.00
	50%		-62.10	-14.24	-0.18	0.58	0.00
	15%		-18.51	-11.86	-0.17	0.52	0.00
	0%		-0.92	-11.83	-0.17	0.26	0.00
Bottom of Well	3%		-3.04	-22.71	-0.08	0.13	0.00

Activities	**100%**	**50%**	**15%**	**0%**	**14%**
aCH_4	-3.71	-3.65	-3.72	-3.69	-3.23
aCO_2	-10.23	-10.18	-10.24	-10.25	-10.24
aO_2	-3.54	-3.84	-4.36	-5.65	-4.89
aH^+	-11.95	-11.76	-11.84	-11.86	-12.07
aSO_4^{2-}	-4.11	-4.05	-4.07	-4.12	-3.79
aHS^-	-8.99	-8.99	-8.69	-8.51	-6.42
$aS_2O_3^{2-}$	-6.40	-6.40	-6.40	-6.40	-6.38
aFe^{3+}	-6.60	-6.60	-6.60	-6.60	-6.59
$aHCO_3^-$	-4.67	-4.62	-4.68	-4.69	-4.68
aCO_3^{2-}	-3.12	-3.07	-3.13	-3.14	-3.13
aFe^{2+}	-6.45	-6.45	-6.46	-6.46	-6.44

AOM = Anaerobic Methane Oxidation

Table 12 - Aqueous Chemistry of CROMO Wells June 2016

		pH	Temp (℃)	Conductivity (µS/cm)	DO (mg/L)	ORP (mV)	SO_4^{2-}	Cl^-	Br^-	NO_3^-	NO_2^-	F^-	Ni	Fe	Cr	DOC	S	Si	H_2	CO
Shallow Wells	**CSW1.4**	7.87	17.34	1978.00	4.40	203.00	429.42	11018.89	43.80	74.99	< 1.45	14.21	9.25	5.87	2.53	66.21	367.51	140.25	0.02	0.14
	N08-C	7.25	16.67	1393.00	0.20	39.80	77.45	7653.45	42.55	72.74	< 1.45	9.47	5.46	21.30	1.40	16.62	41.41	42.02	0.02	0.08
	QV1.2	9.31	16.68	3004.00	0.17	-156.20	0.00	26610.32	76.84	30.48	< 1.45	7.37	8.92	5.39	2.52	15.77	8.99	33.60	BDL	0.05
	CSW1.2	8.80	16.90	4627.00	0.41	-97.50	112.43	118487.17	225.65	14.19	< 1.45	5.26	1.49	4.70	0.31	26.79	149.70	228.58	0.01	0.15
Medium Wells	**CSW1.1**	12.00	18.71	3820.00	0.23	-261.70	389.55	2466.36	30.91	< 1.61	< 1.45	15.79	5.06	3.62	1.41	298.80	752.18	711.77	0.02	0.06
	QV1.1	11.41	16.74	3362.00	0.18	-181.00	76.10	22704.54	71.71	< 1.61	< 1.45	10.53	2.63	19.75	0.32	78.03	71.52	55.11	0.02	0.06
	CSW1.3	10.10	18.83	4787.00	0.21	-275.20	174.79	49937.16	110.51	34.51	< 1.45	10.00	1.81	4.00	0.32	21.02	101.48	401.12	0.02	0.13
	N08-B	10.22	16.87	3047.00	0.15	-78.60	58.30	25214.26	74.71	< 1.61	< 1.45	8.42	1.35	15.16	0.35	28.04	32.30	34.83	0.03	0.15
Deep Wells	**CSW1.5**	9.77	15.69	4780.00	0.49	-206.50	358.21	44051.77	99.74	< 1.61	< 1.45	6.32	1.35	3.92	0.34	40.29	571.18	811.20	0.01	0.11
	QV1.3	9.78	16.55	4735.00	0.22	-207.80	72.25	45098.26	103.12	7.74	< 1.45	5.79	9.14	7.67	2.52	17.25	58.45	330.19	0.02	0.13
	N08-A	10.82	16.32	6040.00	0.27	-216.10	77.14	55218.04	119.64	3.71	< 1.45	7.90	10.36	17.56	2.60	11.82	72.54	383.16	BDL	0.08
	CSW OLD	9.84	18.45	11290.00	1.42	-356.70	170.21	38998.12	94.11	1.94	< 1.45	10.53	6.20	16.21	1.60	22.23	121.70	302.10	0.01	BDL

Table 13 - Family Abundance from 16S rRNA Analysis

Phylum/Class	Family	CSW1.4	N08-C	CSW1.3	N08-B	N08-A	CSW1.1	0%	15%	50%	100%
Betaproteobacteria	Alcaligenaceae	3	106	0	2640	1747	0	0	0	0	0
Betaproteobacteria	Burkholderiaceae	955	0	262	0	0	0	0	0	271	0
Betaproteobacteria	Comamonadaceae	968	2062	5186	43181	71461	38140	82283	77704	99823	2885
Betaproteobacteria	Methylophilaceae	10164	13036	0	2599	0	0	0	0	0	0
Betaproteobacteria	Nitrosomonadaceae	6473	3918	0	0	0	0	0	0	0	0
Betaproteobacteria	Oxalobacteraceae	0	70	0	0	0	0	0	0	55	0
Betaproteobacteria	Rhodocyclaceae	2159	2945	119	911	12673	0	0	0	0	0
Truepera	Trueperaceae	0	0	208	252	1655	36980	6775	14363	4628	9113
Gammaproteobacteria	Alteromonadaceae	0	0	192	363	0	0	0	0	0	0
Gammaproteobacteria	Chromatiaceae	0	0	0	624	0	0	0	0	0	0
Gammaproteobacteria	Coxiellaceae	0	64	0	0	0	0	0	0	0	0
Gammaproteobacteria	Ectothiorhodospiraceae	0	68	0	0	0	0	0	0	0	0
Gammaproteobacteria	Enterobacteriaceae	0	0	51	0	0	0	62	0	0	0
Gammaproteobacteria	Legionellaceae	0	82	0	0	0	0	0	0	0	0
Gammaproteobacteria	Methylococcaceae	16693	1996	74	28876	1436	0	0	0	0	0
Gammaproteobacteria	Moraxellaceae	0	0	266	0	0	0	0	0	0	0
Gammaproteobacteria	Pseudomonadaceae	2531	191	994	0	0	0	0	0	0	20
Gammaproteobacteria	Xanthomonadaceae	17788	4566	0	3413	0	1663	2152	3491	1687	292
Firmicutes	Acholeplasmataceae	0	0	310	0	0	0	0	0	0	0
Firmicutes	Bacillaceae	0	0	63	0	0	0	0	0	0	0
Firmicutes	Caldicoprobacteraceae	0	0	0	316	0	0	0	0	0	0
Firmicutes	Clostridiaceae 4	0	0	0	149	306	0	0	0	0	0
Firmicutes	Erysipelotrichaceae	195	0	4574	122	215	0	0	0	0	0
Firmicutes	Family XI	0	0	0	0	105	0	0	0	0	0
Firmicutes	Family XII	0	0	782	0	0	0	0	0	0	0
Firmicutes	Family XIV	0	0	5931	0	0	0	0	0	0	0
Firmicutes	Lachnospiraceae	0	0	345	0	0	0	0	0	0	0
Firmicutes	P. palm C-A 51	144	0	1603	757	4123	0	0	0	0	0
Firmicutes	Peptococcaceae	0	0	9140	4424	2159	0	0	0	0	0
Firmicutes	SRB2	0	0	1281	8363	2377	82	0	315	96	135
Firmicutes	Staphylococcaceae	0	0	0	0	0	0	57	0	151	0
Firmicutes	Streptococcaceae	0	0	0	0	0	0	302	0	172	0
Firmicutes	Syntrophomonadaceae	89	178	41054	7607	42829	274	184	275	0	16
Alphaproteobacteria	Acetobacteraceae	835	0	183	1477	329	0	0	0	0	0
Alphaproteobacteria	Bradyrhizobiaceae	0	0	560	0	0	0	0	0	0	0
Alphaproteobacteria	Caulobacteraceae	555	0	125	10358	786	0	0	0	0	0
Alphaproteobacteria	Erythrobacteraceae	36259	15175	0	0	101	0	0	0	0	0
Alphaproteobacteria	Parvularculaceae	0	3624	0	0	0	0	0	0	0	0
Alphaproteobacteria	Phyllobacteriaceae	0	0	0	111	0	0	0	0	0	0
Alphaproteobacteria	Xanthobacteraceae	0	0	4592	105	0	0	0	0	0	0
Alphaproteobacteria	Hyphomicrobiaceae	0	62	0	0	0	0	0	0	0	0
Alphaproteobacteria	Methylocystaceae	967	403	3369	0	0	0	0	0	0	0
Alphaproteobacteria	Rhizobiaceae	0	0	0	0	133	0	0	0	0	0
Alphaproteobacteria	Rhodobacteraceae	2595	203	333	199	2687	0	0	0	0	0
Alphaproteobacteria	Rhodobiaceae	0	1068	0	0	0	0	0	0	0	0
Alphaproteobacteria	Rhodospirillaceae	311	248	0	0	0	0	0	0	0	0
Alphaproteobacteria	Rickettsiaceae	0	634	0	0	0	0	0	0	0	0
Alphaproteobacteria	Sphingobacteriaceae	0	0	0	108	0	0	0	0	0	0
Alphaproteobacteria	Sphingomonadaceae	2219	727	182	835	675	0	0	0	0	25
Verrucomicrobia	Chthoniobacteraceae	0	0	0	202	0	0	0	0	0	0
Verrucomicrobia	Opitutaceae	78	2045	210	0	0	0	0	0	0	0
Verrucomicrobia	Verrucomicrobiaceae	0	77	108	144	0	0	0	0	433	0
Acidobacteria	Acidobacteriaceae	0	609	0	0	0	0	0	0	0	0
Actinobacteria	Corynebacteriaceae	0	0	0	0	0	0	0	0	345	0
Actinobacteria	Cellulomonadaceae	0	0	55	0	0	0	0	0	0	0
Actinobacteria	Coriobacteriaceae	0	0	416	849	2570	0	0	0	0	0
Actinobacteria	Streptomycetaceae	0	98	0	0	0	0	0	0	0	0
Actinobacteria	Actinomycetaceae	0	0	0	0	0	0	122	0	0	0
Actinobacteria	Bifidobacteriaceae	0	0	0	0	0	0	147	0	0	0
Actinobacteria	Dietziaceae	0	0	0	0	0	0	396	0	280	0
Actinobacteria	Intrasporangiaceae	0	0	0	0	0	0	0	0	154	0
Actinobacteria	Microbacteriaceae	0	0	83	670	126	0	0	0	0	0
Actinobacteria	Micrococcaceae	0	0	0	0	0	0	0	0	96	0
Actinobacteria	Nocardioidaceae	0	0	0	106	0	0	0	0	0	0
Bacteroidetes	Bacteroidales S24-7 group	85	0	318	279	0	0	0	0	0	0
Bacteroidetes	Chitinophagaceae	0	91	362	0	106	0	0	0	0	0
Bacteroidetes	Cyclobacteriaceae	0	0	0	553	0	0	0	0	0	0
Bacteroidetes	Draconibacteriaceae	0	87	2165	162	554	0	0	0	0	0
Bacteroidetes	Flavobacteriaceae	0	1023	455	160	0	0	0	0	0	0
Bacteroidetes	ML635J-40 aquatic group	0	0	0	483	160	0	0	0	0	0
Bacteroidetes	WCHB1-69	0	72	296	0	87	0	0	0	0	0
Chloroflexi	Anaerolineaceae	494	77	337	7130	2180	0	0	0	0	0
Deltaproteobacteria	Bdellovibrionaceae	0	573	0	0	0	0	0	0	0	0
Deltaproteobacteria	Desulfobulbaceae	198	0	0	0	0	0	0	0	0	0
Deltaproteobacteria	Syntrophaceae	89	179	0	1209	0	0	0	0	0	0
Gemmatimonadetes	Gemmatimonadaceae	2632	1662	0	0	0	0	0	0	0	0
Hydrogenophilalia	Hydrogenophilaceae	180	214	0	0	0	0	0	0	0	0
Nitrospirae	Nitrospiraceae	7752	2647	0	928	143	0	0	0	0	0
Planktomycetes	Phycisphaeraceae	76	4211	0	0	0	0	0	0	0	0
Planktomycetes	Planctomycetaceae	241	1074	0	0	0	0	0	0	0	0
Spirochaetes	Spirochaetaceae	0	87	0	0	0	0	0	0	0	0
Other	Other	23773	54206	3929	73670	15788	0	551	73	95	0

Table 14 - Archaeal qPCR Results from Depth Profile

Content	Sample Name	Starting Quantity (SQ)	Amplicons/mL
Sample	100%	27239.85	2.72E+07
Sample	50%	15291.05	1.53E+07
Sample	15%	2610.50	2.61E+06
Sample	0%	0.90	8.99E+02
Sample	CSW1.1 19.5m	5532.53	5.53E+06
Positive Control	M. jan	2420.52	2.42E+06
Standard	M. jan 16 pg/uL	16.00	1.60E+04
Standard	M. jan 2 pg/uL	2.00	2.00E+03
Standard	M. jan 32 pg/uL	32.00	3.20E+04
Standard	M. jan 4 pg/uL	4.00	4.00E+03
Standard	M. jan 64 pg/uL	64.00	6.40E+04
Standard	M. jan 8 pg/uL	8.00	8.00E+03
Standard	M.jan 128 pg/uL	128.00	1.28E+05
Negative Control	Molec. H2O	0.19	1.86E+02

M. jan = *Methanocaldococcus jannaschii*
pg/ uL = picograms per microliter

REFERENCES

REFERENCES

Albert, D. B. & Martens, C. S. Determination of low-molecular-weight organic acid concentrations in seawater and pore-water samples via HPLC. *Mar. Chem.* **56,** 27–37 (1997).

Albuquerque, L. *et al.* Truepera radiovictrix gen . nov ., sp. nov., a new radiation resistant species and the proposal of Trueperaceae fam. nov. *FEMS Microbiol. Lett.* **247,** 161–169 (2005).

Aloupi, M., Koutrotsios, G., Koulousaris, M. & Kalogeropoulos, N. Trace metal contents in wild edible mushrooms growing on serpentine and volcanic soils on the island of Lesvos, Greece. *Ecotoxicol. Environ. Saf.* **78,** 184–194 (2012).

Amend, J. P. *et al.* Energetics of overall metabolic reactions of thermophilic and hyperthermophilic Archaea and bacteria. *FEMS Microbiol. Rev.* **25,** 175–243 (2001).

Amend, J. P., McCollom, T. M., Hentscher, M. & Bach, W. Catabolic and anabolic energy for chemolithoautotrophs in deep-sea hydrothermal systems hosted in different rock types. *Geochim. Cosmochim. Acta* **75,** 5736–5748 (2011).

Baes III, C. F. & S.B., M. Trace Metal Uptake and Accumulation in Trees as Affected by Environmental Pollution. *NATO ASI Ser.* **G16,** (1987).

Beal, E. J., House, C. H. & Orphan, V. J. Manganese- and Iron-Dependent Marine Methane Oxidation. *Science (80-.).* **325,** 184–187 (2016).

Becquer, T., Quantin, C., Sicot, M. & Boudot, J. P. Chromium availability in ultramafic soils from New Caledonia. *Sci. Total Environ.* **301,** 251–261 (2003).

Brazelton, W. J. *et al.* Metagenomic identification of active methanogens and methanotrophs in serpentinite springs of the Voltri Massif, Italy. *PeerJ* 1–33 (2017). doi:10.7717/peerj.2945

Brazelton, W. J., Mehta, M. P., Kelley, D. S. & Baross, J. A. Physiological differentiation within a single-species biofilm fueled by serpentinization. *MBio* **2,** 1–9 (2011).

Brazelton, W. J., Morrill, P. L., Szponar, N. & Schrenk, M. O. Bacterial communities associated with subsurface geochemical processes in continental serpentinite springs. *Appl. Environ. Microbiol.* **79,** 3906–3916 (2013).

Brazelton, W. J., Nelson, B. & Schrenk, M. O. Metagenomic evidence for H2 oxidation and H2 production by serpentinite-hosted subsurface microbial communities. *Front. Microbiol.* **2,** 1–16 (2012).

Brazelton, W. J., Schrenk, M. O., Kelley, D. S. & Baross, J. A. Methane- and sulfur-metabolizing microbial communities dominate the lost city hydrothermal field ecosystem. *Appl. Environ. Microbiol.* **72,** 6257–6270 (2006).

Callahan, B. J., McMurdie, P. J. & Holmes, S. P. Exact sequence variants should replace operational taxonomic units in marker gene data analysis. *ISME J.* 113597 (2017). doi:doi:10.1038/ismej.2017.119

Cannat, M., Fontaine, F. & Escartin, J. in *Diversity of Hydrothermal Systems on Slow Spreading Ocean Ridges* (2013). doi:10.1029/2008GM000760

Cardace, D. *et al.* Establishment of the Coast Range ophiolite microbial observatory (CROMO): Drilling objectives and preliminary outcomes. *Sci. Drill.* 45–55 (2013). doi:10.5194/sd-16-45-2013

Cardace, D., Meyer-Dombard, D. R., Woycheese, K. M. & Arcilla, C. A. Feasible metabolisms in high pH springs of the Philippines. *Front. Microbiol.* **6,** 10 (2015).

Chavagnac, V. *et al.* Mineralogical assemblages forming at hyperalkaline warm springs hosted on ultramafic rocks: A case study of Oman and Ligurian ophiolites. *Geochemistry, Geophys. Geosystems* **14,** 2474–2495 (2013).

Chavagnac, V., Monnin, C., Ceuleneer, G., Boulart, C. & Hoareau, G. Characterization of hyperalkaline fluids produced by low-temperature serpentinization of mantle peridotites in the Oman and Ligurian ophiolites. *Geochemistry, Geophys. Geosystems* **14,** 2496–2522 (2013).

Cline, J. D. Spectrophotometric determination of hydrogen sulfide in natural waters. *Limnol. Oceanogr.* 454–458 (1969). doi:10.4319/lo.1969.14.3.0454

Crespo-Medina, M. *et al.* Insights into environmental controls on microbial communities in a continental serpentinite aquifer using a microcosm-based approach. *Front. Microbiol.* **5,** 604 (2014).

Crespo-Medina, M. *et al.* Methane Dynamics in a Tropical Serpentinizing Environment: The Santa Elena Ophiolite, Costa Rica. *Front. Microbiol.* **8,** 1–14 (2017).

DeLong, E. F. Archaea in coastal marine environments. *Proc. Natl. Acad. Sci.* **89,** 5685–5689 (1992).

Edgar, R. C. Search and clustering orders of magnitude faster than BLAST. *Bioinformatics* **26,** 2460–2461 (2010).

Edgar, R. C., Haas, B. J., Clemente, J. C., Quince, C. & Knight, R. UCHIME improves sensitivity and speed of chimera detection. *Bioinformatics* **27,** 2194–2200 (2011).

Etiope, G., Ehlmann, B. L. & Schoell, M. Low temperature production and exhalation of methane from serpentinized rocks on Earth: A potential analog for methane production on Mars. *Icarus* **224,** 276–285 (2013).

Etiope, G., Schoell, M. & Hosgörmez, H. Abiotic methane flux from the Chimaera seep and Tekirova ophiolites (Turkey): Understanding gas exhalation from low temperature serpentinization and implications for Mars. *Earth Planet. Sci. Lett.* **310,** 96–104 (2011).

Etiope, G. & Sherwood Lollar, B. Abiotic methane on earth. *Rev. Geophys.* **51,** 276–299 (2013).

Etiope, G., Vance, S., Christensen, L. E., Marques, J. M. & Ribeiro da Costa, I. Methane in serpentinized ultramafic rocks in mainland Portugal. *Mar. Pet. Geol.* **45,** 12–16 (2013).

Ettwig, K. F. *et al.* Nitrite-driven anaerobic methane oxidation by oxygenic bacteria. *Nature* **464,** 543–548 (2010).

Evans, B. W. Lizardite versus antigorite serpentinite: Magnetite, hydrogen, and life(?). *Geology* **38,** 879–882 (2010).

Frost, B. R., Evans, K. A., Swapp, S. M., Beard, J. S. & Mothersole, F. E. The process of serpentinization in dunite from new caledonia. *Lithos* **178,** 24–39 (2013).

Hobbie, J. E., Daley, R. J. & Jasper, S. Use of nuclepore filter counting bacteria by fluoroscence microscopy. *Appl. Environ. Microbiol. Microbiol.* **33,** 1225–1228 (1977).

Hoehler, T. M., Alperin, M. J., Albert, D. B. & Martens S., C. Field and laboratory studies of methane oxidation in an anoxic sediment: evidence for a methanogen-sulfate-reducer consortium. *Glob. Biogeochem Cycles* **8,** 451–464 (1994).

Hoehler, T. M., Alperin, M. J., Albert, D. B. & Martens, C. S. Apparent minimum free energy requirements for methanogenic Archaea and sulfate-reducing bacteria in an anoxic marine sediment. *FEMS Microbiol. Ecol.* **38,** 33–41 (2001).

Holloway, J. M., Goldhaber, M. B., Scow, K. M. & Drenovsky, R. E. Spatial and seasonal variations in mercury methylation and microbial community structure in a historic mercury mining area, Yolo County, California. *Chem. Geol.* **267,** 85–95 (2009).

Hosgormez, H., Etiope, G. & Yalçin, M. N. New evidence for a mixed inorganic and organic origin of the Olympic Chimaera fire (Turkey): A large onshore seepage of abiogenic gas. *Geofluids* **8,** 263–273 (2008).

Huot, F. & Maury, R. C. The Round Mountain serpentinite m??lange, northern Coast Ranges of California: An association of backarc and arc-related tectonic units. *Bull. Geol. Soc. Am.* **114,** 109–123 (2002).

Jørgensen, B. B., Böttcher, M. E., Lüschen, H., Neretin, L. N. & Volkov, I. I. Anaerobic methane oxidation and a deep H2S sink generate isotopically heavy sulfides in Black Sea sediments. *Geochim. Cosmochim. Acta* **68,** 2095–2118 (2004).

Joye, S. B. *et al.* The anaerobic oxidation of methane and sulfate reduction in sediments from Gulf of Mexico cold seeps. *Chem. Geol.* **205,** 219–238 (2004).

Knittel, K. & Boetius, A. Anaerobic oxidation of methane: progress with an unknown process. *Annu. Rev. Microbiol.* **63,** 311–34 (2009).

Kozich, J. J., Westcott, S. L., Baxter, N. T., Highlander, S. K. & Schloss, P. D. Development of a dual-index sequencing strategy and curation pipeline for analyzing amplicon sequence data on the miseq illumina sequencing platform. *Appl. Environ. Microbiol.* **79,** 5112–5120 (2013).

Lang, S. Q. *et al.* Microbial utilization of abiogenic carbon and hydrogen in a serpentinite-hosted system. *Geochim. Cosmochim. Acta* **92,** 82–99 (2012).

Langmuir, D. *Aqueous Environmental Geochemistry*. Prentice Hall, NJ, (1997).

Lee, E. M., Jeon, C. O., Choi, I., Chang, K. S. & Kim, C. J. Silanimonas lenta gen. nov., sp. nov., a slightly thermophilic and alkaliphilic gammaproteobacterium isolated from a hot spring. *Int. J. Syst. Evol. Microbiol.* **55,** 385–389 (2005).

Marques, J. M. *et al.* Origins of high pH mineral waters from ultramafic rocks, Central Portugal. *Appl. Geochemistry* **23,** 3278–3289 (2008).

Mayhew, L. E., Ellison, E. T., McCollom, T. M., Trainor, T. P. & Templeton, A. Hydrogen generation from low-temperature water-rock reactions. *Nat. Geosci.* **6,** 478–484 (2013).

McCollom, T. M. Laboratory Simulations of Abiotic Hydrocarbon Formation in Earth's Deep Subsurface. *Rev. Mineral. Geochemistry* **75,** 467–494 (2013).

McCollom, T. M. & Seewald, J. S. Serpentinites, hydrogen, and life. *Elements* **9,** 129–

McCollom, T. M. & Seewald, J. S. A reassessment of the potential for reduction of dissolved CO2 to hydrocarbons during serpentinization of olivine. *Geochim. Cosmochim. Acta* **65,** 3769–3778 (2001).

McCollom, T. M. & Shock, E. L. Geochemical constraints on chemolithoautotrophic metabolism by microorganisms in seafloor hydrothermal systems. *Geochim. Cosmochim. Acta* **61,** 4375–4391 (1997).

McKay, C. P., Anbar, A. D., Porco, C. & Tsou, P. Follow the Plume: The Habitability of Enceladus. *Astrobiology* **14,** 352–355 (2014).

Meyer-Dombard, D. R. *et al.* High pH microbial ecosystems in a newly discovered, ephemeral, serpentinizing fluid seep at Yanarta?? (Chimera), Turkey. *Front. Microbiol.* **6,** 1–13 (2015).

Miller, H. M. *et al.* Modern water/rock reactions in Oman hyperalkaline peridotite aquifers and implications for microbial habitability. *Geochim. Cosmochim. Acta* **179,** 217–241 (2016).

Möller, F. M., Kriegel, F., Kieß, M., Sojo, V. & Braun, D. Steep pH Gradients and Directed Colloid Transport in a Microfluidic Alkaline Hydrothermal Pore. *Angew. Chemie - Int. Ed.* **56,** 2340–2344 (2017).

Monnin, C. *et al.* Fluid chemistry of the low temperature hyperalkaline hydrothermal system of Prony bay (New Caledonia). *Biogeosciences* **11,** 5687–5706 (2014).

Morrison, J. M. *et al.* Weathering and transport of chromium and nickel from serpentinite in the Coast Range ophiolite to the Sacramento Valley, California, USA. *Appl. Geochemistry* **61,** 72–86 (2015).

Orphan, V. J., House, C. H., Hinrichs, K.-U., McKeegan, K. D. & DeLong, E. F. Multiple archaeal groups mediate methane oxidation in anoxic cold seep sediments. *Proc. Natl. Acad. Sci.* **99,** 7663–7668 (2002).

Ortiz, E. *et al.* Geophysical Characterization of Serpentinite Hosted Hydrogeology at the McLaughlin Natural Reserve, Coast Range Ophiolite. *(In Submission)*

Oze, C. & Sharma, M. Have olivine, will gas: Serpentinization and the abiogenic production of methane on Mars. *Geophys. Res. Lett.* **32,** 1–4 (2005).

Proskurowski, G. *et al.* Abiogenic hydrocarbon production at lost city hydrothermal field. *Science* **319,** 604–7 (2008).

Proskurowski, G., Lilley, M. D., Kelley, D. S. & Olson, E. J. Low temperature volatile production at the Lost City Hydrothermal Field, evidence from a hydrogen stable isotope geothermometer. *Chem. Geol.* **229,** 331–343 (2006).

Pruesse, E., Peplies, J. & Glöckner, F. O. SINA: Accurate high-throughput multiple sequence alignment of ribosomal RNA genes. *Bioinformatics* **28,** 1823–1829 (2012).

Reeburgh, W. Oceanic methane biogeochemistry. *Am. Chem. Soc.* **107,** 486–513 (2007).

Sanchez-Murillo, R. *et al.* Geochemical evidence for active tropical serpentinization in the Santa Elena Ophiolite, Costa Rica: An analog of a humid early Earth? *Geochemistry Geophys. Geosystems* **18,** 1–16 (2014).

Schink, B. Energetics of syntrophic cooperation in methanogenic degradation. *Microbiol. Mol. Biol. Rev.* **61,** 262–280 (1997).

Schloss, P. D. & Westcott, S. L. Assessing and improving methods used in operational taxonomic unit-based approaches for 16S rRNA gene sequence analysis. *Appl. Environ. Microbiol.* **77,** 3219–3226 (2011).

Schloss, P. D. *et al.* Introducing mothur: Open-source, platform-independent, community-supported software for describing and comparing microbial communities. *Appl. Environ. Microbiol.* **75,** 7537–7541 (2009).

Schrenk, M. O., Brazelton, W. J., Carolina, N. & Lang, S. Q. Serpentinization, Carbon, and Deep Life. *Rev. Mineral.* **75,** 575–606 (2013).

Schrenk, M. O., Kelley, D. S., Delaney, J. R. & Baross, J. A. Incidence and diversity of microorganisms within the walls of an active deep-sea sulfide chimney. *Appl. Environ. Microbiol.* **69,** 3580–3592 (2003).

Schwarzenbach, E. M. *et al.* Sulfur geochemistry of peridotite-hosted hydrothermal systems: Comparing the Ligurian ophiolites with oceanic serpentinites. *Geochim. Cosmochim. Acta* **91,** 283–305 (2012).

Schwarzenbach, E. M., Gill, B. C., Gazel, E. & Madrigal, P. Sulfur and carbon geochemistry of the Santa Elena peridotites: Comparing oceanic and continental processes during peridotite alteration. *Lithos* **252–253,** 92–108 (2016).

Seyfried, W. E., Foustoukos, D. I. & Fu, Q. Redox evolution and mass transfer during serpentinization: An experimental and theoretical study at 200 ??C, 500 bar with implications for ultramafic-hosted hydrothermal systems at Mid-Ocean Ridges. *Geochim. Cosmochim. Acta* **71,** 3872–3886 (2007).

Shervais, J. W. & Kimbrough, D. L. Geochemical evidence for the tectonic setting of the Coast Range ophiolite: a composite island arc-oceanic crust terrane in western California. *Geology* **13,** 35–38 (1985).

Shervais, J. W. *et al.* Multi-Stage Origin of the Coast Range Ophiolite, California: Implications for the Life Cycle of Supra-Subduction Zone Ophiolites. *Int. Geol. Rev.* **46,** 289–315 (2004).

Sleep, N. H., Meibom, a, Fridriksson, T., Coleman, R. G. & Bird, D. K. H2-rich fluids from serpentinization: geochemical and biotic implications. *Proc. Natl. Acad. Sci. U. S. A.* **101,** 12818–12823 (2004).

Sleep, N. H., Bird, D. K. & Pope, E. C. Serpentinite and the dawn of life. *Philos. Trans. R. Soc. B Biol. Sci.* **366,** 2857–2869 (2011).

Sogin, M. L. *et al.* Microbial diversity in the deep sea and the underexplored 'rare biosphere'. *Proc. Natl. Acad. Sci. U. S. A.* **103,** 12115–20 (2006).

Srinivas, T. N. R., Kailash, T. B. & Anil Kumar, P. Silanimonas mangrovi sp. nov., a member of the family Xanthomonadaceae isolated from mangrove sediment, and emended description of the genus Silanimonas. *Int. J. Syst. Evol. Microbiol.* **63,** 274–279 (2013).

Stadnitskaia, A. *et al.* Carbonate formation by anaerobic oxidation of methane: Evidence from lipid biomarker and fossil 16S rDNA. *Geochim. Cosmochim. Acta* **72,** 1824–1836 (2008).

Suda, K. *et al.* Origin of methane in serpentinite-hosted hydrothermal systems: The CH4-H2-H2O hydrogen isotope systematics of the Hakuba Happo hot spring. *Earth Planet. Sci. Lett.* **386,** 112–125 (2014).

Suzuki, S. *et al.* Microbial diversity in The Cedars, an ultrabasic, ultrareducing, and low salinity serpentinizing ecosystem. *Proc. Natl. Acad. Sci. U. S. A.* **110,** 15336–15341 (2013).

Suzuki, S. *et al.* Physiological and genomic features of highly alkaliphilic hydrogen-utilizing Betaproteobacteria from a continental serpentinizing site. *Nat. Commun.* **5,** 3900 (2014).

Szponar, N. *et al.* Geochemistry of a continental site of serpentinization, the Tablelands Ophiolite, Gros Morne National Park: A Mars analogue. *Icarus* **224,** 286–296 (2013).

Twing, K. I. *et al.* Serpentinization-influenced groundwater harbors extremely low diversity microbial communities adapted to high pH. *Front. Microbiol.* **8,** 308 (2017).

Twing, K. I. Microbial Diversity and Metabolic Potential of the Serpentinite Subsurface Environment. (Ph.D. Thesis). Order No. 3739219 Michigan State University. Ann Arbor: *ProQuest* (2015).

Visioli, G., Menta, C., Gardi, C. & Conti, F. D. Metal toxicity and biodiversity in serpentine soils: Application of bioassay tests and microarthropod index. *Chemosphere* **90,** 1267–1273 (2013).

Wang, D. T. *et al.* Methane cycling. Nonequilibrium clumped isotope signals in microbial methane. *Science* **348,** 428–31 (2015).

Weber, H. S., Thamdrup, B. & Habicht, K. S. High Sulfur Isotope Fractionation Associated with Anaerobic Oxidation of Methane in a Low-Sulfate, Iron-Rich Environment. *Front. Earth Sci.* **4,** 1–14 (2016).

Woycheese, K. M., Meyer-Dombard, D. R., Cardace, D., Argayosa, A. M. & Arcilla, C. A. Out of the dark: Transitional subsurface-to-surface microbial diversity in a terrestrial serpentinizing seep (Manleluag, Pangasinan, the Philippines). *Front. Microbiol.* **6,** 1–12 (2015).